Copyright Warning & Restrictions

The copyright law of the United States (Title 17, United States Code) governs the making of photocopies or other reproductions of copyrighted material.

Under certain conditions specified in the law, libraries and archives are authorized to furnish a photocopy or other reproduction. One of these specified conditions is that the photocopy or reproduction is not to be "used for any purpose other than private study, scholarship, or research." If a, user makes a request for, or later uses, a photocopy or reproduction for purposes in excess of "fair use" that user may be liable for copyright infringement,

This institution reserves the right to refuse to accept a copying order if, in its judgment, fulfillment of the order would involve violation of copyright law.

Please Note: The author retains the copyright while the New Jersey Institute of Technology reserves the right to distribute this thesis or dissertation

Printing note: If you do not wish to print this page, then select "Pages from: first page # to: last page #" on the print dialog screen

NJIT New Jersey's Science & Technology University

The Van Houten library has removed some of the personal information and all signatures from the approval page and biographical sketches of theses and dissertations in order to protect the identity of NJIT graduates and faculty.

ABSTRACT

Application of Imaging Pyrometry for Remote Temperature Measurements

by

Michael B. Kaplinsky

The radiometric model of an IR image sensor has been developed. Based on this model, the application of imaging pyrometry to remote temperature measurements has been investigated. This analysis provides the estimation of temperature accuracy achievable by imaging pyrometry in conjunction with a number of radiometric methods. The detection of radiation emitted across the full spectral bandwidth of the imager as well as utilization of narrow-passband filters was analyzed for a target with known emissivity.

The methods of two-wavelength ratio radiometry and multi-wavelength radiometry were considered for the targets with unknown emissivity. The optimal selection of the wavelengths for the method of ratio radiometry was investigated. It was shown that in the case of a blackbody radiator at 1000 °C the ratio radiometry yields temperature resolution of 0.5 °C for the 10^6 electrons per pixel signal level detected by 320x244 IR imager with PtSi Schottky-barrier detectors and operated with 100-nm-wide Gaussian filters positioned at 1.5 μm and 3.0 μm. The temperature accuracy achievable by least-squares-based multi-wavelength imaging pyrometry (MWIP) was

analyzed for linear and quadratic emissivity models. The presented results have shown that for targets with quadratic spectral emissivity at 1000 °C the 6-filter MWIP is capable of providing temperature resolution of about 1 °C for target temperature of 1000 °C and the maximum signal of $4x10^6$ electrons per pixel. For targets at 500 °C the corresponding accuracy is equal to 0.4 °C.

APPLICATION OF IMAGING PYROMETRY FOR REMOTE TEMPERATURE MEASUREMENTS

by
Michael B. Kaplinsky

A Thesis
Submitted to the Faculty of the
New Jersey Institute of Technology
in Partial Fulfillment of the Requirements for the Degree of
Master of Science

Department of Electrical and Computer Engineering
January, 1993

APPROVAL PAGE

Application of Imaging Pyrometry for Remote Temperature Measurements

by

Michael B. Kaplinsky

Dr. Walter F. Kosonocky, Thesis Advisor
Distinguished Professor of Electrical and Computer Engineering,
NJIT Foundation Chair for Optoelectronics and Solid State Circuits

---

Dr. Constantine N. Manikopoulos, Committee Member
Associate Professor of Electrical and Computer Engineering, NJIT

Dr. Edwin Hou, Committee Member
Assistant Professor of Electrical and Computer Engineering, NJIT

BIOGRAPHICAL SKETCH

Author: Michael B. Kaplinsky

Degree: Master of Science in Electrical Engineering

Date: January, 1993

Education:

- Master of Science in Electrical Engineering,
  New Jersey Institute of Technology, Newark, NJ, 1993

- Master of Science in Mechanical Engineering,
  Moscow Institute of Steel and Alloys, Moscow, USSR, 1989

Publications and Presentations:

Kaplinsky, M. B. "Research Into Heat Transfer in Furnaces with Screen Systems," *Steel in the USSR*, 16 (9), London, 1986.

Patel, V., M. Kaplinsky, W.F. Kosonocky, S. Ayyagari, and B. Singh, "Heat Transfer Analysis of Silicon Wafers During Reactive Ion Etching," presented at 39th National AVS Symposium, SRC ID# N92039 (1992)

This thesis is dedicated to
my daughter Diana

ACKNOWLEDGMENT

The author wishes to express his sincere gratitude to his advisor, Professor Walter F. Kosonocky for providing technical guidance and moral support throughout the term of this work. The author would like to take this opportunity to acknowledge the financial support for this research provided by NJIT Foundation Chair for Optoelectronics and Solid State Circuits held by Professor Kosonocky.

The author is also grateful to Dr. Constantine N. Manikopoulos for providing technical suggestions during the term of this work.

Special thanks are due to Professor Dr. Edwin Hou for serving as member of the committee.

The author also wishes to express his appreciation to Vipulkumar Patel and Nathaniel McCaffrey, NJIT graduate students, who have helped with experimental verification of the model.

TABLE OF CONTENTS

Chapter Page

1 INTRODUCTION 1

2 BASIC CONCEPTS OF RADIATION THERMOMETRY 4

2.1 Black Body Radiation 5

2.1.1 Planck Spectral Distribution and Wien's Approximation 5

2.1.2 Wien's Displacement Law and Stefan-Boltzmann Law 8

2.2 Emissivity of Real Surfaces 10

3 IR IMAGE SENSOR AS RADIOMETER 13

3.1 Basic Principles of Radiation Measurement 13

3.2 IR Image Sensors 17

3.2.1 320x244 IR CCD and 640x480 IR MOS Image Sensors 17

3.2.2 PtSi Schottky-Barrier Detector 20

3.2.3 Radiometric Model of the IR Imager 22

3.3 Accuracy of Wide-Band Temperature Measurements. 25

3.4 Single Wavelength Radiometry 29

3.4.1 Reference Wavelength Approach 30

3.4.2 Accuracy of Narrow-Band Radiometry 40

3.4.2.1 Noise Equivalent Temperature 41

3.4.2.2 Effects of an Inaccurate Filter Specification 45

Chapter Page

4 TWO WAVELENGTHS RATIO RADIOMETRY 52

4.1 Basic Theory of Two Wavelengths Ratio Radiometry 53

4.2 Accuracy of the Temperature Measurement 56

5 MULTI-WAVELENGTH RADIOMETRY 61

5.1 Basic Principles of MWIP 61

5.2 Accuracy of Temperature Measurements 65

5.2.1 Theoretical Estimation of the Accuracy 65

5.2.2 Linear and Quadratic Emissivity Models 68

6 COMPARISON OF RADIOMETRIC METHODS 78

6.1 Temperature Accuracy 79

6.1.1 Wide-Band vs. Narrow-Band Radiometry 80

6.1.2 Ratio and Multi-wavelength Radiometry 85

6.2 Improvement of Temperature Accuracy 90

6.2.1 Independently Repeated Measurements 91

6.2.2 Calibration 94

7 CONCLUSIONS 97

APPENDIX 101

REFERENCES 124

LIST OF TABLES

Table Page

1 NEΔT resulting from 1 measurement per filter. 80

2 NEΔT resulting from 4 measurements per filter. 92

3 NEΔT resulting from 25 measurements per filter. 93

4 NEΔT resulting from 100 measurements per filter..... 93

LIST OF FIGURES

Figure		Page
1	Spectral radiance of a blackbody radiator	6
2	Comparison of blackbody and real body emission	10
3	Imaging radiation thermometer with lens	14
4	Pixel layout of Sarnoff 320x244 IR imager	18
5	Low-noise MOS readout multiplexer of Sarnoff 640x480 IR MOS imager	19
6	Operation of Schottky-barrier detector.	20
7	Measured responsivity of PtSi Schottky-Barrier detector array	22
8	Total signal detected by 640x480 IR MOS imager	23
9	Calculated optical integration time of 640x480 IR MOS imager for detected signal of Q_{max} electrons per pixel.	24
10	Calculated NEΔT of 640x480 IR MOS imager with f/1.4 optics	27
11	Calculated NEΔT of 640x480 IR MOS imager with f/1.4 optics for detected signal of Qmax electrons per pixel	28
12	Normalized moments of various filters	36
13	Calculated and measured signal of 320x244 IR-CCD imager without lens	38

Figure Page

14 Calculated and measured signal of 320x244 IR-CCD imager operating with optical integration time of 33 ms, f/2 optics and 500-nm Gaussian filter with 60% 39

15 Calculated and measured signal of 320x244 IR-CCD imager operating with optical integration time of 33 ms, f/2 optics and 20-nm Gaussian filter with 60% peak of transmission..... 40

16 Calculated and measured signal of 320x244 IR-CCD imager operating with optical integration time of 33 ms, f/2 optics and 20-nm Gaussian filter with 60% peak of transmission..... 44

17 Effect on ΔT of 5-nm error in the estimation of the center wavelength of 100-nm Gaussian filter..... 49

18 Error in the detected by a 320x244 IR-CCD imager signal resulting from modeling Gaussian-shaped filter by the square-shaped filter of the same area..... 50

19 Temperature is inferred from the ratio of signals measured at two distinct wavelengths..... 54

20 Calculated NEΔT for 320x244 IR CCD camera operating with optical integration time of 33 ms, f/2 optics, and 500 nm Gaussian filter with 60% peak transmission..... 58

21 Calculated NEΔT for 320x244 IR CCD camera operating with optical integration time of 33 ms, f/2 optics, and 20 nm Gaussian filter with 60% peak transmission..... 59

Figure Page

22 Dependence of ΔT on the positioning of two Gaussian 100 nm filters. The center wavelength of one of the filters is given on horizontal axis. 60

23 Least-squares fit to the simulated signal detected by a 320x244 IR CCD imager. The fit is based on 8 measurements per filter. The temperature of the simulated target is 1073 K..... 63

24 Spectral emissivity of single crystal n-type silicon disc..... 71

25 Temperature accuracy of MWIP with linear emissivity model. The computations assume 4 independent measurements per filter, 100-nm -wide Gaussian filters and Qmax=106 electrons per pixel..... 73

26 Temperature accuracy of MWIP with linear emissivity model and 5-nm error in the estimation of the center wavelengths of 100-nm-wide Gaussian filters. The computations assume 25 independent measurements per filter and Qmax=106 electrons/pixel..... 74

27 Temperature accuracy of MWIP vs. total spectral bandwidth of measurement for target temperature of 1000 °C 76

28 Accuracy of MWIP measurements with linear and quadratic emissivity models 89

CHAPTER 1

INTRODUCTION

The research work reported in this thesis represents theoretical analysis performed in support of the effort of the Electronic Imaging Center of the NJIT Foundation for Optoelectronics and Solid-State Circuits under DARPA contract F33615-92-C-5817 "Multi-Wavelength Imaging Pyrometry for Semiconductor Process Monitoring and Control" and under NASA contract NAS1-18226 "Radiometric Infrared Focal Plane Array Imaging System for Thermographic Applications". This work was done under general direction of Professor Walter Kosonocky. The graduate students who contributed the experimental results reported in this thesis include Nathaniel McCaffrey, Vipulkumar Patel, and Mehul Patel.

The objectives of this work include the development of a radiometric model of an IR image sensor and the estimation of its performance for measurement of temperature of remote radiant targets. The thesis also provides the comparative study of various radiometric techniques, including wide-band, narrow-band, ratio, and multi-wavelength radiometry. For the purpose of this analysis the radiometric performance of a 320x244 IR CCD image sensor, developed at the David Sarnoff Research Center, was investigated in conjunction with each of the above techniques. The analysis presented in this work places special emphasis on the accurate description of

narrow-passband filters used for radiometric temperature measurement, thus providing a realistic model of the spectral properties of filter-imager system.

Chapter 2 gives a brief description of the basic radiometric concepts used in this thesis. The concept of the ideal emitter and radiator (blackbody) is introduced in the first section of this chapter. This section provides the information on the basic characteristics of the blackbody spectral emission. The second section of this chapter describes radiation emission by real (non-idealized) surfaces.

Chapter 3 provides the description of the radiometric model of the IR image sensor. Based on this model the radiometric performance of the imager is investigated for the cases of wide-band and narrow-band radiometry. The concept of the *reference wavelength* is introduced in order to facilitate the analysis of radiometric performance of an imager viewing the radiant target through a narrow-passband infrared filter. The chapter concludes with the analysis of the effects of the filter characteristics on the temperature accuracy of the radiometric temperature measurements.

Chapter 4 describes the theory of ratio radiometry. It is shown that this radiometric technique allows to perform accurate temperature measurements for graybodies with unknown emissivity. The noise equivalent temperature, $NE\Delta T$[1] , resulting from employing this technique is analyzed. This chapter

---

[1] It should be noted that the concepts of *noise equivalent temperature*, $NE\Delta T$, *minimum resolvable temperature*, and *noise-limited temperature accuracy* are used interchangeably throughout the thesis.

concludes with the discussion of various factors affecting the accuracy of temperature measurement by the method of ratio radiometry.

Chapter 5 describes the techniques of multi-wavelength imaging pyrometry (MWIP). It is shown that for a wide variety of targets the MWIP technique provides the means of radiometric temperature measurement without prior knowledge of the emissivity of the target. In this chapter a special emphasis is placed on the analysis of noise equivalent temperature for linear and quadratic models of spectral emissivity.

Chapter 6 provides a comparative analysis of the NEΔT achievable by the radiometric techniques described in the thesis. The advantages and limitations of each approach are analyzed. This chapter concludes with a discussion of the calibration procedure of the IR imager which should be conducted in order to improve the accuracy of the measurements.

CHAPTER 2

BASIC CONCEPTS OF RADIATION THERMOMETRY

All matter emits radiant energy as a consequence of its temperature. The non-contact measurement of temperature based on the detection of the emitted radiation is referred to as Radiation Thermometry or Radiometry.

To obtain a quantitative description of the emitted radiation the concept of spectral radiance has been introduced. The spectral radiance, $L_{\lambda,em}$, is defined as the radiant flux, Φ_{em} , emitted at the wavelength λ in a given direction, per unit of the emitting surface normal to this direction, per unit solid angle about this direction, and per unit wavelength interval $d\lambda$ about λ. The spectral radiance, which has the units of $[W/m^2 \cdot sr \cdot \mu m]$, may then be expressed as

$$L_{\lambda,em}(\lambda,\theta) = \frac{d^3\Phi_{em}}{dA_n d\omega\, d\lambda} \qquad (2\text{-}1)$$

If the spectral and directional distributions of the spectral radiance are known, the radiant power per unit area of the emitting surface may be determined by integration of Eq. (2-1) over finite solid angle and wavelength interval. In particular, the radiant power per unit area, emitted into the hemispheric space above the surface is defined as the total self-exitance, M_{em} $[W/m^2]$.

It is important to note that, in general, the directional distribution of surface emission varies according to the conditions of the surface. However, many real surfaces can be reasonably approximated by so-called lambertian surface. For a lambertian surface (also known as isotropically diffuse emitter) the radiance of the emitted radiation is independent of the direction. In this case the following relationship between radiance and exitance holds

$$M_{em} = \pi L_{em} \tag{2-2}$$

where L_{em} - is the total radiance of the emitted radiation $[W / m^2 \cdot sr^{-1}]$

In this work all considerations will be restricted to emitters which can be closely approximated by lambertian surfaces within reasonably small solid angles.

2.1 Black Body Radiation

2.1.1 Planck Spectral Distribution and Wien's Approximation

When describing the radiation characteristics of real surfaces, it is useful to introduce the concept of the blackbody. The blackbody is an ideal surface with the following properties:

(1) A blackbody absorbs all incident radiation, regardless of wavelength and direction.

(2) For a given temperature and wavelength, no surface can emit more thermal radiation than a blackbody.

(3) The blackbody is an isotropically diffuse (lambertian) emitter. Therefore, its radiation is independent of direction.

As a perfect absorber or emitter, the blackbody serves as the ideal radiator against which the properties of actual surfaces may be compared.

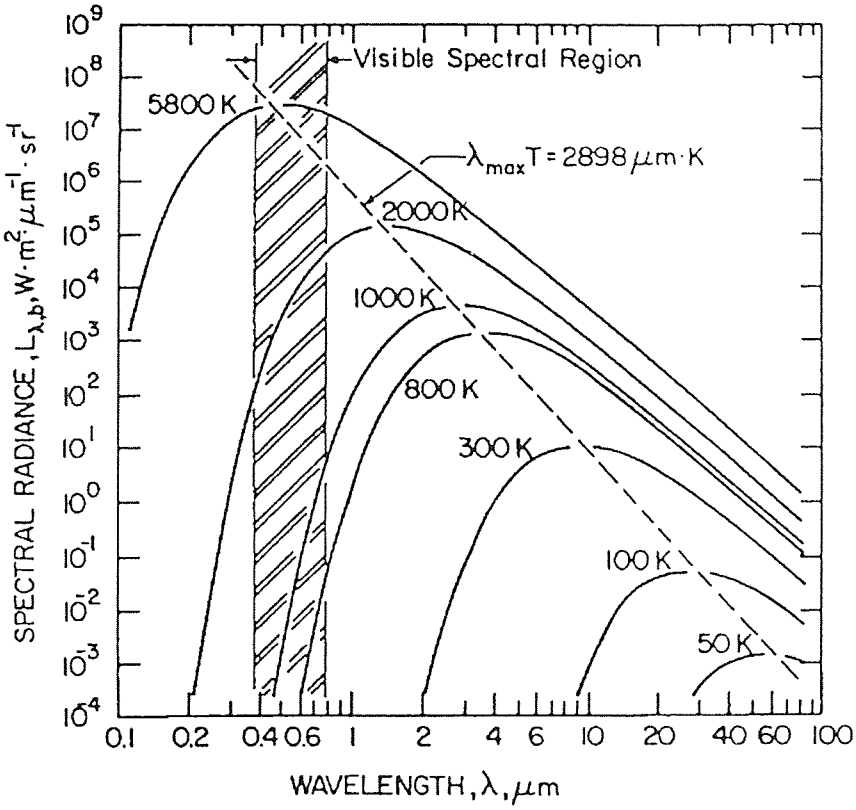

Figure 1 Spectral radiance of a blackbody radiator [1].

The spectral distribution of the radiation associated with blackbody emission was first derived by Planck from quantum mechanical considerations. The spectral radiance of a blackbody has the form

$$L_{\lambda,b}(\lambda,T)=\frac{C_1}{\lambda^5\left(\exp\left(\frac{C_2}{\lambda T}\right)-1\right)} \qquad (2\text{-}3)$$

where

$L_{\lambda,b}(\lambda,T)$ - is the blackbody spectral radiance $[W/m^2\cdot\mu m]$,

T - is the temperature of the blackbody radiator [K],

λ - is the wavelength [μm],

$C_1=1.1911\times10^8$ – is the first radiation constant $[W\cdot\mu m^4/m\cdot sr]$,

$C_2=1.4388\times10^4$ – is the second radiation constant $[\mu m\cdot K]$.

The spectral radiance of a blackbody is shown in Figure 1 for selected temperatures [1]. The following important characteristics of this distribution should be noted:

(1) The emitted radiation varies continuously with wavelength.

(2) At any wavelength the magnitude of the emitted radiation increases with increasing temperature.

(3) The spectral region in which the radiation is concentrated depends on temperature, with comparatively more radiation appearing at shorter wavelengths as the temperature increases.

Since the form of Eq. (2-3) is inconvenient for analytical manipulations a number of approximations to Planck's law have been developed. One of the most useful approximations to Eq. (2-3) is known as Wien's approximation and has the form

$$L_{\lambda,b}(\lambda,T)=\frac{C_1}{\lambda^5 \exp\left(\frac{C_2}{\lambda T}\right)} \tag{2-4}$$

For $\lambda T<2900\ \mu m\cdot K$ Plank's law and Wien's approximation produce almost indistinguishable results. Therefore, Wien's approximation is especially useful for short wavelengths or relatively low temperatures.

2.1.2 Wien's Displacement Law and Stefan-Boltzmann Law

It can be seen from Figure 1 that the blackbody spectral radiance is characterized by a maximum and that the wavelength associated with this maximum, λ_{max} , depends on blackbody temperature. Differentiating the Planck distribution given by Eq. (2-3) with respect to wavelength and setting the result equal to zero, we obtain

$$\lambda_{max}\cdot T=2897.7\ [\mu m\cdot K] \tag{2-5}$$

Equation (2-5) is known as Wien's displacement law. According to this law, the maximum of spectral radiance is displaced to shorter wavelengths with increasing temperature of the radiant surface. Thus, for a blackbody at 1000 K peak emission occurs at 2.9 μm, and for 300 K peak corresponds to 9.7 μm.

It can be shown that the value of the blackbody spectral radiance at its maximum is proportional to the fifth power of the blackbody temperature. Performing the substitution of Eq. (2-5) into Eq. (2-3) and multiplying the constants we obtain

$$L_{\lambda,b}(\lambda_{max},T) = 1.288\times10^{-11}\cdot T^5 \left[\frac{W}{m^2\cdot\mu m}\right] \qquad (2\text{-}6)$$

The value of the total radiant power emitted from a unit of blackbody surface area over the wavelength range from zero to infinity can be obtained by integration of Eq. (2-3) for any given temperature T. The result of this integration can be expressed as

$$L_{0\rightarrow\infty,b} = \sigma\cdot T^4 \quad \left[\frac{W}{m^2}\right] \qquad (2\text{-}7)$$

where $\sigma = 1.8049\times10^{-8}\ [W/m^2\cdot K^4]$ - is the Boltzmann constant.

Equation (2-7), known as the Stefan-Boltzmann law, shows that the total radiant power emitted by a blackbody is proportional to the fourth power of temperature.

2.2 Emissivity of Real Surfaces

Emissivity is a property of the emitting surface and is defined as the ratio of the radiation emitted by the surface to the radiation emitted by a blackbody at the same temperature and for the same spectral and directional conditions. It should be noted that emissivity may assume different values according to whether one is interested in emission at a given wavelength, in a given direction or in weighted averages over all possible wavelengths and directions as shown in Figure 2 [1].

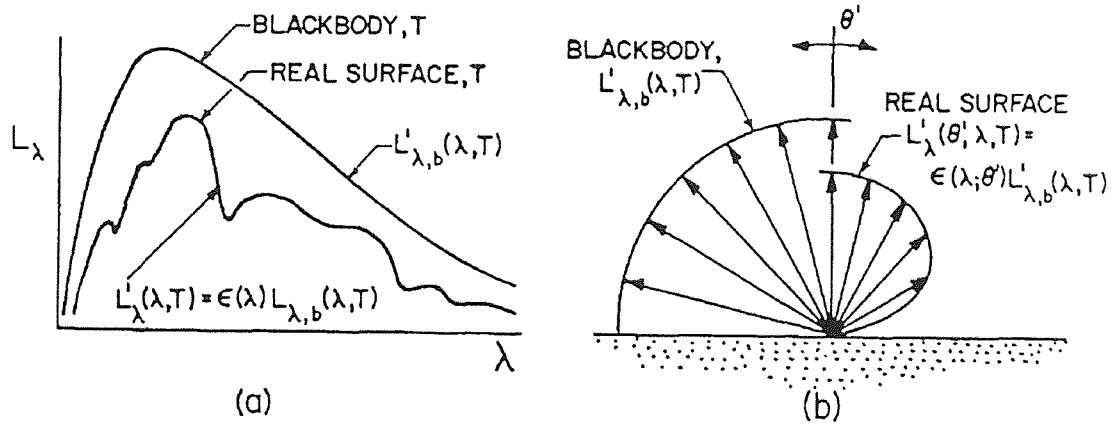

Figure 2. Comparison of blackbody and real body emission:

(a) spectral distribution and (b) directional distribution of radiance [1].

The spectral-directional emissivity $\varepsilon(\lambda,\theta,T)$ of a surface at temperature T is defined (assuming azimuthal isotropy for clarity) as the ratio of radiance of the radiation emitted at wavelength λ and in the direction θ to the radiance of the radiation emitted by a blackbody at the same temperature and wavelength

$$\varepsilon(\lambda,\theta,T) = \frac{L_{\lambda,em}(\lambda,\theta,T)}{L_{\lambda,b}(\lambda,T)} \tag{2-8}$$

It should be recognized that the spectral-directional emissivity is the most basic of the radiative properties from which other expressions for surface emissivity can be derived. The spectral-hemispherical emissivity (later referred to as spectral emissivity) represents a weighted average over all directions within the hemispherical space above a surface and is defined as

$$\varepsilon(\lambda,T) = \frac{\int_0^{\pi/2} L_{\lambda,em}(\lambda,\theta,T)\cos\theta\sin\theta\,d\theta}{\int_0^{\pi/2} L_{\lambda,b}(\lambda,T)\cos\theta\sin\theta\,d\theta} = \frac{\int_0^{\pi/2} L_{\lambda,em}(\lambda,\theta,T)\cos\theta\sin\theta\,d\theta}{\pi\cdot L_{\lambda,b}(\lambda,T)} \tag{2-9}$$

From Eq. (2-9) it follows that for lambertian surfaces the spectral-directional emissivity is equal to the spectral-hemispherical emissivity

$$\varepsilon(\lambda,\theta) = \varepsilon(\lambda,2\pi) \tag{2-10}$$

Finally, the total-hemispherical emissivity represents an average over the entire spectral range and for all possible directions and is defined as

$$\varepsilon(t,2\pi) = \frac{M_{em}(T)}{M_b(T)} \tag{2-11}$$

where $M_b(T)$ is the total exitance of the blackbody radiator [W/m^2] and $M_{em}(T)$ is the total self-exitance of the radiant surface given by Eq. (2-2).

CHAPTER 3

IR IMAGE SENSOR AS RADIOMETER

In this chapter it will be shown that an IR imager can be used as a imaging radiometer, later referred to as radiometer or radiation thermometer. We will discuss the methods by which the temperature of the remote radiant surface can be inferred from the spectral radiance measured by a radiometer. We will also consider the limitations imposed on the accuracy of temperature measurements by the presence of the radiation (shot) noise and rms detector read-out noise.

3.1 Basic Principles of Radiation Measurement

The concept of spectral radiance described by Eq (2-1) is of fundamental importance in radiation thermometry for the following reasons:

(1) The spectral radiance of a blackbody is accurately expressible in terms of its temperature and certain radiometric constants, as shown by Eq. (2-2). The same is true for non-blackbodies (gray or color bodies), but with the additional requirement that spectral emissivity must be known.

(2) An electro-optical system designed to measure spectral radiance provides the means for remote sensing of the temperature of a radiating surface.

(3) Spectral radiance has the very useful property of invariance along a beam of radiant flux [1]. Due to this property the radiant flux input to an IR imager can be calculated independently of the distance between the imager and the emitting surface.

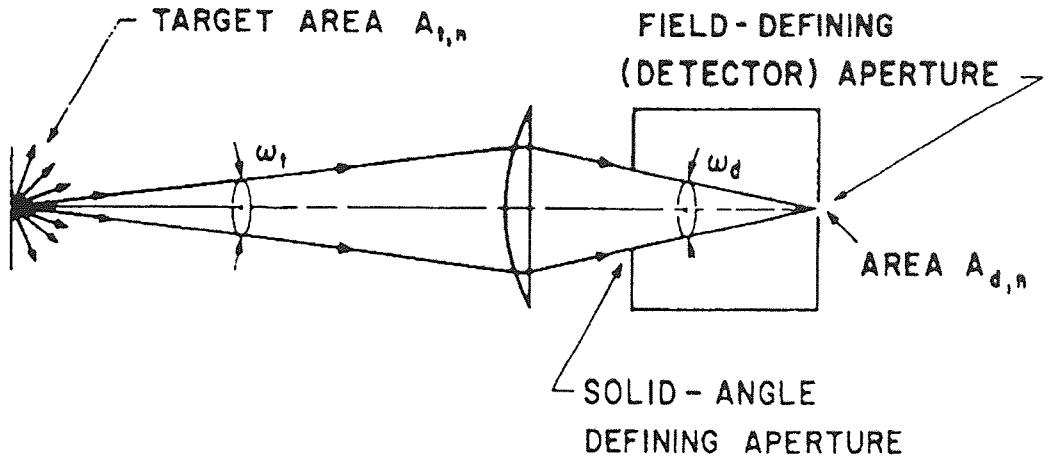

Figure 3 Imaging radiation thermometer with lens.

An approximate expression for the radiant flux originating from a remote radiant surface and entering the radiation detector can be obtained by integrating Eq. (2-1) over the area of the emitting surface within the field of view of the detector, solid angle subtended by the detector aperture, and the total bandwidth of the radiometer (see Figure 3)

$$\Phi(T) = \int_{\omega_t} \int_{A_{t,n}} \int_{0}^{\infty} L_\lambda(\lambda, T)\, dA_{t,n}\, d\omega_t\, d\lambda \qquad (3\text{-}1)$$

where

$A_{t,n}$ - is the area of the projection of the emitting surface in the field of view to the plane perpendicular to the optical axes;

ω_t - is the solid angle subtended by the radiation beam leaving the surface of the radiant target and reaching the radiation detector;

For a lambertian emitting surface, radiance is essentially constant over the $A_{t,n}$, and, for sufficiently remote target, $d\omega_t$ has nearly the same value from all points on $A_{t,n}$. In addition to the above assumptions we use the concept of optical invariant [2] in the following form

$$A_{d,n}\,\omega_d = A_{t,n}\,\omega_t \tag{3-2}$$

where

$A_{d,n}$ - is the area of projection of the detector aperture onto a plane perpendicular to the optical axes;

ω_d - is the solid angular field of view determined by the aperture.

Therefore, the Eq. (3-1) can be rewritten as

$$\Phi(T) = A_{d,n} \cdot \omega_d \cdot \int_0^\infty L_\lambda(\lambda,T)\, d\lambda \tag{3-3}$$

In order to obtain the output signal of the radiometer, we must also know its spectral responsivity function which is defined as

$$R(\lambda) = \frac{dS}{d\Phi(\lambda)} \tag{3-4}$$

Substituting Eq. (3-4) into Eq. (3-3) and taking into consideration the transmission curve $\tau(\lambda)$ of the filter (if applicable) positioned between the radiant target and detector, we obtain the following expression for the signal detected by the imager viewing the radiant target

$$S(T) = A_{d,n} \cdot \omega_d \cdot \int_0^\infty \tau(\lambda) \cdot R(\lambda) \cdot L_\lambda(\lambda, T)\, d\lambda \tag{3-5}$$

The signal given by Eq. (3-5) represents the output current of the radiation detector. For the purpose of this thesis, however, it is more convenient to represent the detected signal in terms of the electrical charge accumulated in the detector (pixel) during the optical integration time. The representation of the output signal of an imager in terms of electrons per pixel makes it easier to define radiation (shot) noise and to compare the signal under consideration with the maximum charge handling capacity of the detector. Therefore, in this thesis we will use the following expression

for the signal detected by the imager

$$S(T) = A_{d,n} \cdot \omega_d \cdot \frac{t_i}{Q_{el}} \cdot \int_0^{\infty} \tau(\lambda) \cdot R(\lambda) \cdot L_\lambda(\lambda, T)\, d\lambda \qquad (3\text{-}6)$$

where

t_i - is the optical integration time [s];

$Q_{el} = 1.6 \times 10^{-19}$ - is the charge of the electron [q].

Finally, we note that the spectral radiance L_λ of the radiation incident on the detector can be expressed by the product of the spectral emissivity of the emitting surface times the spectral radiance of the blackbody, in accordance with the Eq. (2-8). Substitution of Eq. (2-8) into Eq. (3-6) leads us to the most general expression for the output signal of the radiation detector viewing the radiant target

$$S(T) = A_{d,n} \cdot \omega_d \cdot \frac{t_i}{Q_{el}} \cdot \int_0^{\infty} \varepsilon(\lambda, T) \cdot \tau(\lambda) \cdot R(\lambda) \cdot L_{\lambda,b}(\lambda, T)\, d\lambda \qquad (3\text{-}7)$$

3.2 IR Image Sensors

3.2.1 320x244 IR CCD and 640x480 IR MOS Image Sensors

The radiometric analysis presented in this thesis is applied to the 320x244 IR CCD and 640x480 IR MOS image sensors (imagers) developed at the David Sarnoff Research Center. The IR detectors used in these imagers are

the PtSi Schottky-barrier detectors (SBDs) which are most sensitive to the radiation emitted in the SWIR (1 to 3 μm) and MWIR (3 to 5 μm) bands.

The 320x244 IR CCD imager has 40-μm x 40-μm pixels and a fill factor of 43%. This imager employs buried-channel CCD (BCCD) readout registers and has the pixel layout shown in Figure 4 [3]. The BCCD readout registers of this imager provide maximum charge handling capacity of $1.4x10^6$ electrons per pixel.

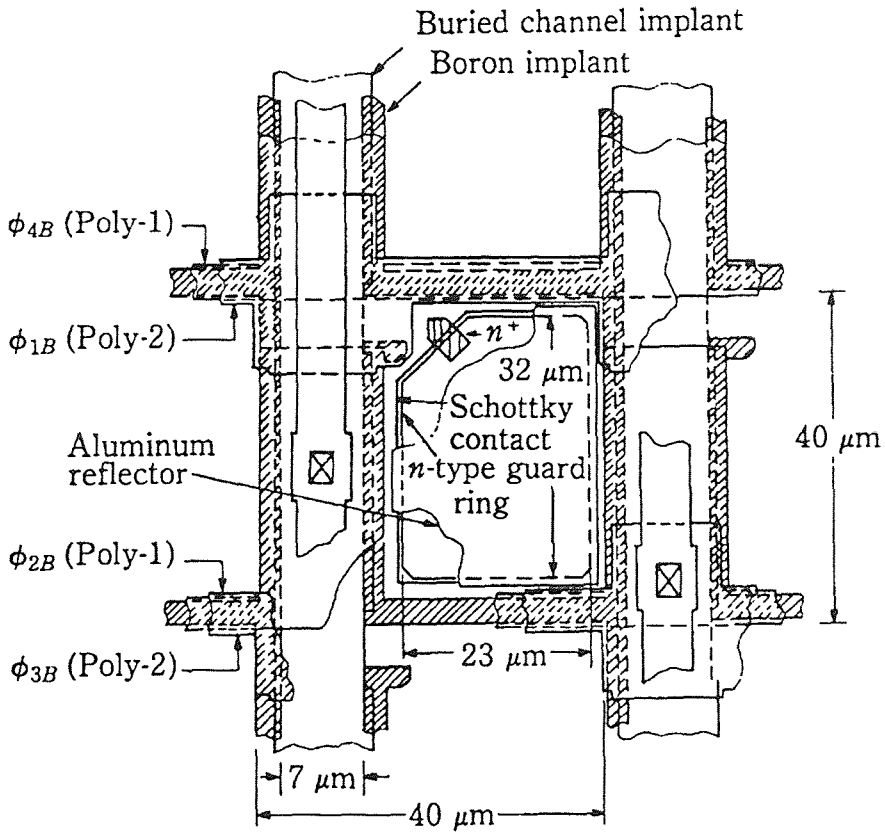

Figure 4 Pixel layout of Sarnoff 320x244 IR imager [3].

The 640x480 IR MOS imager has 24-μm x 24-μm pixel size and fill

factor of 38%. This imager has a low-noise X-Y addressable readout multiplexer with two MOS switches per SBD, and a MOS source follower at the output of each row with 8:1 multiplexing to a shared on-chip output amplifier. The readout noise of this device is under 300 rms electrons per pixel [3]. The readout structure of this imager is shown in Figure 5. Its saturation charge level is 1.5×10^6 electrons per pixel. It should also be noted that the Sarnoff 640x480 IR MOS imager can be operated with subframe imaging capability for any subframe size and location. In addition, this imager provides electronic integration time control down to a minimum of 60 μs for operation at 30 frames per second.

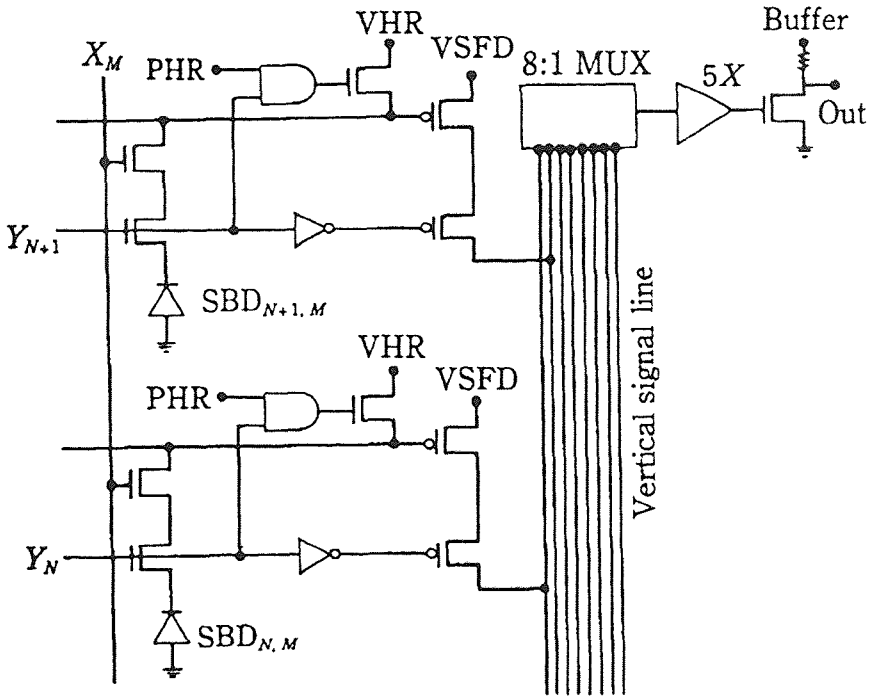

Figure 5 Low-noise MOS readout multiplexer of Sarnoff 640x480 IR MOS imager [3].

3.2.2 PtSi Schottky-Barrier Detector

Both IR imagers described in the previous section employ PtSi Schottky-barrier photon detectors. The basic construction and operation of PtSi SBD is illustrated in Figure 6.

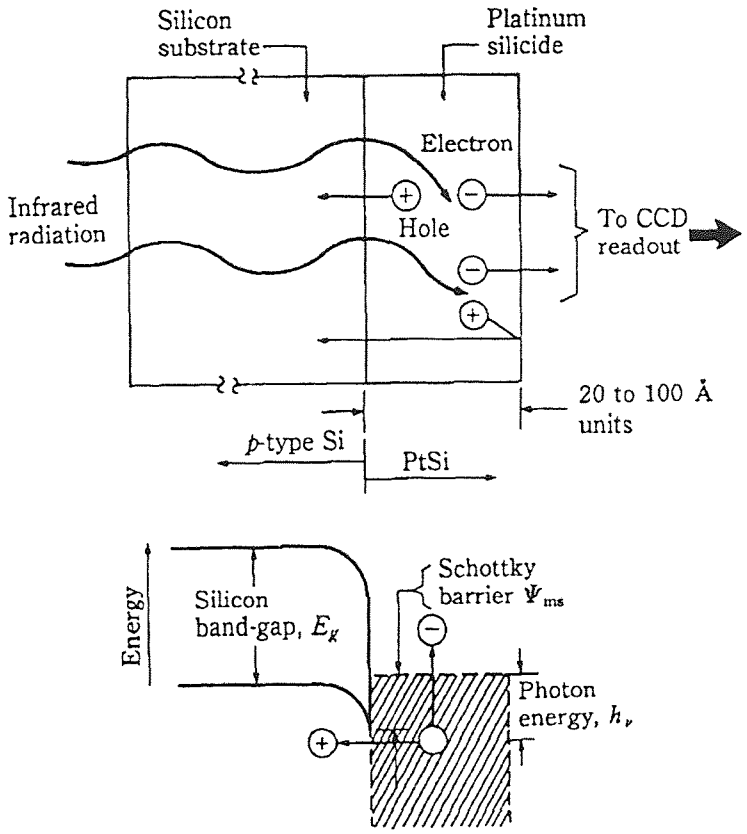

Figure 6 Operation of Schottky-barrier detector [3].

The infrared radiation with photon energy less than the bandgap of silicon (E_g=1.12 eV) is transmitted through the substrate. The absorption of the infrared radiation in the silicide layer results in the excitation of photocurrent across the Schottky-barrier (Ψ_{ms}) by internal photoemission.

The Schottky-barrier is the barrier that is formed between the silicide layer and the p-type silicon substrate. The absorbed IR photons excite the valence electrons above the Fermi level, generating hole-electron pairs. The holes with energy levels exceeding the Schottky-barrier are injected into the silicon substrate. The result of this process is the accumulation of negative charge on the silicon electrode. The detection of the optical signal is completed by transferring the negative charge from the silicide electrode into the readout structure.

The spectral responsivity $R(\lambda)$ of the IR imager depends on the quantum efficiency of the PtSi Schottky-barrier detectors and can be approximated by the Fowler equation [3] as

$$R(\lambda) = C_1\left(1 - \frac{\Psi_{ms} \cdot \lambda}{1.24}\right)^2 \qquad (3\text{-}8)$$

The spectral responsivity and quantum efficiency of the PtSi SBD array corresponding to C_1=0.124 eV^{-1} and Ψ_{ms}=0.2272 eV is shown in Figure 7.

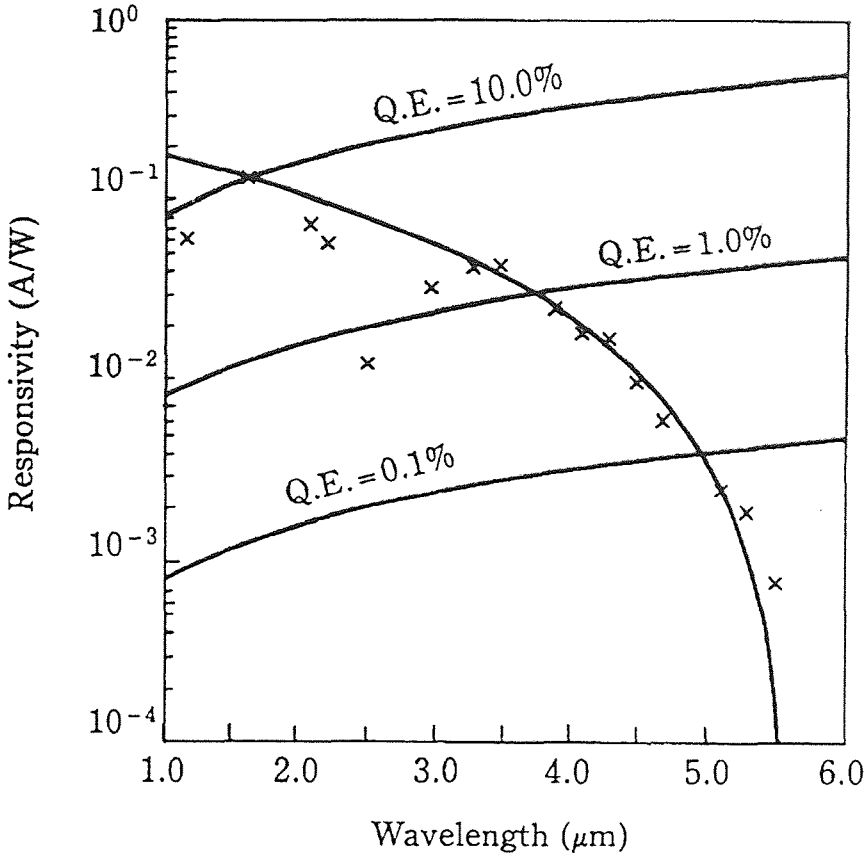

Figure 7 Measured responsivity of PtSi Schottky-Barrier detector array [3].

3.2.3 Radiometric Model of the IR Imager

In order to adapt the theory of the preceding section to the description of the IR CCD imager output signal we note that for targets sufficiently remote from the lens of the imager the solid angle given by Eq. (3-7) can be approximated as [4]

$$\omega_d \approx \frac{\pi}{4 \cdot (f/\#)^2} \tag{3-9}$$

Substituting Eq. (3-9) into Eq. (3-7) we obtain

$$S(T) = A_{d,n} \cdot \frac{\pi}{4 \cdot (f/\#)^2} \cdot \frac{t_i}{Q_{el}} \cdot \int_0^{\infty} \varepsilon(\lambda) \cdot \tau(\lambda) \cdot R(\lambda) \cdot L_{\lambda,b}(\lambda, T)\, d\lambda \quad (3\text{-}10)$$

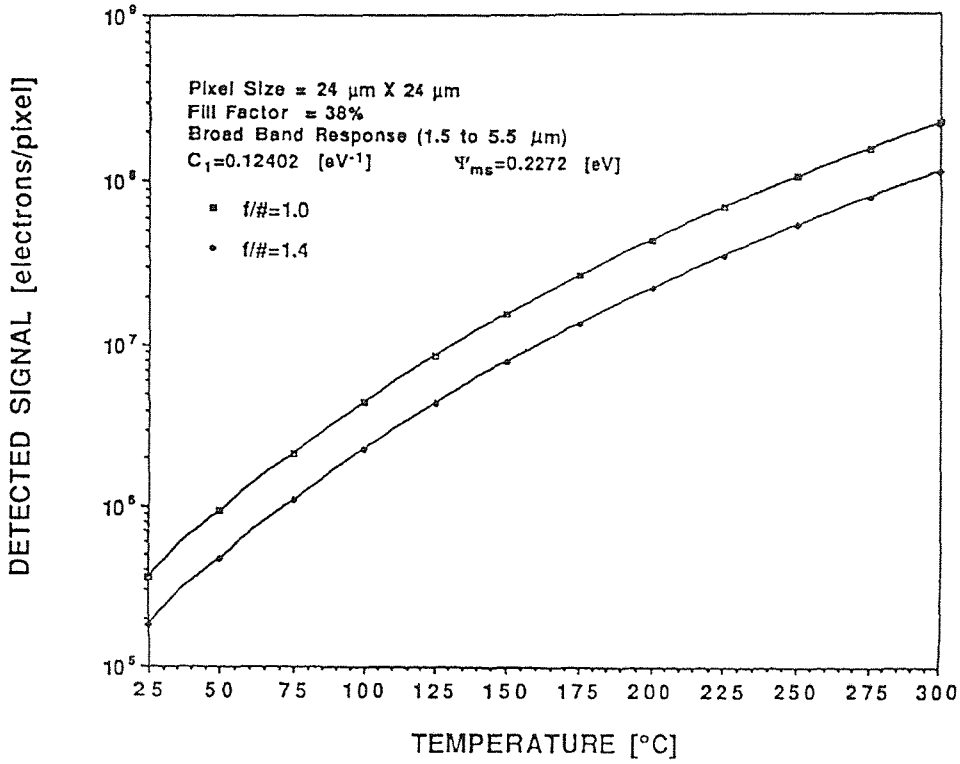

Figure 8 Total signal detected by 640x480 IR MOS imager operating at 30 frames per second with f/1.0 and f/1.4 optics.

At this point we can apply our analysis to the estimation of radiometric performance of the 640x480 IR imager developed at the David Sarnoff Research Center.

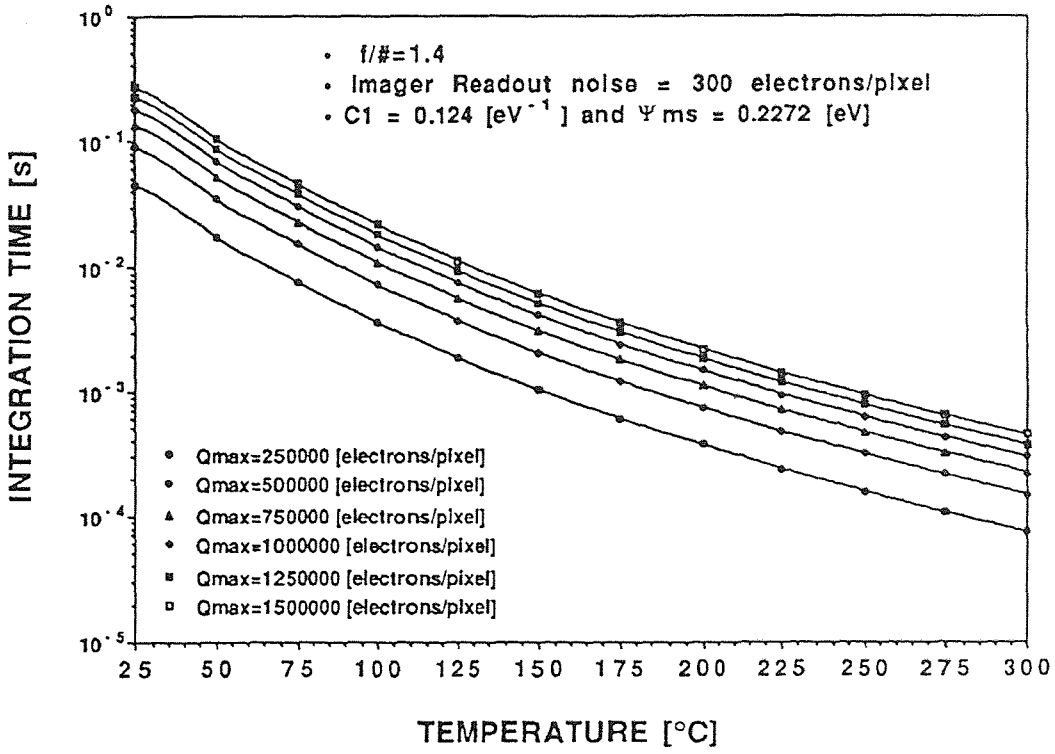

Figure 9 Calculated optical integration time of 640x480 IR MOS imager for detected signal of Qmax electrons per pixel.

The total detected signal for the 640x480 IR imager calculated from Eq. (3-10) is shown in Figure 8. These calculations assume that the pixel size of the imager is 24-μm x 24-μm, the fill factor is 38%, that it is operated at 30 frames per second, and is characterized by the spectral responsivity function given above.

Inspection of Figure 8 shows that for blackbody temperatures in excess of 50-75 °C, the signal exceeds the 10^6 electrons per pixel charge handling capacity of the imager (Q_{max}). In order to overcome this

limitation the signal should be limited by the control of optical integration time. This is illustrated in Figure 9. This Figure shows the integration times which should be used in order to maintain a prescribed signal level at different temperatures.

3.3 Accuracy of Wide-Band Temperature Measurements.

It can be shown from statistical considerations [5] that the process of photon emission from a radiant surface, i.e. the number of photons emitted per unit time per unit area of emitter surface, can be described by the Poisson distribution. The same is equally true for the process of photon detection by a photodetector. In other words, the probability of detecting x photons in the time interval Δt is given by

$$P(x,\mu) = \frac{\mu^x}{x!} \cdot e^{-\mu} \qquad (3\text{-}11)$$

where μ is the average number of photons detected in the interval Δt.

One of the fundamental properties of Poisson distribution is the fact that its standard deviation is equal to the square root of its mean. Applying this property to the process of photon detection by the radiation detector we conclude that rms radiation (shot) noise in the detected signal is equal to the square root of the signal itself.

Another source of noise in the output signal of the imager is the rms readout noise connected to the mechanism of sensing the accumulated charge in the detector by the capacitor. The readout noise is considered to be independent of the radiation shot noise and has been estimated to be 300 electrons per pixel for the IR 640x480 MOS imager. Therefore, the total noise in the imager output can be expressed as

$$\Delta S_{noise} = \sqrt{N^2_{readout} + S(\lambda, T)} \tag{3-12}$$

If the emissivity of the target is known, Eq. (3-10) can be solved numerically for target temperature, T, as a function of measured imager output signal S(T). The accuracy of the temperature measurement in this case will be limited by the noise in the output signal, ΔS_{noise}, and is referred to as noise equivalent temperature NEΔT. Using Eq. (3-12) we can express NEΔT as

$$S(T + NE\Delta T) - S(T) = \sqrt{N^2_{readout} + S(\lambda, T)} \tag{3-13}$$

Considering the first order terms in a Taylor's series expansion of S(T) and using Eq. (3-13) we can express NEΔT as

$$NE\Delta T(T) = \frac{\sqrt{N^2_{readout} + S(\lambda, T)}}{\frac{dS(\lambda, T)}{dT}} \tag{3-14}$$

In order to obtain the partial derivative of the signal with respect to temperature, we note that the only temperature dependent term in Eq. (3-10) is the blackbody spectral radiance, $L_{\lambda,b}$, therefore

$$\frac{dS(T)}{dT} = A_{d,n} \cdot \frac{\pi}{4 \cdot (f/\#)^2} \cdot \frac{t_i}{Q_{el}} \cdot \int_0^{\infty} R(\lambda) \cdot \left(\frac{dL_{\lambda,b}(\lambda, T)}{dT} \right) d\lambda \quad (3\text{-}15)$$

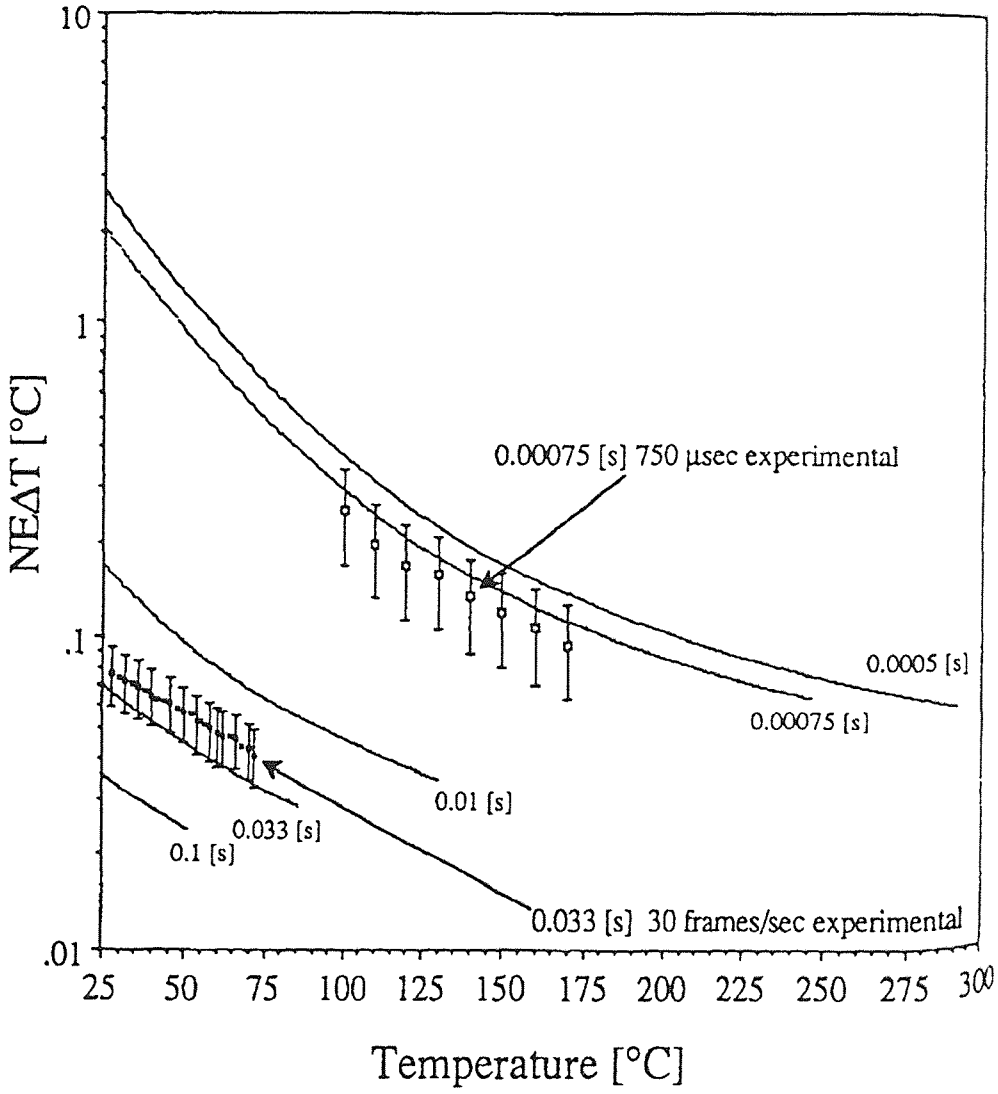

Figure 10 Calculated NEΔT of 640x480 IR MOS imager with f/1.4 optics.

The derivative of Planck's equation with respect to temperature is

$$\frac{dL_{\lambda,b}(\lambda,T)}{dT} = \frac{C_1 \cdot C_2 \cdot e^{\left(\frac{C_2}{\lambda T}\right)}}{\lambda^6 \cdot T^2 \cdot \left(e^{\left(\frac{C_2}{\lambda T}\right)} - 1\right)^2} \qquad (3\text{-}16)$$

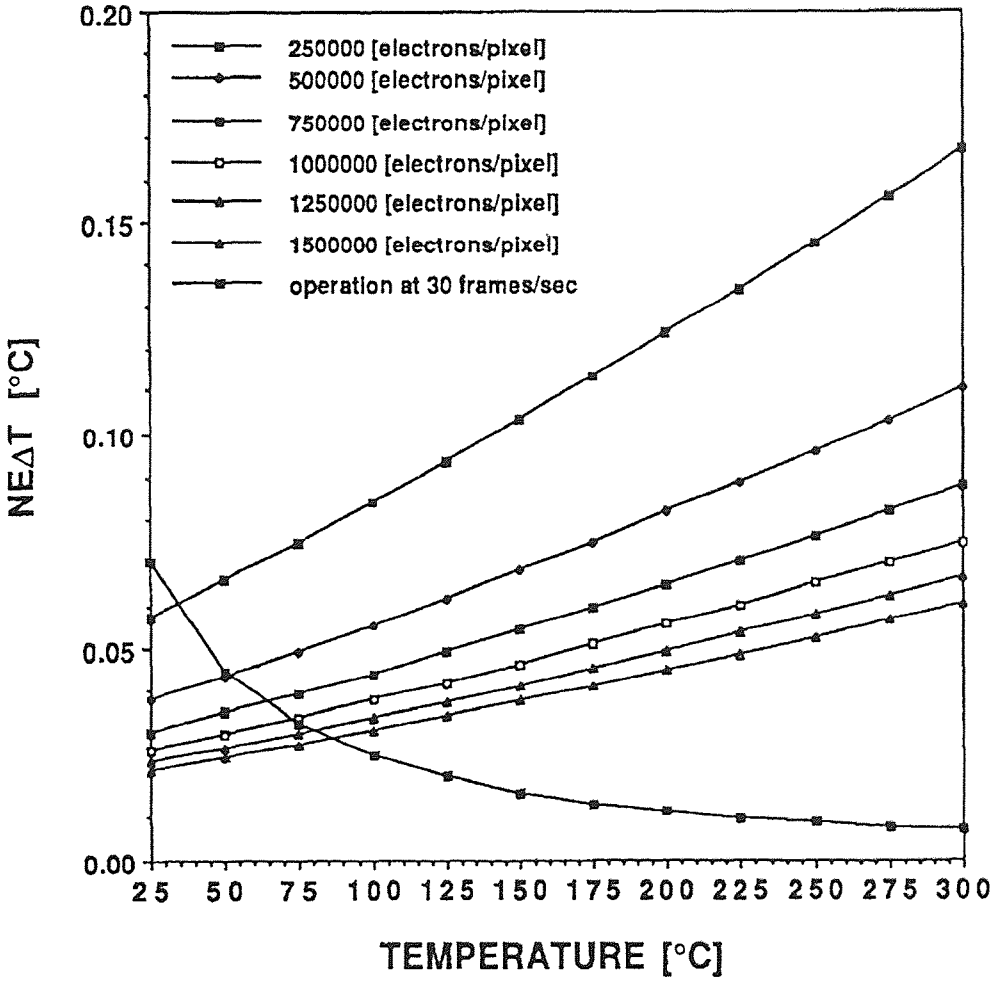

Figure 11 Calculated NEΔT of 640x480 IR MOS imager with f/1.4 optics for detected signal of Qmax electrons per pixel.

By the substitution of Eqs. (2-3) and (3-16) into Eq. (3-15) and (3-14) and performing the numerical integration we can evaluate NEΔT for any given value of the optical integration time t_i, and radiant target temperature T. The values computed from Eq. (3-14) along with the experimentally obtained ones of NEΔT for 640x480 IR MOS imager for different optical integration times and target temperatures are shown in Figure 10. Each curve in this Figure is shown only up to the point where the signal level reaches the maximum charge handling capacity of the imager ($Q_{max} = 1.5 \times 10^6$ electrons per pixel). The values of NEΔT resulting from the operation of the IR imager with constant signal level are shown in Figure 11.

3.4 Single Wavelength Radiometry

The wideband radiometric temperature measurements described in the previous section have the advantage of achieving high signal-to-noise ratio even for relatively low temperatures of radiant target. However, at the elevated target temperatures the signal level has to be limited by decreasing the optical integration time in order to keep the signal below the maximum charge handling capacity of the detector. Inspection of Figure 10 shows that even for the moderate target temperature of 300 °C the integration time of the IR imager should be less than 0.5 ms.

In addition to the control of the optical integration time the signal level can also be limited by the use of the narrow passband filter positioned between the target and the detector. This approach (referred to as monochromatic or single wavelength radiometry) is especially attractive because it does not require the knowledge of total emissivity. Instead, the spectral emissivity within the passband of the filter or even just at its center wavelength is being used.

Eq. (3-10) developed in section 3.2 is applicable to the case of single wavelength radiometry. The temperature of the radiant target can be inferred from the detected signal by solving Eq. (3-10) for temperature, T. However, for real time on-line temperature measurements the iterative nature of the numerical solution of Eq. (3-10) is undesirable. In fact, for sufficiently narrow filters the spectral emissivity of the target and the spectral responsivity of the detector can be described within the passband of the filter by a continuous smooth function of wavelength. In such cases, the analytical solution of Eq. (3-10) can be obtained.

3.4.1 Reference Wavelength Approach

A number of methods designed to provide an approximate analytical solution of Eq. (3-10) have been described in the radiometric literature [6,7] One of these methods, the technique developed by Coates [6] provides very high accuracy for the solution when the fractional bandwidth of the

filter, $\Delta\lambda/\lambda$, is less then 0.1. It should be noted that this technique, known as *reference wavelength* method, in addition to high accuracy and ease of interpretation, provides the means to account for the variation of spectral emissivity across the passband of the filter. The discussion presented here follows the development by Coates [6].

This *reference wavelength* method is based on the description of the spectral transmission of a narrow-bandpass filter in terms of the moments of its spectral transmittance $\tau(\lambda)$ about the mean wavelength of the filter, λ_o. The n^{th} moment of the transmittance, a_n, is defined by

$$\int_0^\infty (\lambda - \lambda_o)^n \cdot \tau(\lambda) d\lambda = a_n \cdot \tau(\lambda_o) \cdot (\Delta\lambda)^{n+1} \qquad (3\text{-}17)$$

where $\Delta\lambda$ - is the bandwidth of the filter at half of its peak transmittance.

At this point it should be noted that the moments reflect the shape of the filter and are independent of the peak transmission t_o and the filter width $\Delta\lambda$. Since the reference wavelength λ_o is taken as the mean wavelength of the filter, the first moment, a_1, is zero by definition.

The output signal of the IR imager viewing radiant target with temperature T and spectral emissivity $\varepsilon(\lambda)$ is given by Eq. (3-10) reproduced here for convenience

$$S(T) = A_{d,n} \cdot \frac{\pi}{4 \cdot (f/\#)^2} \cdot \frac{t_i}{Q_{el}} \cdot \int_0^\infty \varepsilon(\lambda) \cdot \tau(\lambda) \cdot R(\lambda) \cdot L_{\lambda,b}(\lambda, T)\, d\lambda \qquad (3\text{-}10)$$

This signal can be described to a good first approximation by

$$S_o(T) = A_{d,n} \cdot \omega_d \cdot a_o \cdot \tau(\lambda_o) \cdot \Delta\lambda \cdot R(\lambda_o) \cdot \varepsilon(\lambda_o) \cdot L_{\lambda,b}(\lambda_o, T) \quad (3\text{-}18)$$

where the factor a_o has been included to make the product $a_o\tau(\lambda_o)\Delta\lambda$ equal to the area under the $\tau(\lambda)$ curve. We now define the correction factor C(T) as

$$C(T) = \frac{S(T)}{S_o(T)} = \int_0^\infty \frac{\tau(\lambda)}{a_o\tau(\lambda_o)\Delta\lambda} \cdot \frac{R(\lambda)}{R(\lambda_o)} \cdot \frac{\varepsilon(\lambda)}{\varepsilon(\lambda_o)} \cdot \frac{L_{\lambda,b}(\lambda, T)}{L_{\lambda,b}(\lambda_o, T)} \cdot d\lambda \quad (3\text{-}19)$$

Once the correction factor C(T) has been determined, the signal S(T) can be obtained from the computed signal $S_o(T)$. Each of factors in the integrand, except that involving the filter transmission, is now expanded in a Taylor series about reference wavelength λ_o

$$\frac{R(\lambda)}{R(\lambda_o)} = 1 + r_1 \cdot (\lambda - \lambda_o) + r_2 \cdot (\lambda - \lambda_o)^2 + \ldots \quad (3\text{-}20)$$

$$\frac{\varepsilon(\lambda)}{\varepsilon(\lambda_o)} = 1 + \varepsilon_1 \cdot (\lambda - \lambda_o) + \varepsilon_2 \cdot (\lambda - \lambda_o)^2 + \ldots \quad (3\text{-}21)$$

and

$$\frac{L_{\lambda,b}(\lambda,T)}{L_{\lambda,b}(\lambda_o,T)} = 1 + L_1 \cdot (\lambda - \lambda_o) + L_2 \cdot (\lambda - \lambda_o)^2 + \ldots \qquad (3\text{-}22)$$

where

$$r_n = \frac{1}{n! R(\lambda_o)} \cdot \frac{d^n R(\lambda)}{d\lambda^n} \qquad (3\text{-}23)$$

$$\varepsilon_n = \frac{1}{n! \varepsilon(\lambda_o)} \cdot \frac{d^n \varepsilon(\lambda)}{d\lambda^n} \qquad (3\text{-}24)$$

and

$$L_n(T) = \frac{1}{n! L_{\lambda,b}(\lambda_o,T)} \cdot \frac{d^n L_{\lambda,b}(\lambda,T)}{d\lambda^n} \qquad (3\text{-}25)$$

Expressions for $L_1(T)$ and $L_2(T)$ can be obtained by differentiating the Plank's distribution function to find

$$\lambda_o \cdot L_1(T) = \frac{x e^x}{(e^x - 1)} - 5 \qquad (3\text{-}26)$$

$$\lambda_o^2 \cdot L_2(T) = \frac{x^2 e^x}{(e^x - 1)^2} + \frac{\left[(x^2/2) - 6x\right] \cdot e^x}{(e^x - 1)} + 15 \qquad (3\text{-}27)$$

where

$$x = \frac{C_2}{\lambda_o T} \qquad (3\text{-}28)$$

The computations performed for Gaussian filter with fractional bandwidth $\Delta\lambda/\lambda_o$=0.05 and target temperatures between 100 °C and 1000 °C show that $L_3(T)$ and $L_4(T)$ enter only those terms of C(T) which constitute less than 0.49% of its absolute value. Therefore, $L_3(T)$ and $L_4(T)$ can be sufficiently accurately evaluated by using Wien's law

$$\lambda_o^3 \cdot L_3(T) = \frac{x^3}{6} - \frac{7x^2}{2} + 21x - 35 \qquad (3\text{-}29)$$

$$\lambda_o^4 \cdot L_4(T) = \frac{x^4}{24} - \frac{4x^3}{3} + 14x^2 - 56x + 70 \qquad (3\text{-}30)$$

The Eqs. (3-23) through (3-30) are now substituted into Eqs. (3-20), (3-21), and (3-22), and those expressions are substituted in turn into Eq. (3-19). After the substitution is performed the coefficients of each order of the terms $[(\lambda\text{-}\lambda_o)/\lambda_o]^n$ are collected. Designating the sum of the coefficients of the term of degree n as $\Sigma_n(T)$ we can express the correction factor as

$$C(T) = 1 + \Sigma_1(T)\int_0^\infty \frac{(\lambda-\lambda_o)\tau(\lambda)d\lambda}{a_o\tau(\lambda_o)\lambda_o\Delta\lambda} + \Sigma_2(T)\int_0^\infty \frac{(\lambda-\lambda_o)^2\tau(\lambda)d\lambda}{a_o\tau(\lambda_o)\lambda_o^2\Delta\lambda} + \ldots \qquad (3\text{-}31)$$

Substituting from Eq. (3-17) into Eq. (3-31) we obtain

$$C(T) = 1 + \Sigma_2(T) \cdot A_2 \cdot \left(\frac{\Delta\lambda}{\lambda_o}\right)^2 + \ldots + \Sigma_n(T) \cdot A_n \cdot \left(\frac{\Delta\lambda}{\lambda_o}\right)^n + \ldots \qquad (3\text{-}32)$$

where $A_n = a_n/a_o$ and $A_1 = 0$ since $a_1 = 0$ by definition.

In most practical cases [6] $\varepsilon(\lambda)$ and $R(\lambda)$ change relatively slow across the passband of the filter and can be accurately represented by the first three terms in Eqs. (3-20) and (3-21). Under these conditions the expressions for $\Sigma_n(T)$ up to $\Sigma_4(T)$ are found to be as follows

$$\Sigma_1(T) = \lambda_o\left[L_1(T) + (r_1 + \varepsilon_1)\right] \qquad (3\text{-}33)$$

$$\Sigma_2(T) = \lambda_o^2 \cdot \left[L_2(T) + (r_1 + \varepsilon_1) \cdot L_1(T) + (r_2 + r_1\varepsilon_1 + \varepsilon_2)\right] \qquad (3\text{-}34)$$

$$\Sigma_3(T) = \lambda_o^3 \cdot \left[L_3(T) + (r_1 + \varepsilon_1) \cdot L_2(T) + (r_2 + r_1\varepsilon_1 + \varepsilon_2) \cdot L_1(T) + (r_3 + r_2\varepsilon_1 + r_1\varepsilon_2 + \varepsilon_3)\right] \qquad (3\text{-}35)$$

$$\Sigma_4(T) = \lambda_o^4 \cdot \left[L_4(T) + (r_1 + \varepsilon_1) \cdot L_3(T) + (r_2 + r_1\varepsilon_1 + \varepsilon_2) \cdot L_2(T) + (r_3 + r_2\varepsilon_1 + r_1\varepsilon_2 + \varepsilon_3) \cdot L_1(T) + (r_4 + r_3\varepsilon_1 + r_2\varepsilon_2 + r_2\varepsilon_3 + \varepsilon_4)\right] \qquad (3\text{-}36)$$

Moments up to A_4 have been computed by numerical integration for several transmission curves of interest and are given in Figure 12. It may

be noted that in the case of symmetrical filters, An is zero for odd values of n. Therefore, for symmetrical filters with moderate bandwidths, the third term in Eq. (3-32) is zero. For filters with $\Delta\lambda/\lambda_0<0.1$ the fourth term in Eq. (3-32) is at least two orders of magnitude smaller than the second term. In this case the correction factor C(T) can be approximated by

$$C(T)=1+\Sigma_2(T)\cdot A_2\cdot\left(\frac{\Delta\lambda}{\lambda_0}\right)^2 \tag{3-37}$$

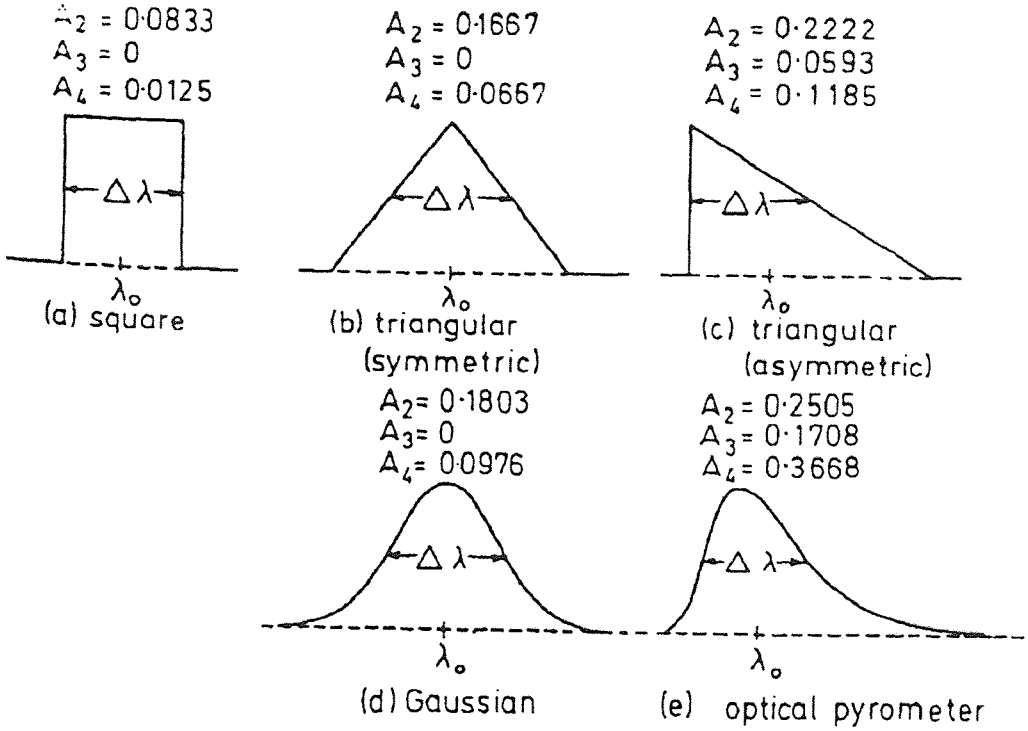

Figure 12 Normalized moments of various filters [6].

Substituting C(T) from Eq. (3-37) into Eq. (3-19) we obtain the expression for the output signal of the imager viewing the radiant surface

through the narrow-passband filter

$$S(T) = A_{d,n} \cdot \omega_d \cdot a_o \cdot \tau(\lambda_o) \cdot \Delta\lambda \cdot R(\lambda_o) \cdot \varepsilon(\lambda_o) \times \\ \times \left[1 + \Sigma_2(T) \cdot A_2 \cdot \left(\frac{\Delta\lambda}{\lambda_o} \right)^2 \right] \cdot L_{\lambda,b}(\lambda_o, T) \tag{3-38}$$

In order to further simplify the expression (3-38) we define the filter shape factor $K(\lambda_O,T)$ as

$$K(\lambda, T) = A_{d,n} \cdot \omega_d \cdot a_o \cdot \tau(\lambda_o) \cdot \Delta\lambda \cdot \left[1 + \Sigma_2(T) \cdot A_2 \cdot \left(\frac{\Delta\lambda}{\lambda_o} \right)^2 \right] = \\ = G \cdot \left[1 + \Sigma_2(T) \cdot A_2 \cdot \left(\frac{\Delta\lambda}{\lambda_o} \right)^2 \right] \tag{3-39}$$

where the geometric factor G is given by

$$G = A_{d,n} \cdot \omega_d \cdot a_o \cdot \tau(\lambda_o) \cdot \Delta\lambda \tag{3-40}$$

Finally, substituting Eq. (3-39) into Eq.(3-38) we obtain the simplified expression for the output signal of the imager

$$S(\lambda, T) = K(\lambda, T) \cdot \varepsilon(\lambda) \cdot R(\lambda) \cdot L_{\lambda,b}(\lambda, T) \tag{3-41}$$

The accuracy of Eq. (3-38) was verified experimentally by measuring the output signal of a 320x244 IR CCD Camera viewing the blackbody radiator through the filter with various mean wavelengths. The blackbody had the aperture of 0.2 inches in diameter and was positioned 18 inches in front of the camera with lens of objective removed. The experimental values of the signal along with the theoretical results based on (3-38) are shown in Figure 13. Inspection of the Figure 13 shows that there is good agreement between theoretical and experimental data. Nevertheless, slight discrepancies between model and experiment dictate the need for accurate filter and detector calibration which will be discussed in Section 3.4.3.

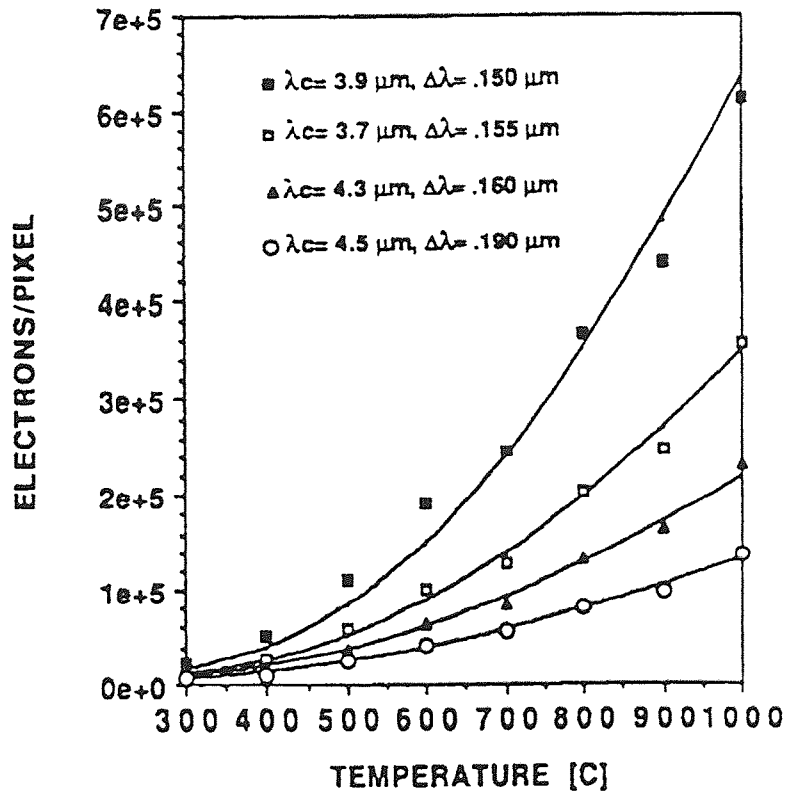

Figure 13 Calculated and measured signal of 320x244 IR-CCD imager without lens.

The values of the output signal calculated from (3-38) for 320x244 IR CCD camera operating with optical integration time of 33 ms, f/2 optics, and 500-nm-wide Gaussian filter having 60% peak transmission are shown in Figure 14. The output signal of the same imager viewing the blackbody radiator through a 20-nm-wide Gaussian filter was calculated for a broad range of temperatures and is shown in Figure 15.

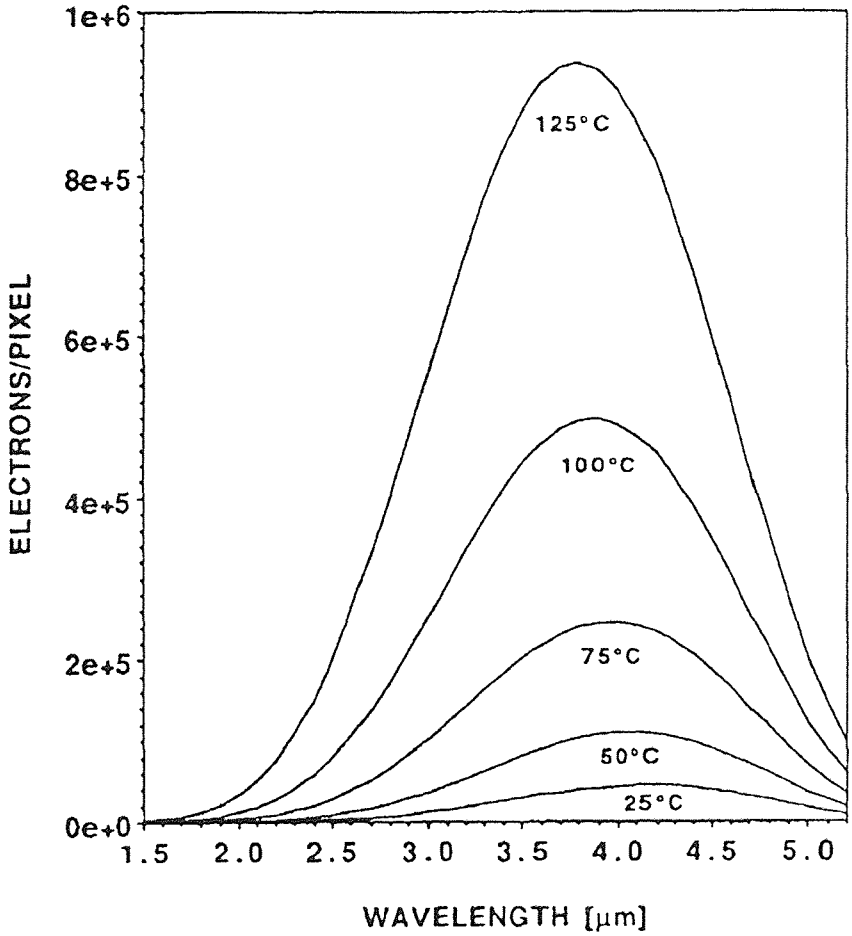

Figure 14 Calculated and measured signal of 320x244 IR-CCD imager operating with optical integration time of 33 ms, f/2 optics and 500-nm Gaussian filter with 60% peak of transmission.

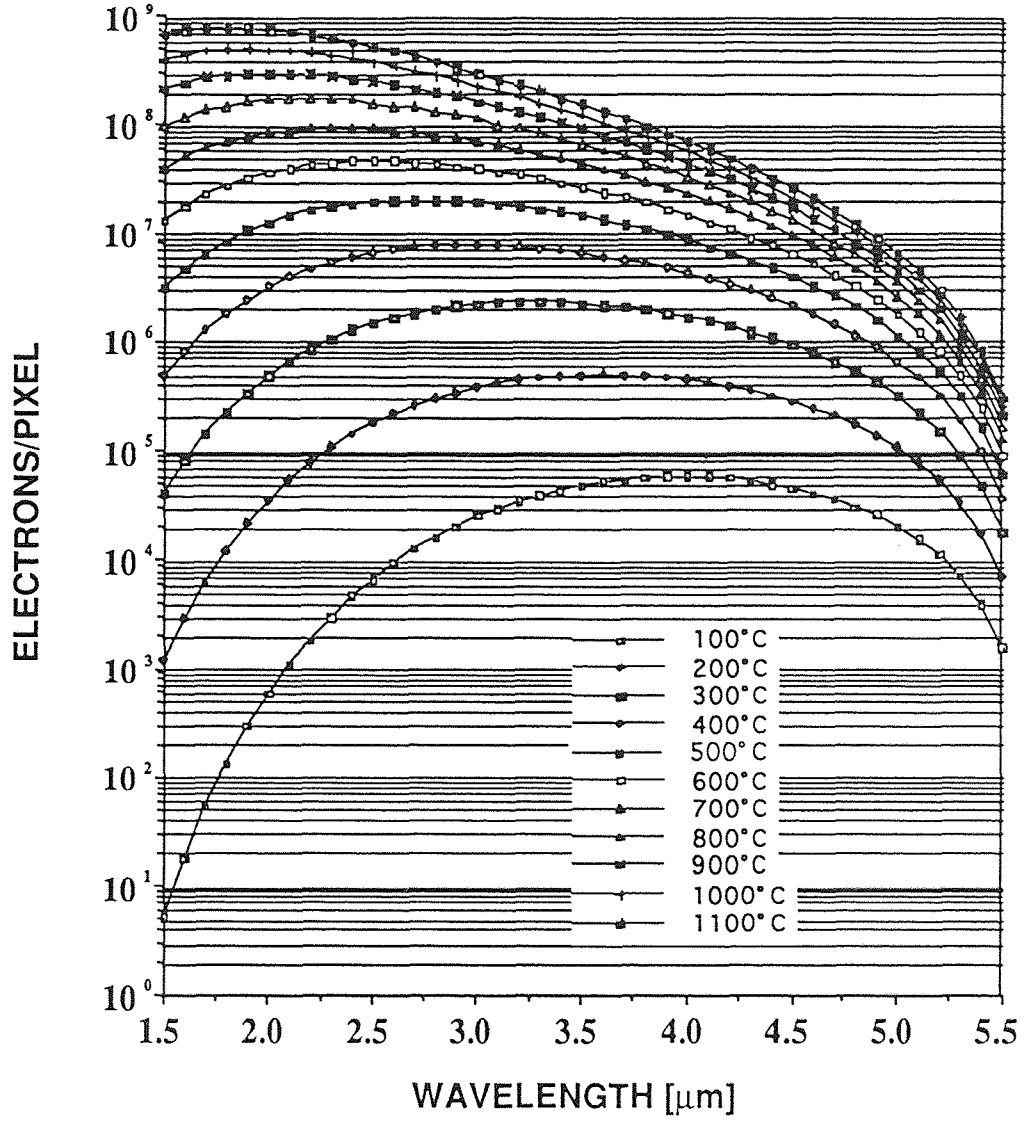

Figure 15 Calculated and measured signal of 320x244 IR-CCD imager operating with optical integration time of 33 ms, f/2 optics and 20-nm Gaussian filter with 60% peak of transmission.

3.4.2 Accuracy of Narrow-Band Radiometry

The general expression for the noise equivalent temperature (NEΔT) developed in section 3.3 can also be used in the case of narrow bandwidth

radiometry. Moreover, the noise equivalent temperature can be directly calculated from Eq. (3-17) provided the integrand of this expression is multiplied by the spectral transmittance, $\tau(\lambda)$, of the filter under consideration. However, the reference wavelength approach, introduced in the previous section, allows us to develop an expression for NEΔT which does not require numerical integration. It should be noted that the expressions developed in this section will also be used in the accuracy analysis of multi wavelength radiometry described in Section 5.

3.4.2.1 Noise Equivalent Temperature We will start this section with the application of the reference wavelength technique to the development of the analytical expression for the partial derivative of the IR imager output signal with respect to temperature. Similarly to Eqs. (3-23)-(3-25) let us define the normalized derivative of the blackbody spectral radiance with respect to temperature as

$$L_T = \frac{1}{L_{\lambda,b}(\lambda_o, T)} \cdot \frac{dL_{\lambda,b}(\lambda, T)}{dT} = \frac{x e^x}{T\left(e^x - 1\right)} \qquad (3\text{-}42)$$

where x is given by Eq. (3-28).

We will also define relative derivative of the filter shape factor $K(\lambda,T)$

with respect to temperature as

$$K_T = \frac{1}{K(\lambda,T)} \cdot \frac{dK(\lambda,T)}{dT} \tag{3-43}$$

where dK/dT can be evaluated by differentiating Eq. (3-39) as

$$\frac{dK(\lambda,T)}{dT} = G \cdot A_2 \cdot \left(\frac{\Delta\lambda}{\lambda_o}\right)^2 \frac{d\Sigma_2(T)}{dT} \tag{3-44}$$

In turn, the expression for $d\Sigma_2(T)/dT$ may be obtained by differentiating Eq. (3-34) to find

$$\frac{d\Sigma_2(T)}{dT} = \lambda_o^2 \cdot \left[\frac{dL_2(T)}{dT} + (r_1 + \varepsilon_1) \cdot \frac{dL_1(T)}{dT}\right] \tag{3-45}$$

where L_1, L_2, r_1 and ε_1 are defined in (3-23)-(3-25).

The values of dL_1/dT and dL_2/dT can be evaluated based on Wien's approximation

$$\frac{dL_1(T)}{dT} = \frac{x^2 e^x}{C_2\left(e^x - 1\right)} \cdot \left[\frac{x}{\left(e^x - 1\right)} - 1\right] \tag{3-46}$$

and

$$\frac{dL_2(T)}{dT} = \frac{x}{\lambda^2 T} \cdot [6 - x] \tag{3-47}$$

Finally, we note that ε_1 defined in Eq. (3-24) is equal to zero for blackbody radiator and r_1 can be estimated by performing the substitution from Eq. (3-8) into Eq. (3-23) as

$$r_1 = -\frac{2\Psi_{ms}}{1.24} \cdot \sqrt{\frac{C}{R(\lambda)}} \tag{3-48}$$

At this point we can use Eqs. (3-42) and (3-43) in order to write the partial derivative of the signal expression given by Eq. (3-41) with respect to temperature as follows

$$\begin{aligned} \frac{dS(\lambda,T)}{dT} &= \frac{K(\lambda,T)}{dT} \cdot \varepsilon(\lambda) \cdot R(\lambda) \cdot L_{\lambda,b}(\lambda,T) + \\ &+ K(\lambda,T) \cdot \varepsilon(\lambda) \cdot R(\lambda) \cdot \frac{L_{\lambda,b}(\lambda,T)}{dT} = \\ &= S(\lambda,T) \cdot [K_T + L_T] \end{aligned} \tag{3-49}$$

The expression for NEΔT can now be obtained by substitution of Eq. (3-49) into Eq. (3-14). In the case of shot noise limited mode of

operation (also referred to as BLIP) we have

$$NE\Delta T = \frac{1}{\sqrt{S(\lambda,T)}\cdot[K_T + L_T]} \tag{3-50}$$

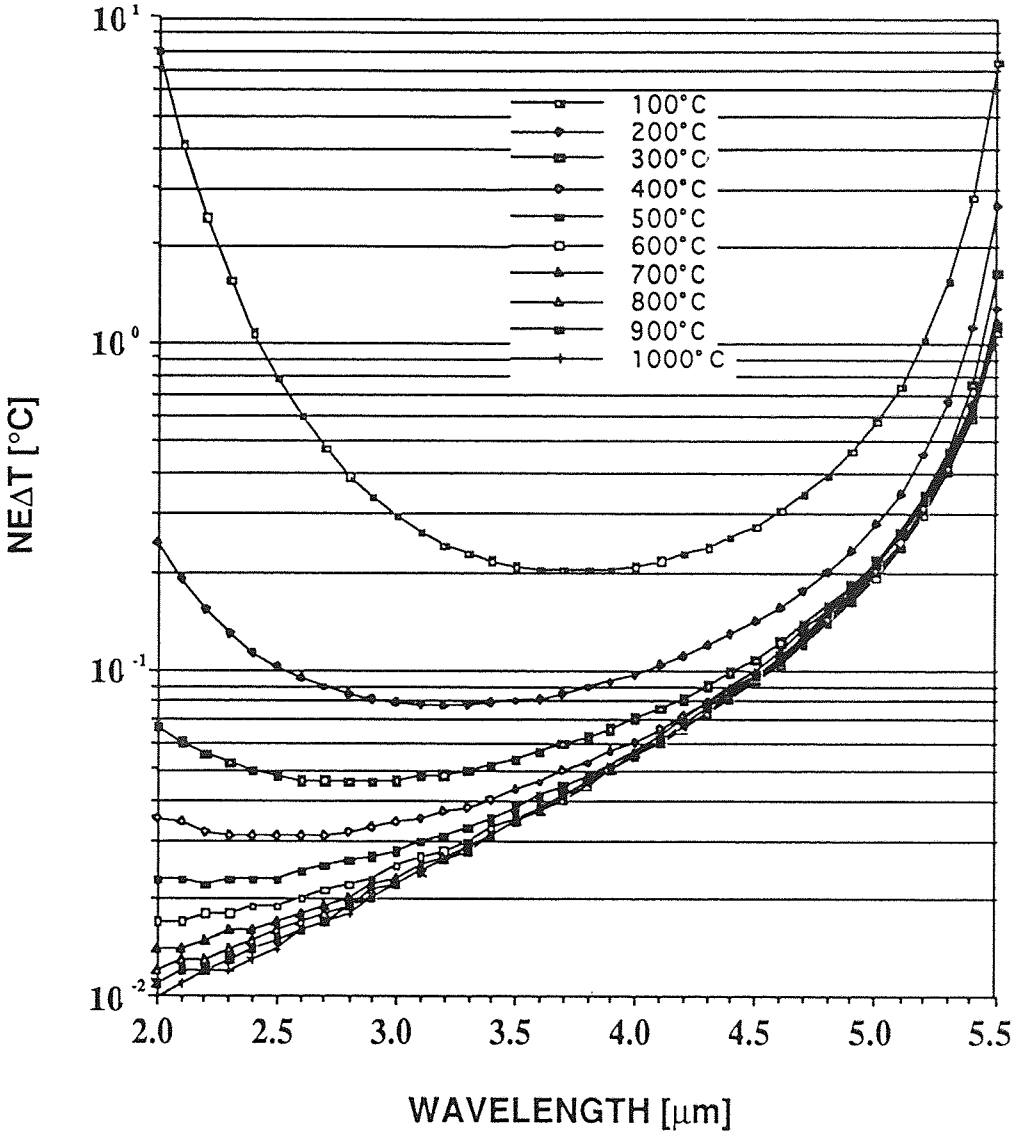

Figure 16 Calculated and measured signal of 320x244 IR-CCD imager operating with optical integration time of 33 ms, f/2 optics and 20-nm Gaussian filter with 60% peak of transmission.

The values of NEΔT calculated from Eq. (3-50) for 320x244 IR CCD camera operating with optical integration time of 33 ms, f/2 optics, and 20-nm-wide Gaussian filter having 60% peak transmission are shown in Figure 16. It should be noted, however, that these calculations were performed with the assumption of unlimited charge handling capacity. Therefore, the values of NEΔT shown in Figure 16 are not realizable in practice for elevated temperatures of the radiant target. The values of NEΔT achievable by the imager with the maximum charge handling capacity of 10^6 electrons per pixel are shown in Figure 17, discussed in the next section.

3.4.2.2 Effects of an Inaccurate Filter Specification In radiometric measurements the temperature of the target is inferred from the signal detected by the photodetector viewing the radiant surface. Therefore, any source of uncertainty in the value of the detected signal will have an effect on the accuracy of the measured temperature. In the analysis given in the preceding sections it was assumed that the only uncertainties in the level of the detected signal are those that can be attributed to the radiation shot noise and the rms readout noise of the detector. However, in the case of the detector viewing the radiant target through the narrow passband filter, any inaccuracy in the description of the filter

transmittance, $\tau(\lambda)$, will contribute to the uncertainty in the detected signal and, therefore, will affect the accuracy of the temperature measurement.

In this analysis we will assume that the filter can be represented by the shape of its transmission curve, the area under the transmission curve, and the value of the peak wavelength (considering only single-peak filters for clarity). In this section we will consider the consequences of the error in the measurement of the effective center wavelength of the filter as well as the inaccuracy in the description of its shape. The effect of inaccuracy in the specification of the area under the transmission curve is indistinguishable from an error in the determination of the spectral emissivity of the target and will be treated in Chapter 5.

The inaccuracy in the detected signal due to the error in specification of the peak wavelength of the filter, $\delta\lambda$, can be expressed as

$$\Delta S = \frac{d\,S(\lambda,T)}{d\,\lambda}\cdot\delta\lambda \qquad (3\text{-}51)$$

where the partial derivative is evaluated at peak wavelength.

In order to evaluate the partial derivative of the detected signal $S(\lambda,T)$ with respect to wavelength we will again employ the reference wavelength approach described in Section 3.4.1. Proceeding in much the same way as in the previous section we define the relative partial derivative of the filter

shape factor $K(\lambda,T)$ with respect to wavelength as

$$K_1 = \frac{1}{K(\lambda,T)} \cdot \frac{dK(\lambda,T)}{d\lambda} \tag{3-52}$$

where $dK/\Delta\lambda$ can be evaluated by differentiating Eq. (3-39) as

$$\frac{dK(\lambda,T)}{d\lambda} = G \cdot A_2 \cdot \left(\frac{\Delta\lambda}{\lambda_o}\right)^2 \left[\frac{d\Sigma_2(\lambda,T)}{d\lambda} - \frac{2}{\lambda} \cdot \Sigma_2(\lambda,T)\right] \tag{3-53}$$

In turn, expression for $d\Sigma_2(T)/d\lambda$ can be obtained by differentiating Eq. (4-34)

$$\begin{aligned}\frac{d\Sigma_2}{d\lambda} = \frac{2\cdot\Sigma_2}{\lambda} + \lambda^2 \cdot \left[3L_3 - L_1 \cdot L_2 + \left(2r_2 - r_1^2 - \varepsilon_1^2\right)\cdot L_1 + \right. \\ \left. + (r_1 + \varepsilon_1)\cdot\left(2L_1 - L_2^2\right) + \varepsilon_1 \cdot \left(2r_2 - r_1^2\right) - \varepsilon_1^2 \cdot r_1\right]\end{aligned} \tag{3-54}$$

where L_1, L_2, r_1, r_2 and ε_1 are defined in Eqs. (3-23)-(3-25).

We note that ε_1 defined in Eq. (3-24) is equal to zero for a blackbody radiator, r_1 is given by Eq. (3-48), and r_2 can be estimated by performing the substitution from Eq. (3-8) into Eq. (3-23) as

$$r_2 = \frac{1}{2R(\lambda)} \cdot \frac{2\cdot C\cdot \Psi_{ms}^2}{(1.24)^2} \tag{3-55}$$

At this point we can use Eqs. (3-23), (3-26), (3-48) and (3-52) in order to obtain the partial derivative of the signal given by Eq. (3-41) with respect to wavelength as follows

$$\frac{dS(\lambda,T)}{d\lambda} = S(\lambda,T)\cdot\left[\varepsilon_1 + K_1 + r_1 + L_1\right] \tag{3-56}$$

Now we can write the expression for NEΔT which would take into account not only the radiation shot noise and the rms detector readout noise but also the "noise" produced by the error in specification of the effective center wavelength of the filter. Substituting Eqs. (3-49), (3-51), and (3-56) into Eq. (3-14) and treating all noise sources as being independent of each other, we have

$$NE\Delta T = \frac{\sqrt{S(\lambda,T) + N_{readout}^2 + \left(\frac{dS(\lambda,T)}{d\lambda}\cdot\delta\lambda\right)^2}}{\frac{dS(\lambda,T)}{dT}} \tag{3-57}$$

The values of NEΔT computed from Eq. (3-57) for the case of precise knowledge of the peak wavelength of the filter as well as for the case where 5-nm error has been made are shown in Figure 17. These computations were performed for IR CCD MOS imager viewing the blackbody radiator through a 100-nm-wide Gaussian filter. It should also be pointed out that these computations assume that by adjusting the optical

integration time the signal level was kept at 10^6 electrons per pixel for each simulated measurement. It might be interesting to note that each pair of curves in Figure 17 has one common point which corresponds to the maximum of the spectral density of the detected signal. This effect is due to the fact that at the maximum of the spectral density of the signal the value of $dS(\lambda,T)/d\lambda$ is equal to zero and, therefore, the small error in the spectral positioning of the filter does not have any effect on the outcome of the measurement.

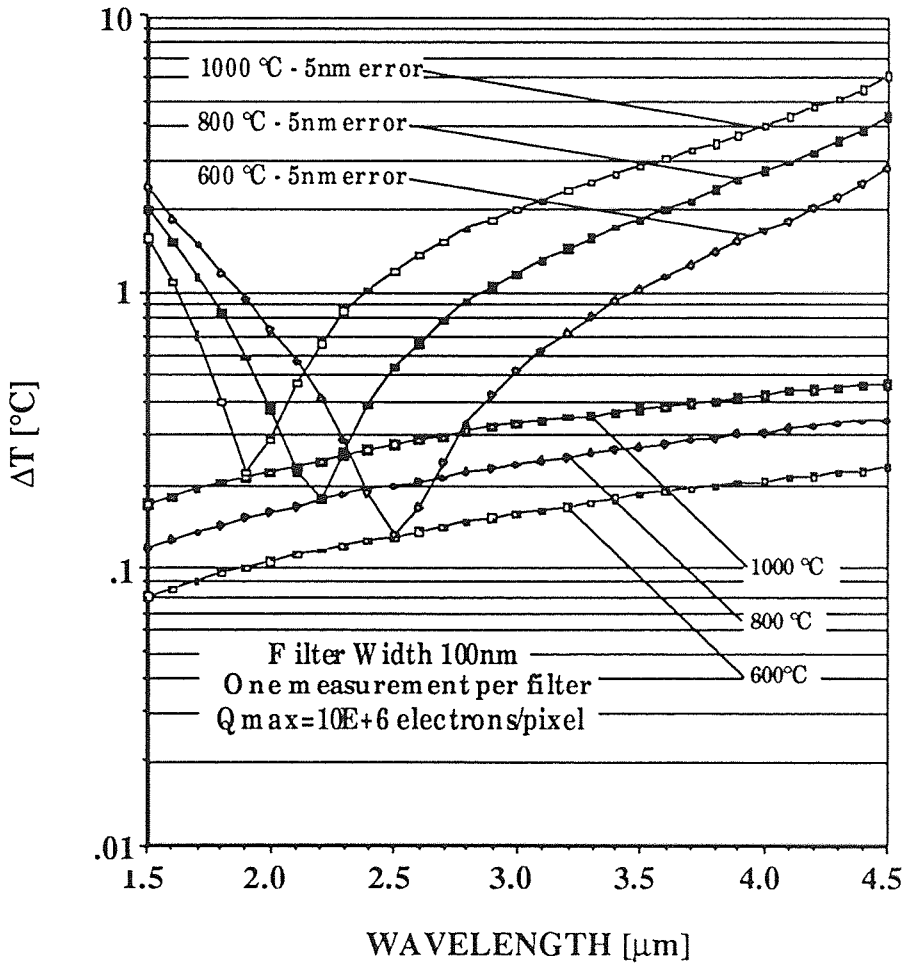

Figure 17 Effect on ΔT of 5-nm error in the estimation of the center wavelength of 100-nm Gaussian filter.

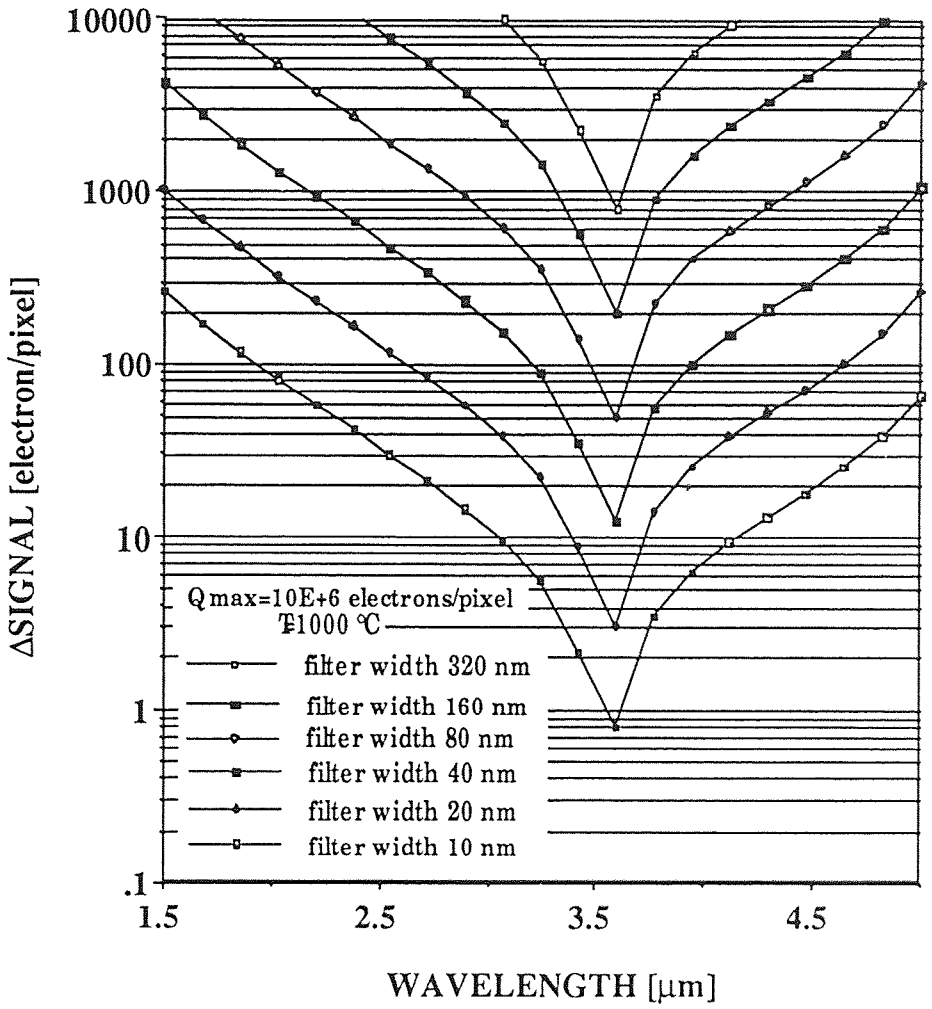

Figure 18 Error in the detected by a 320x244 IR-CCD imager signal resulting from modeling Gaussian-shaped filter by the square-shaped filter of the same area.

As was mentioned at the beginning of this section, another potential source of the error in the detected signal is the inaccurate description of shape of the transmission curve of the filter. In order to estimate this effect the output signal of the IR imager was calculated for both Gaussian and square shaped filters having the same area under transmission curve. These

computations assume that the optical integration time was adjusted to provide 10^6 electrons per pixel signal for square shaped filter. The absolute values of the difference of the signals detected through Gaussian and square filters are shown in Figure 18. The inspection of this figure shows that for filter width under 40-nm the difference in signal levels does not substantially exceed the value of the radiation shot noise. Therefore, for sufficiently narrow passband the shape of the filter does not have crucial effect on the accuracy of temperature measurement. However, if the filters with wider passband are to be used for temperature measurements the imager calibration should be performed prior to measurements in order to account for inaccuracy of filter specifications.

CHAPTER 4

TWO WAVELENGTHS RATIO RADIOMETRY

The analysis given in the preceding chapter shows that some knowledge about the emissivity of the radiant target is essential to the temperature measurement techniques based on either wide band or single wavelength radiometry. In particular, in order to infer the temperature of the target from a wide band measurement of the emitted radiation the value of the total emissivity $\varepsilon(T)$ should be known. Similarly, the technique based on the measurement of the radiation through the narrow filter (single wavelength radiometry) requires the knowledge of spectral emissivity, $\varepsilon(\lambda,T)$, of the target within the passband of the filter. Therefore, in situations where the emissivity of the target is changing rapidly or the conditions of the process preclude the independent measurement of target emissivity the methods of Chapter 3 will not yield the true temperature of the radiant target.

The extensive study of the radiometric literature shows that there exists a wide variety of methods designed to circumvent the problem of unknown emissivity. Some of these methods provide satisfactory results if certain usually rather restrictive assumptions about the spectral emissivity of the target are met. Other methods require more extensive measurements but provide acceptable results without placing substantial restrictions on the shape of the spectral emissivity curve.

It would appear that most of the suggested methods to date can be divided into two general classes. The methods in the first class can be described as "interpolation based techniques". In these methods the spectral radiance of the target is being measured at n+1 distinct wavelengths and these measurements are being used in order to determine the unknown temperature of the radiant target and n parameters of the particular emissivity model. The methods in the second class are referred to as "least-square-based techniques". In these methods the radiant measurements are made at m wavelengths, such that m>n, where n is the number of unknowns in the model. The redundancy in the data obtained here is used to smooth out the effects of noise in the data and allow more accurate estimation of the spectral emissivity.

The "interpolation based techniques" can be further separated into two distinct approaches. Some of these methods lead to evaluation of both temperature and emissivity [8,9], while others provide the target temperature by elimination of the emissivity parameters [10] The latter methods are referred to as ratio radiometry. One of them will be subject of this chapter. It should be noted that the theoretical errors associated with the interpolation methods which provide both temperature and emissivity have been analyzed by Coates [8]. The analysis given in [8] shows that when the number of unknowns n>3 the accuracy of these methods is unacceptable.

4.1 Basic Theory of Two Wavelengths Ratio Radiometry

The two wavelength ratio radiometry (later referred to as ratio radiometry) involves measuring the spectral radiance of the target at two different wavelengths (see Figure 19) and inferring the temperature from the ratio of these two measurements. Although measuring two signals, rather than one, introduces the additional uncertainty due to the noise present in both measurements, the method of ratio radiometry can successfully circumvent the problem of unknown emissivity for graybody radiators.

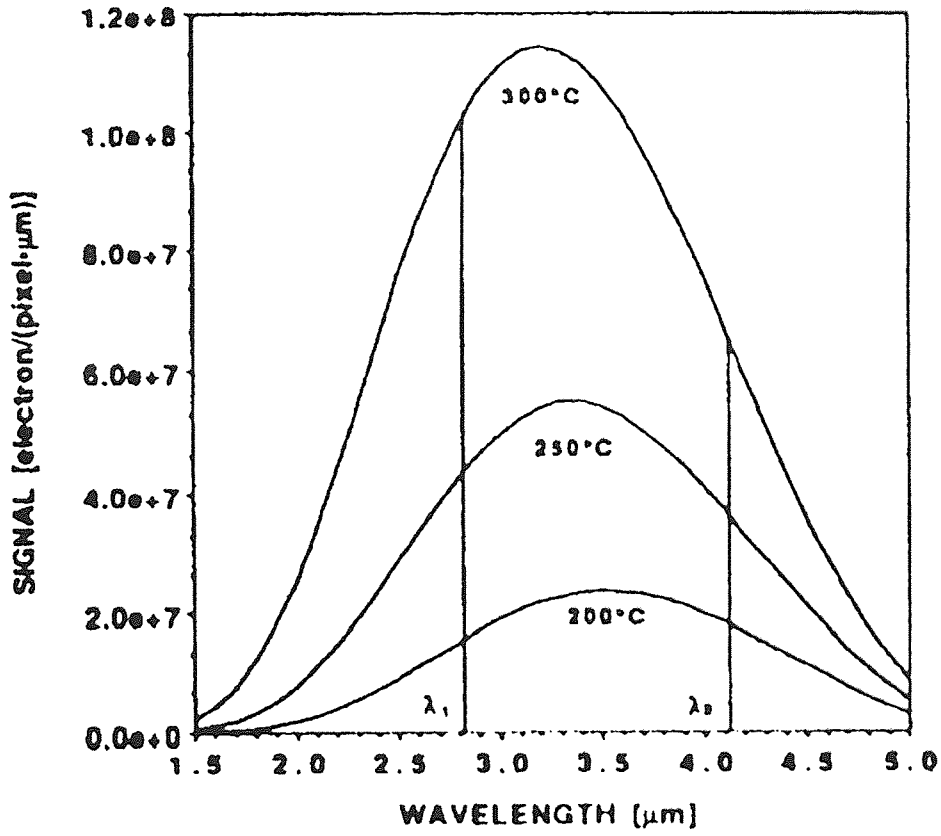

Figure 19 Temperature is inferred from the ratio of signals measured at two distinct wavelengths.

Using Eq. (3-41) and Plank's law we can express the radio of the signals detected at two distinct wavelengths λ_1 and λ_2 as

$$\frac{S_1(T)}{S_2(T)} = \frac{\varepsilon(\lambda_1)\cdot K(\lambda_1)\cdot R(\lambda_1)\cdot \lambda_1^{-5}\cdot e^{(-C_2/\lambda_1 T)}}{\varepsilon(\lambda_2)\cdot K(\lambda_2)\cdot R(\lambda_2)\cdot \lambda_2^{-5}\cdot e^{(-C_2/\lambda_2 T)}} \tag{4-1}$$

where $S_1(T)$ and $S_2(T)$ are the signals measured at λ_1 and λ_2 respectively.

By solving Eq. (4-1) for temperature, we obtain

$$\frac{1}{T} = \frac{\lambda_1\lambda_2}{C_2(\lambda_1-\lambda_2)}\left[\ln\left(\frac{S_2}{S_1}\right)+\ln\left(\frac{K_1}{K_2}\right)+\ln\left(\frac{R_1}{R_2}\right)+5\ln\left(\frac{\lambda_2}{\lambda_1}\right)+\ln\left(\frac{\varepsilon(\lambda_1)}{\varepsilon(\lambda_2)}\right)\right] \tag{4-2}$$

Though Eq. (4-2) has the temperature-dependent term $K(\lambda_1)/K(\lambda_2)$ in its right-hand side, it can be solved iteratively, because the dependence of this term on temperature is very weak. It should also be noted that in the case of a graybody radiator with $\varepsilon(\lambda_1)=\varepsilon(\lambda_2)$ equation (4-2) does not include the value of the target emissivity. Therefore the method of ratio radiometry can be used to determine the temperature of a graybody radiator with unknown emissivity. Furthermore, the target need not to be totally gray; it is sufficient for the target to have just two spectral regions where the spectral emissivities are equal. Moreover, even if the target is occluded by spectrally non-selective transparent media the results given by the method of ratio radiometry will still be correct.

4.2 Accuracy of the Temperature Measurement

It has already been mentioned that ratio radiometry yields the correct temperature for the case of graybody radiators. However, if the spectral emissivities of the target $\varepsilon(\lambda_1)$ and $\varepsilon(\lambda_2)$ are not exactly equal, then the measured temperature will differ from the true temperature of the target. The magnitude of this error can be estimated from Eq. (4-2) and is given by

$$\Delta T_{\varepsilon_1 \neq \varepsilon_2} = \frac{\lambda_1 \cdot \lambda_2 \cdot T^2 \cdot \ln\left(\frac{\varepsilon(\lambda_1)}{\varepsilon(\lambda_2)}\right)}{\lambda_1 \cdot \lambda_2 \cdot T \cdot \ln\left(\frac{\varepsilon(\lambda_1)}{\varepsilon(\lambda_2)}\right) + C_2(\lambda_1 - \lambda_2)} \tag{4-3}$$

However, assuming true graybody radiator, the accuracy of ratio radiometry is determined by the noise level of the detected signals.

In order to estimate the effect of radiation shot noise on the accuracy of the ratio radiometry we note that the noise levels of both signals $S(\lambda_1)$ and $S(\lambda_2)$ have to be taken into account. Since the signal measurements at two wavelengths are independent of each other we can express the accuracy of the temperature measurement as

$$\Delta T_{\lambda_1,\lambda_2} = \left[\left(\frac{dT}{dS_1} \cdot \Delta S_1\right)^2 + \left(\frac{dT}{dS_2} \cdot \Delta S_2\right)^2\right]^{\frac{1}{2}} \tag{4-4}$$

where from Eq. (4-2)

$$\left|\frac{dT}{dS_i}\right| = \frac{\lambda_1 \cdot \lambda_2}{C_2 \cdot (\lambda_1 - \lambda_2)} \cdot \frac{T^2}{S_i} \tag{4-5}$$

and the total noise in the signal, ΔS_i, measured at wavelength λ_i is

$$\Delta S_i = N_{shot} + N_{readout} + N_{filter} =$$

$$= \sqrt{S(\lambda_i, T) + N_{readout}^2 + \left(\frac{dS(\lambda, T)}{d\lambda} \cdot \delta\lambda\right)^2} \tag{4-6}$$

The values of ΔT corresponding to the positioning of one of the filters at 3.5 μm and of the second filter at various positions are shown in Figures 20 and 21. It should be noted that the computations were performed for a 320x244 IR CCD camera operating with an optical integration time of 33 ms and with f/2 optics. Figure 20 corresponds to the use of 500-nm-wide Gaussian filters, whereas the use of 20-nm-wide Gaussian filters for higher temperature range is reflected in Figure 21.

The analysis of Eqs. (4-3) and (4-4) shows that the effects of shot noise and emissivity variations on the accuracy of temperature measurement are minimized by proper selections of the filters. The optimum selection of the filter wavelengths is unique for each target temperature and can be determined from the following competing considerations:

(a) According to Eqs. (4-3) and (4-4) the increase in the separation of the filter wavelengths leads to improvement of ΔT. In other words, the filters should be positioned far enough from each other so that the difference in the detected signal is much larger than the total noise levels. It might be noted that the selection of the wavelengths on different sides of the maximum of the signal spectral density will tend to maximize the accuracy of temperature measurements.

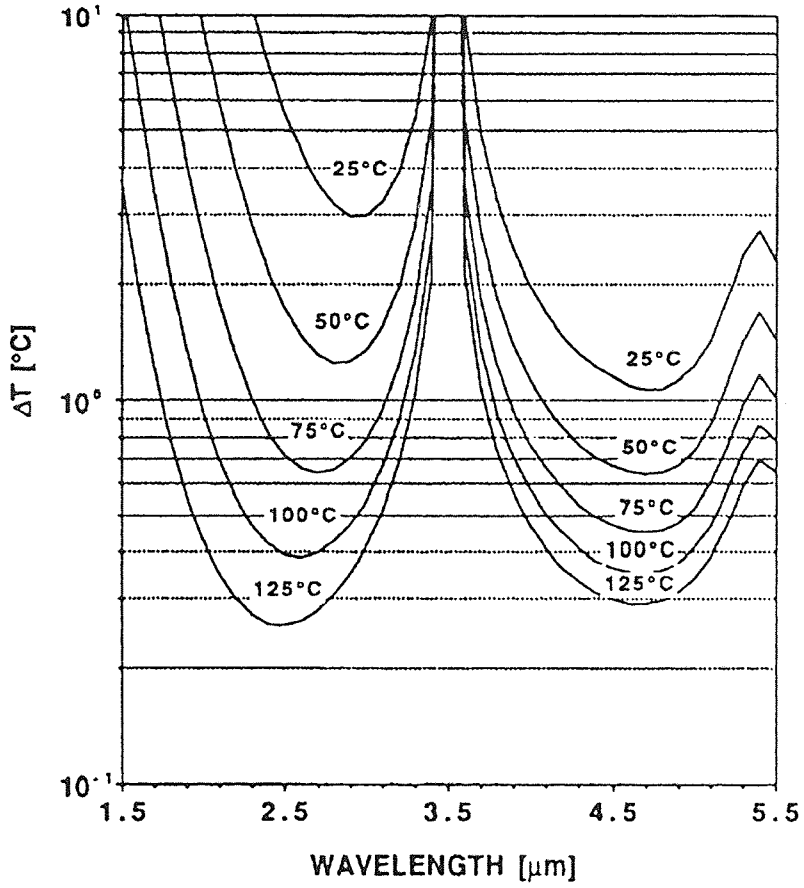

Figure 20 Calculated NEΔT for 320x244 IR CCD camera operating with optical integration time of 33 ms, f/2 optics, and 500 nm Gaussian filter with 60% peak transmission.

(b) On the other hand, it can be seen from Eqs. (4-3) and (4-4) that for a given wavelength separation smaller values of the product $\lambda_1 \cdot \lambda_2$ correspond to better accuracy.

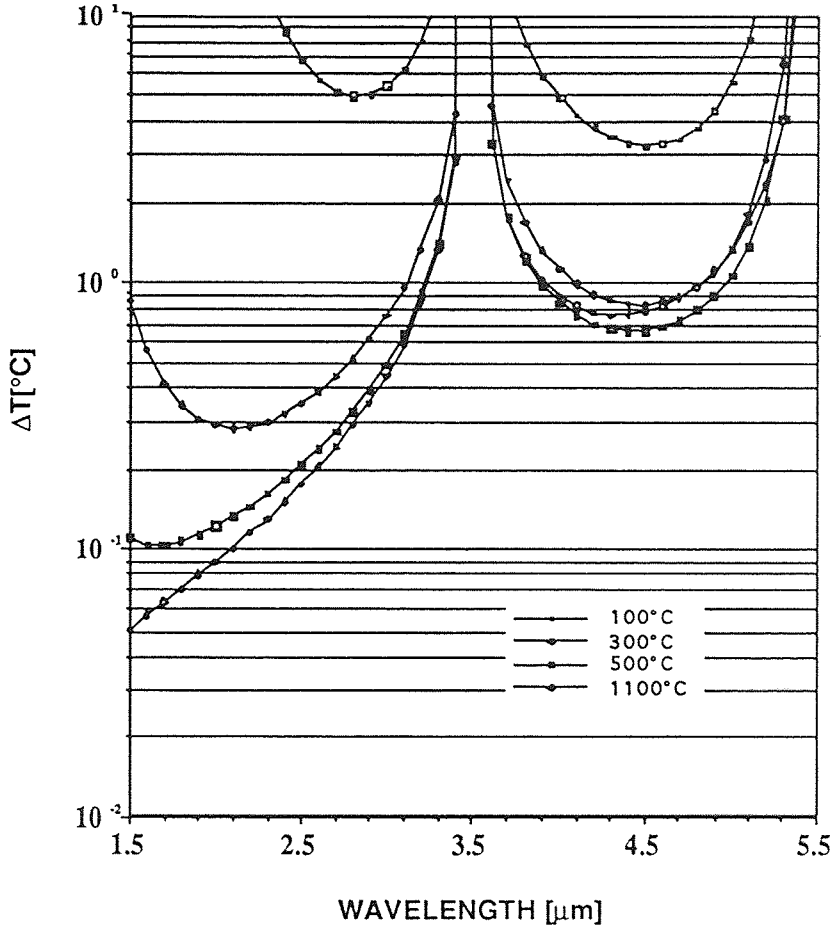

Figure 21 Calculated NEΔT for 320x244 IR CCD camera operating with optical integration time of 33 ms, f/2 optics, and 20 nm Gaussian filter with 60% peak transmission.

The analysis of the above mentioned factors leads to the conclusion that control of the optical integration time may be used to improve the accuracy of the temperature measurement by the method of ratio radiometry. In particular, the shortest wavelength should be chosen as short as the spectral

responsivity of the system permits, provided the signal level is kept high by setting the optical integration time appropriately. In that case the only factor which has to be optimized is the positioning of the filter corresponding to the longer wavelength. In order to illustrate this concept the values of ΔT computed for the signal level of 10^6 electrons per pixel and 1000 °C temperature are shown in Figure 22. It should be pointed out that these computations assume a 320x244 IR CCD Imager operating with f/2 optics and viewing the blackbody radiator through the 100 nm-wide Gaussian filter

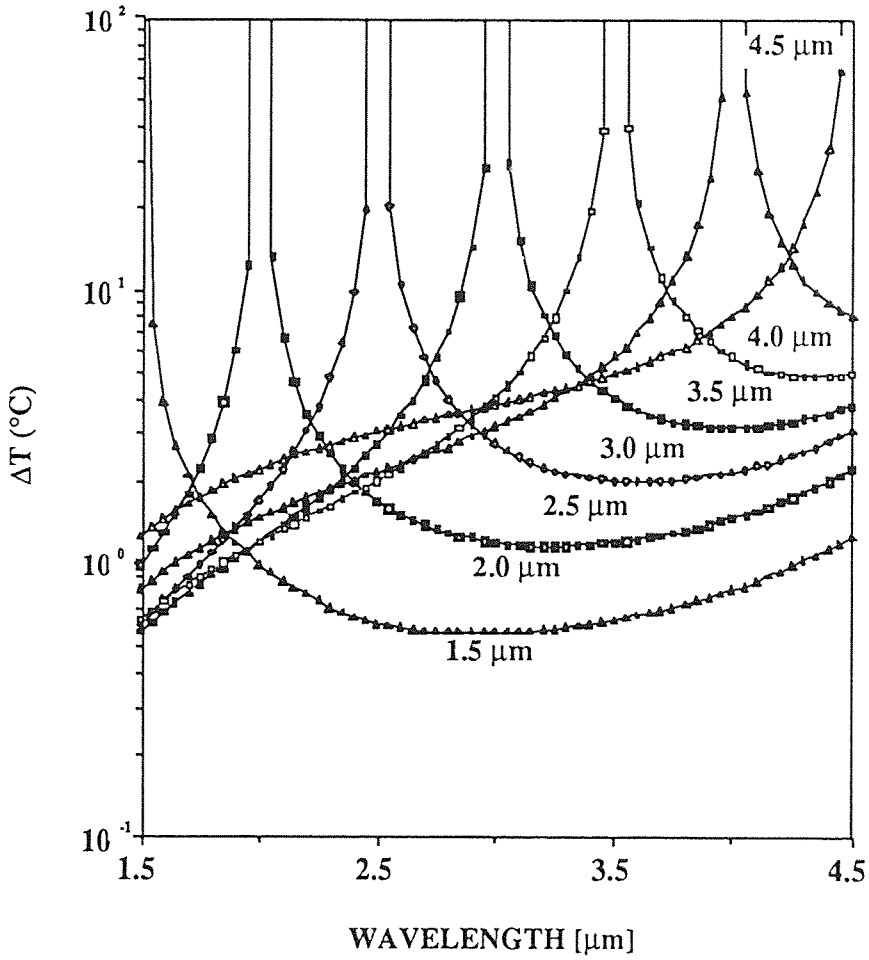

Figure 22 Dependence of ΔT on the positioning of two Gaussian 100 nm filters. The center wavelength of one of the filters is given on horizontal axis.

CHAPTER 5

MULTI-WAVELENGTH RADIOMETRY

The technique of ratio radiometry described in Chapter 4 belongs to the class of the radiometric methods which are designed to circumvent the problem of the unknown emissivity by eliminating the emissivity factor from the ratios of the measured signals. These techniques have not, in general, provided adequately accurate temperature estimates for broad industrial usage [11]. The often large inaccuracies of ratio techniques have been attributed to the fact that they require unrealistic assumption of constant spectral emissivity. The multi-wavelength least-squares-based technique presented in this chapter is more promissing, since it allows a more realistic assumption of a wavelength-dependent emissivity function.

The method of least-square-based multi-wavelength radiometry also referred to as multi-wavelength imaging pyrometry (MWIP) will be described in this chapter. Special emphasis will be placed on the analysis of the temperature accuracy achievable by MWIP for linear and quadratic emissivity models.

5.1 Basic Principles of MWIP

The first step in MWIP is to assume certain kind of functional dependency of the target spectral emissivity with wavelength. Analysis of the published

data on spectral emissivity of various materials [13] shows that in most cases the spectral emissivity can be adequately represented by the following polynomial function of wavelength

$$\varepsilon(\lambda) = a_1 + a_2 \cdot \lambda + a_3 \cdot \lambda^2 + \ldots \tag{5-1}$$

where $a_1, a_2, a_3 \ldots$ are the parameters of the emissivity model.

Substituting the emissivity model expressed by Eq. (5-1) into the expression for the detected signal given by Eq. (3-41) we obtain the parametric model of the output signal of the imager viewing the target with unknown emissivity

$$S(\lambda, a_1, \ldots, a_n) = K(\lambda, a_1, \ldots, a_n) \cdot \varepsilon(\lambda, a_1, \ldots, a_n) \cdot R(\lambda) \cdot L_{\lambda,b}(\lambda, T) \tag{5-2}$$

where the temperature of the target $T=a_n$ is also an unknown parameter of the model.

The central idea of radiometric temperature measurement by MWIP (see Figure 23) is to determine the temperature and the emissivity of the radiant target from the fit of the signal model given by Eq. (5-2) to the set of experimental values of the signal, $S_1, \ldots, S_N$ measured by the IR imager at N distinct wavelengths. It should also be noted that in order to obtain meaningful results, the number of wavelengths, N, should exceed the

number of unknown parameters, n, of the model.

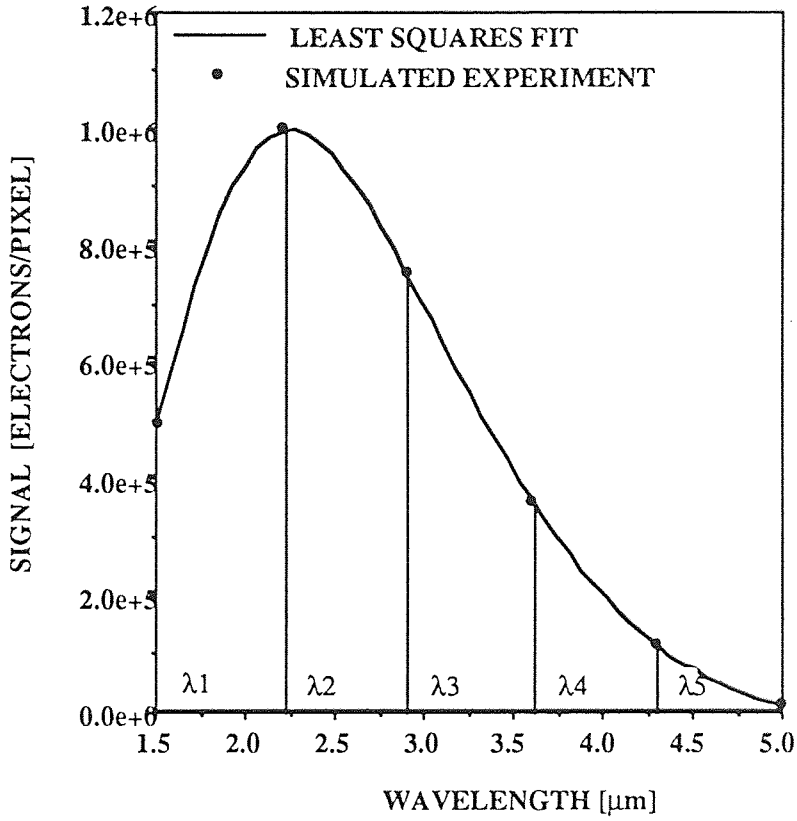

Figure 23 Least-squares fit to the simulated signal detected by a 320x244 IR CCD imager. The fit is based on 8 measurements per filter. The temperature of the simulated target is 1073 K.

Let us assume that the noise present in the experimental measurement S_i can be described by a Gaussian distribution with standard deviation σ_i (also referred to as rms noise). In this case the method known in classical statistics as the "method of maximum likelihood" can be applied to the development of the criteria which will provide the best fit of the parameters

of the theoretical model, a1,...,an, to the experimental values $S_1,...,S_N$. According to the method of maximum likelihood the best possible least-squares fit of the given model to the experimental values is achieved when the parameters of the model correspond to the minimum of the following function [5]

$$\min_{a_1,...,a_n} \chi^2 = \sum_{i=1}^{N} \left\{ \frac{1}{\sigma_i^2} [S_i - S(\lambda_i, a_1,...,a_n)]^2 \right\} \rightarrow a_1,...,a_n \qquad (5\text{-}3)$$

It might be noted that in the case of MWIP Eq. (5-3) calls for minimization of the weighted sum of squares of differences between the theoretical and experimental values of the detected signal, where the points with higher values of the rms shot noise are given less weight.

It is generally not convenient to derive an analytical expression for calculating the parameters of a non-linear function $S(\lambda, a_1,...,a_n)$. Instead, χ^2 must be considered to be a continuous function of the n parameters a_j describing a hypersurface in n-dimensional space which must be searched for a minimum. The description of a wide variety of methods designed to perform the search for the minimum in an n-dimensional hypersurface is given in the literature [see, for example, reference 5] and is beyond the scope of the present discussion. For the purpose of performing the least-squares fit in this thesis the software package ODRPACK developed in the National

Institute of Standards and Technology was utilized[1] .

5.2 Accuracy of Temperature Measurements

There are two approaches to the estimation of the temperature accuracy achievable by MWIP. The first approach involves simulation of the "experimental" values of the detected IR imager signal and performing the actual least- squares fit on this data. The estimation of the accuracy can then be obtained by the comparison of the results of the least-squares fit against "true" values of parameters used in the simulation. The second approach to the estimation of the temperature accuracy leads to the development of the approximate analytical solution to the least-squares problem defined by Eq. (5-3). For the sake of completeness and verification both approaches will be considered in this chapter.

5.2.1 Theoretical Estimation of the Accuracy

The fitting function $S(\lambda, a_1, \ldots, a_n)$ defined in Eq. (5-2) can be approximated in the close proximity of the solution by its expansion in a Taylor's series. Neglecting all terms of the second and higher orders we have

$$S(\lambda) = S_o(\lambda) + \sum_{j=1}^{n}\left[\frac{dS_o(\lambda)}{da_j}\cdot\delta a_j\right] + \frac{dS_o(\lambda)}{d\lambda}\cdot\delta\lambda \qquad (5\text{-}4)$$

[1] This software and its documentation [14] is not copyrighted and can be obtained free of charge through the AT&T software distribution system. The text of the user supplied subroutine appropriate to the present analysis is given in the Appendix.

The approximate solution to the minimization problem given by Eq. (5-3) can be obtained by setting the partial derivatives of χ^2 with respect to each of the parameter increments equal to zero

$$-2\sum_{i=1}^{N}\left(\frac{1}{\sigma_i^2}\left\{S_i - S_o(\lambda_i) - \sum_{j=1}^{n}\left[\frac{dS_o(\lambda)}{da_j}\cdot\delta a_j\right] - \frac{dS_o(\lambda)}{d\lambda}\cdot\delta\lambda\right\}\cdot\frac{dS_o(\lambda)}{da_k}\right) = 0 \tag{5-5}$$

where σ_i is the standard deviation of the signal detected at the wavelength λ_i. It should be noted that for the purpose of the present discussion the σ_i is equal to the total rms noise level in the signal and according to the development of Chapter 3 can be expressed as

$$\sigma_i^2 = S(\lambda,T) + N_{readout}^2 + \left(\frac{dS(\lambda,T)}{d\lambda}\cdot\delta\lambda\right)^2 \tag{5-6}$$

The Eq. (5-5) can be written in matrix form as

$$\overline{\beta} = \delta\overline{a}\cdot\overline{\alpha} \tag{5-7}$$

where

$$\alpha_{jk} = \sum_{i=1}^{N}\left(\frac{1}{\sigma_i^2}\cdot\frac{dS_o(\lambda)}{da_j}\cdot\frac{dS_o(\lambda)}{da_k}\right) \tag{5-8}$$

and

$$\beta_k = \sum_{i=1}^{N}\left(\frac{1}{\sigma_i^2}\left\{S_i - S_o(\lambda_i) - \frac{dS_o(\lambda)}{d\lambda}\cdot\delta\lambda\right\}\cdot\frac{dS_o(\lambda)}{da_k}\right) \qquad (5\text{-}9)$$

The matrix $\bar{\alpha}$ is referred to as "curvature matrix" because of its relationship to the curvature of χ^2 in coefficient space. Defining the symmetric matrix $\bar{\gamma}$ as the inverse of matrix $\bar{\alpha}$ we can obtain the expression for the approximate solution of the minimization problem (5-3) as

$$\delta\bar{a} = \bar{\beta}\cdot\bar{\gamma} \quad \text{or} \quad \delta a_j = \sum_{k=1}^{n}\left(\gamma_{jk}\cdot\beta_k\right) \qquad (5\text{-}10)$$

where $\bar{\gamma} = \bar{\alpha}^{-1}$

In order to find the accuracy of the parameter estimation by least-squares fit we note that each of our experimental data points Si has been used in the determination of the parameters, and each has contributed some fraction of its own noise to the uncertainty in the computed parameters. Therefore, the accuracy (standard deviation) of any parameter a_j can be expressed as the root sum square of the rms noise levels of each data point multiplied by the effect which that data point has on the determination of the

parameter a_j

$$\sigma_{a_j}^2 = \sum_{i=1}^{N} \sigma_i^2 \cdot \left(\frac{d a_j}{d S_i} \right)^2 = \sum_{i=1}^{N} \sigma_i^2 \cdot \left(\frac{d \delta a_j}{d S_i} \right)^2 \qquad (5\text{-}11)$$

The partial derivatives of the parameters with respect to each experimental data point can be obtained by differentiating Eq. (5-10) as

$$\frac{d \delta a_j}{d S_i} = \sum_{k=1}^{n} \left[\gamma_{jk} \cdot \frac{1}{\sigma_i^2} \cdot \frac{d S_o(\lambda)}{d a_k} \right] \qquad (5\text{-}12)$$

Performing the substitution of the partial derivatives given by Eq. (5-12) into Eq. (5-11) and taking into account the fact that matrix $\bar{\gamma}$ is the inverse of the matrix $\bar{\alpha}$ we obtain the final expression for the standard deviations of the parameters of the theoretical model fitted to the experimentally measured values of the detected IR imager signal.

$$\sigma_{a_j}^2 = \sum_{i=1}^{N} \sigma_i^2 \cdot \left\{ \sum_{k=1}^{n} \left[\gamma_{jk} \cdot \frac{1}{\sigma_i^2} \cdot \frac{d S_o(\lambda)}{d a_k} \right] \right\}^2 = \gamma_{jj} \qquad (5\text{-}13)$$

5.2.2 Linear and Quadratic Emissivity Models

At this point it should be noted that in order to implement the error analysis described in the preceding section we have to obtain analytical expressions

for the partial derivatives of the signal model with respect to each of its parameter. The expressions of the partial derivatives of the signal model with respect to temperature and wavelength were developed in Chapter 3 and are given by Eqs. (3-49) and (3-56) respectively. We will now derive the expressions for the partial derivatives of the signal model with respect to the parameters of the emissivity model. For the sake of clarity only a linear emissivity model with two unknown parameters a and b will be considered. Let us define the relative partial derivatives of the emissivity with respect to the coefficients a and b by analogy with Eq. (3-24) as

$$\varepsilon_a = \frac{1}{\varepsilon(a,b)} \cdot \frac{d\varepsilon(a,b)}{da} = \frac{1}{\varepsilon(a,b)} \tag{5-14}$$

and

$$\varepsilon_b = \frac{1}{\varepsilon(a,b)} \cdot \frac{d\varepsilon(a,b)}{db} = \frac{\lambda_o}{\varepsilon(a,b)} \tag{5-15}$$

similarly, the relative partial derivatives of the shape coefficient $K(a,b,T)$ can be defined by analogy with Eq. (3-43) as

$$K_a = \frac{1}{K(a,b,T)} \cdot \frac{dK(a,b,T)}{da} \tag{5-16}$$

and

$$K_b = \frac{1}{K(a,b,T)} \cdot \frac{dK(a,b,T)}{db} \tag{5-17}$$

where dK/da and dK/db can be obtained by differentiating (3-39) as

$$\frac{dK(a,b,T)}{da} = -G \cdot A_2 \cdot \lambda_o^2 \cdot \frac{b}{\varepsilon^2(a,b)} \cdot \left(\frac{\Delta\lambda}{\lambda_o}\right)^2 \cdot (r_1 + L_1) \tag{5-18}$$

and

$$\frac{dK(a,b,T)}{db} = G \cdot A_2 \cdot \lambda_o^2 \cdot \frac{a}{\varepsilon^2(a,b)} \cdot \left(\frac{\Delta\lambda}{\lambda_o}\right)^2 \cdot (r_1 + L_1) \tag{5-19}$$

Using the definitions of Eqs. (5-14) through (5-17) we can now obtain the expressions for the partial derivatives of the signal with respect to the coefficients a and b of the emissivity model

$$\frac{dS(a,b,T)}{da} = S(a,b,T) \cdot (\varepsilon_a + K_a) \tag{5-20}$$

and

$$\frac{dS(a,b,T)}{db} = S(a,b,T) \cdot (\varepsilon_b + K_b) \tag{5-21}$$

Having defined all necessary partial derivatives of the signal model we are now ready to proceed with the numerical evaluation of the temperature accuracy achievable by the least-squares based MWIP. In order to perform these computations we have to assume some values of the coefficients a and b which would be realistic and representative of the practical situations. For the purpose of this analysis the data on the spectral emissivity of pure silicon published by Sato [15] and shown in Figure 24 has been used. The coefficients of the linear emissivity model were obtained by performing the least-squares fit of the first degree polynomial to the data given in this figure for the spectral emissivity of silicon at 1073K and the wavelength range from 1.5 to 5.0 μm.

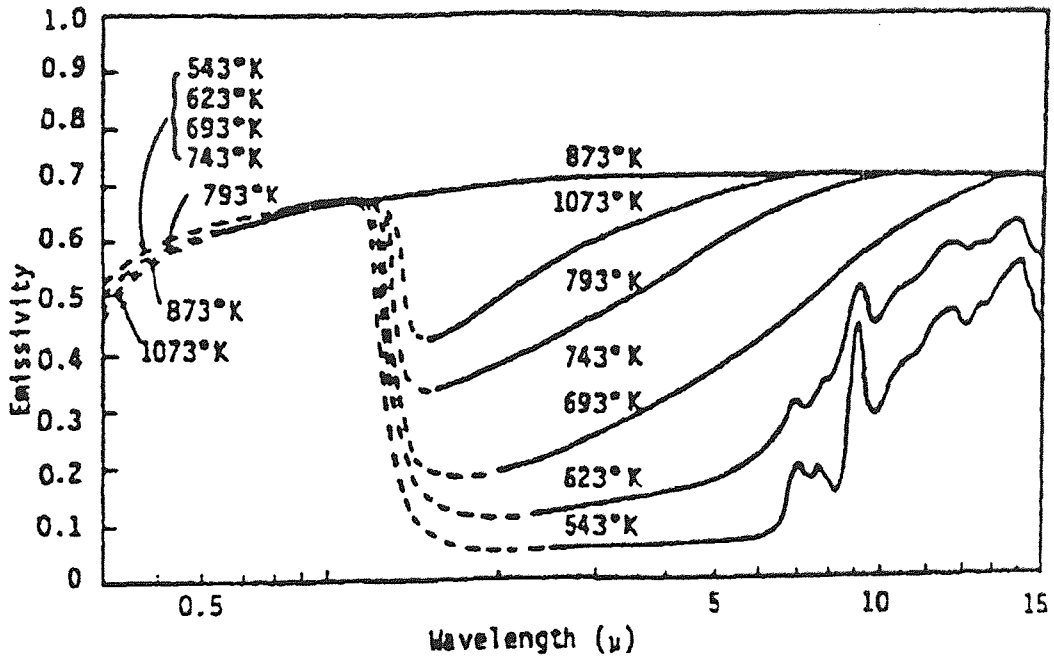

Figure 24 Spectral emissivity of single crystal n-type silicon disc [15].

The coefficients of the non-linear emissivity model were obtained by fitting the second degree polynomial to the spectral emissivity data corresponding to 793K for wavelength interval given above. The results of this fitting procedure show that the spectral emissivity of pure silicon at 1073K can be represented by a first degree polynomial as

$$\varepsilon_{1073K}(\lambda) = 0.6871 + 0.0086 \cdot \lambda \tag{5-22}$$

whereas for the specimen at 793 K the expression of the spectral emissivity requires second degree polynomial

$$\varepsilon_{793K}(\lambda) = 0.2253 + 0.1586 \cdot \lambda + 0.0148 \cdot \lambda^2 \tag{5-23}$$

As was mentioned at the beginning of this chapter two different methods have been used for the estimation of the temperature accuracy achievable by MWIP. The first method is based on the simulation of the detected signal using the signal model given by Eq. (3-38) with the spectral emissivity model given by Eqs. (5-22) and (5-23). As part of these simulations a random number generator was utilized in order to simulate normally distributed noise in the signal with the rms value given by Eq. (3-12). The simulated signal was then used as the input data to the least-squares software package [14]. The temperature accuracy (standard deviation of the parameter T) was obtained by a comparison of the results of the least-

squares fit with the "true" value of the signal used in the simulation experiments. The second method is based on the development given in Section 5.2.1 and involves direct computation of the standard deviation from Eq. (5-13). It should be noted, however, that this method is based on the first order approximation of the outcome of the least- squares fit and, as illustrated in Figure 25, leads to higher errors in the estimation of the temperature accuracy in comparison to what is achievable by MWIP.

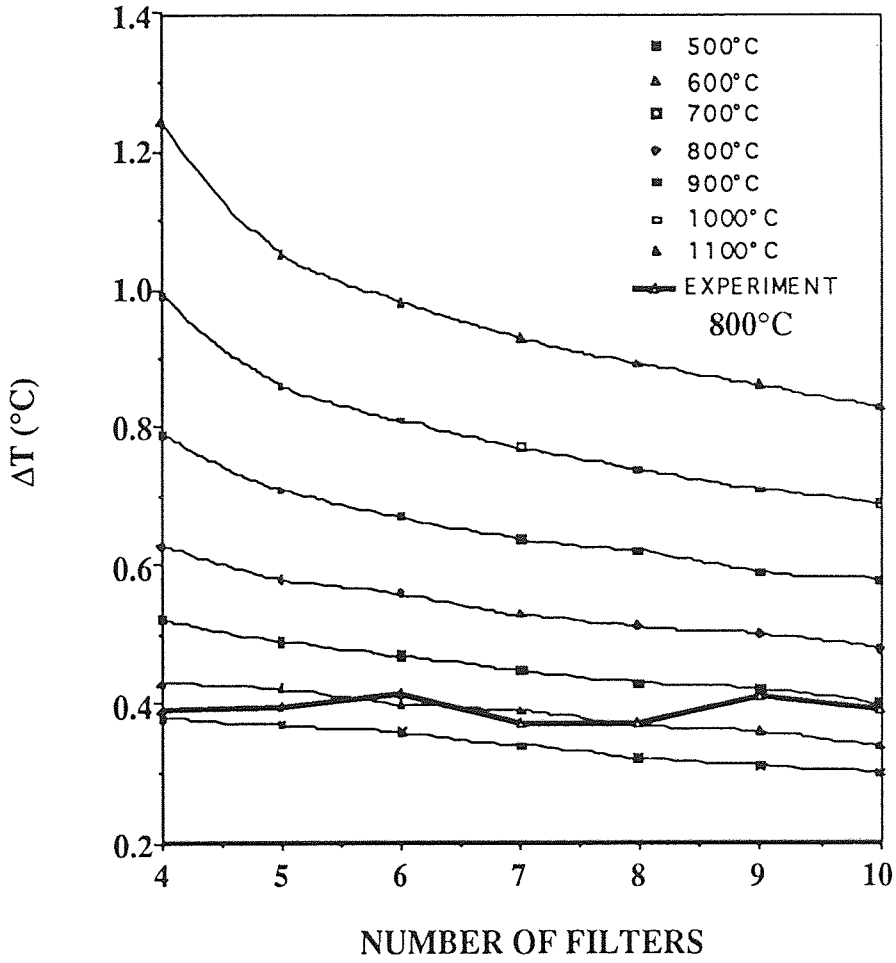

Figure 25 Temperature accuracy of MWIP with linear emissivity model. The computations assume 4 independent measurements per filter, 100-nm -wide Gaussian filters and $Q_{max}=10^6$ electrons per pixel.

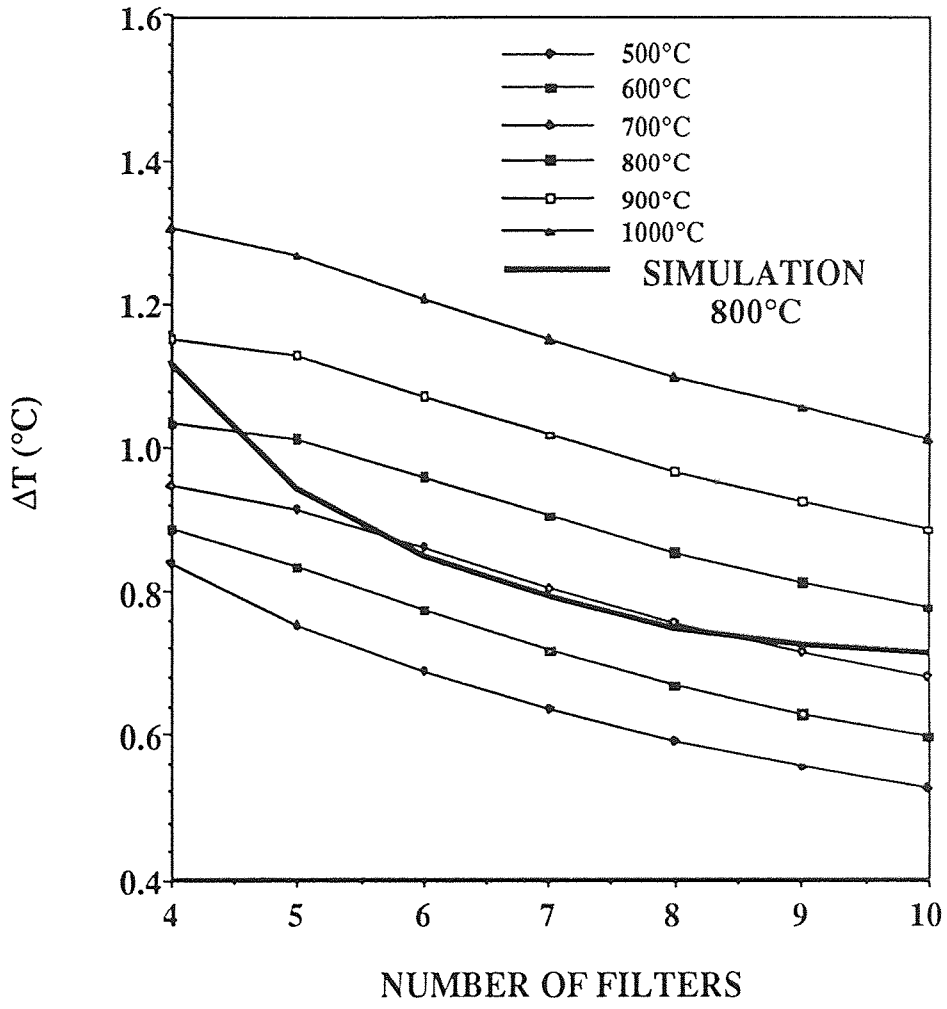

Figure 26 Temperature accuracy of MWIP with linear emissivity model and 5-nm error in the estimation of the center wavelengths of 100-nm-wide Gaussian filters. The computations assume 25 independent measurements per filter and $Q_{max}=10^6$ electrons/pixel.

The results obtained by both methods for the case of a linear emissivity model and maximum charge handling capacity of the IR imager equal to 10^6 electrons per pixel are shown in Figures 25 and 26. It should be pointed out that the results shown in these figures were obtained with the filters having Gaussian shape and 100-nm effective width of spectral

transmittance. It should also be emphasized that these computations are based on the assumption that a number of repeated independent measurements were performed at each wavelength and their averages were used as the input to the least-squares fitting algorithm. The technique of taking the average of n independent measurements as a single value has the same effect as an n-fold increase in charge handling capacity of the IR imager and leads to the decrease of rms noise in the signal by the factor of square root of n.

Inspection of Figure 25 shows that in the case of a linear emissivity model with three unknown parameters the amount of filters does not have an appreciable effect on the accuracy of the resulting temperature estimation, provided that a minimum of four filters are used. The fact that the bold simulated curve representing simulation experiment does not show the expected smooth behavior is due to the randomness of the simulated radiation noise.

As expected, averaging of repeated independent measurements leads to improvement in the effective signal-to-noise ratio. However, this can only lead to the reduction of the effects of temporal noise sources, such as radiation shot noise and detector readout noise. The uncertainty in the signal measurement introduced by such permanent factors as the inaccuracy in the description of the filter transmittance can only be reduced by the increase in the number of filters and the more accurate estimation of their spectral

transmittances. This fact is reflected in the Figure 26 which shows the accuracy of least-squares based MWIP in the case of 5-nm errors in the specifications of effective center wavelengths of the 100-nm-wide filters. Inspection of this figure shows that the increase in the number of filters used for MWIP has a much more pronounced effect on the outcome of the measurements with appreciable errors in the specification of the filter spectral transmittance.

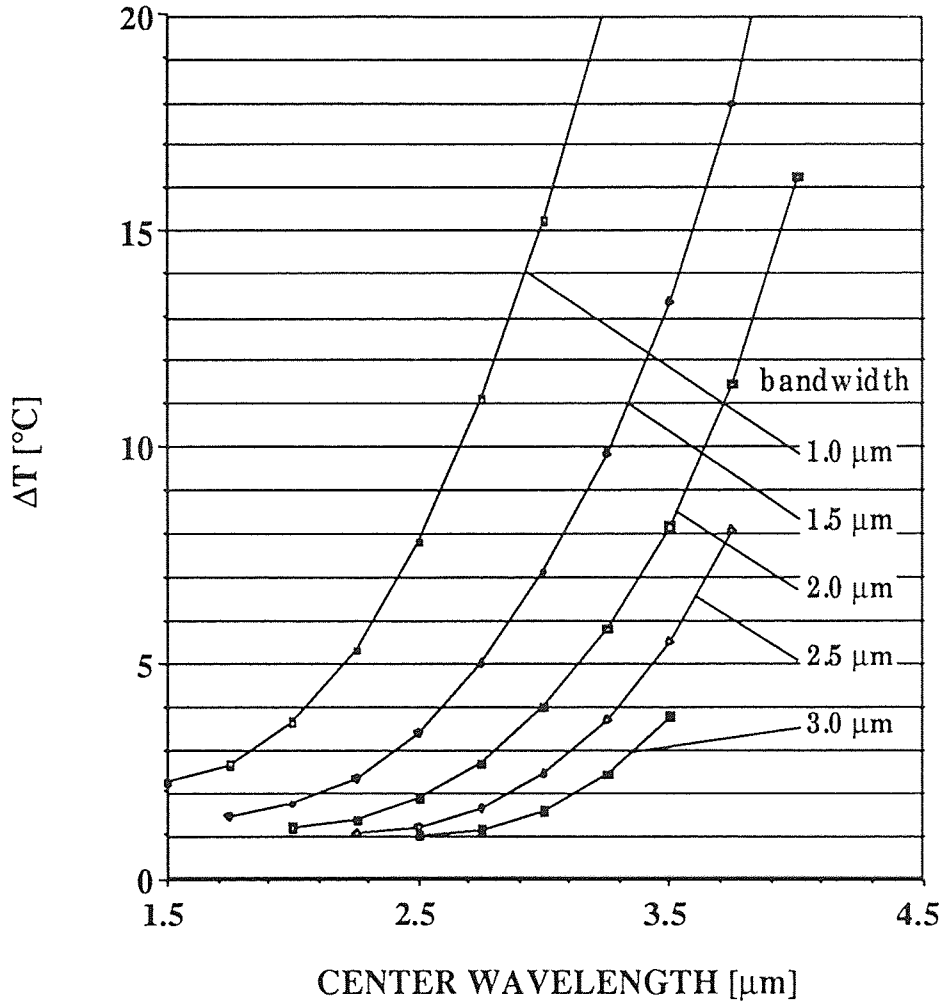

Figure 27 Temperature accuracy of MWIP vs. total spectral bandwidth of measurement for target temperature of 1000 °C.

Another factor affecting MWIP accuracy is the total bandwidth of the measurements, i.e. the separation between the filters corresponding to the shortest and longest wavelengths. This effect is illustrated in Figure 27 where the horizontal axis corresponds to the center wavelength of the total bandwidth used for MWIP measurement. These computations assume 6 equally spaced filters and target temperature of 1000 °C. The inspection of this figure shows that wider bandwidth range of MWIP measurement provides better accuracy of temperature estimation. Gardener [12] points out that in the case of small spectral bandwidth of MWIP measurement the relative dependence of the spectral radiance distribution on temperature is reduced. This leads to the greater errors in the estimated temperature, since the changes in emissivity are difficult to distinguish from changes in temperature.

CHAPTER 6

COMPARISON OF RADIOMETRIC METHODS

In the three previous chapters we have analyzed a number of radiometric methods which can be used for non-contact temperature measurement of the remote radiant target. The methods described in this thesis include:

(1) Wideband radiometry, where the full bandwidth of the IR imager is being used for the detection of the radiation emitted by the target. The application of this method to the temperature measurements of gray and color bodies requires the knowledge of the total emissivity of the target.

(2) Narrow-band (monochromatic) radiometry which employs narrow passband filters in order to detect the radiation emitted by the target within small wavelength interval. The temperature estimation by this method requires the knowledge of the spectral emissivity of the target in the proximity of the center wavelength of the filter transmittance.

(3) Two wavelength radio radiometry, where the temperature of the radiant target is inferred from the ratio of emitted radiation measured at two distinct wavelengths. This method allows the measurement of the temperature of a gray target with unknown emissivity, but does require the knowledge of the spectral emissivity in the case of color targets.

(4) Multi-wavelength least-squares based radiometry which employs the measurement of the emitted radiation at more than two wavelengths. This method does not require prior knowledge of spectral emissivity and can be applied to the temperature measurement of color targets. In order to apply this method some assumption about the dependency of the spectral emissivity on wavelength must be made. Therefore, some general knowledge about the shape of the spectral emissivity curve is desirable.

In this chapter we will compare the temperature accuracy achievable by each of the above radiometric methods. The discussion presented here assumes that all methods are used with a 320x244 IR-CCD camera with f/2 optics.

6.1 Temperature Accuracy

The estimated values of the temperature accuracy achievable by the methods considered in this thesis are shown in Tables 1-4. It should be noted that the data shown in these tables correspond to radiant target with the temperature equal to 1000 °C. Table 1 provides the data on the accuracy of the temperature measurements of blackbody targets, targets with linear spectral emissivity, and targets with quadratic linear emissivity. The data shown in The accuracy achievable by wide-band, narrow-band, ratio, and multi-

wavelength radiometry is shown for each of the above targets. Table 1 corresponds to the maximum signal of 10^6 electrons per pixel. Tables 2-4, shown at the end of this chapter, provide the accuracy data for levels of the maximum signal of $4x10^6$ electrons per pixel, $2.5x10^7$ electrons per pixel, and $1.0x10^8$ electrons per pixel respectively.

Table 1 NEΔT resulting from 1 measurement per filter.

Method of Temperature Measurement	Black Body $\varepsilon = 1$ (°C)	Color Body $\varepsilon = a + b \cdot \lambda$ (°C)	Color Body $\varepsilon = a + b \cdot \lambda + c \cdot \lambda^2$ (°C)
Wide-Band Radiometry ($\Delta\lambda$ = 3 μm)	0.251		
Narrow-Band Radiometry (λ = 1.5 μm)	0.169		
Ratio Radiometry (λ_1 = 1.5 μm , λ_2 = 3.0 μm)	0.564		
Multi Wavelength Radiometry (linear emissivity model)	0.407	0.601	56.0
Multi Wavelength Radiometry (quadratic emissivity model)	1.684	5.655	3.445

6.1.1 Wide-Band vs. Narrow-Band Radiometry

The inspection of Table 1 shows that the best accuracy achievable by a 320x244 IR-CCD imager viewing the blackbody radiator at 1000 °C corresponds to the method of a one filter narrow-bandwidth radiometry. In order to verify this result it might be useful to obtain an approximate analytical expression for the temperature accuracy of narrow-band

radiometry. Assuming that for a sufficiently narrow filter the variations in spectral radiance and responsivity across the passband are negligible, Eq. (3-50) can be approximated as

$$NE\Delta T = \frac{1}{\sqrt{S(\lambda,T)} \cdot L_T} \tag{6-1}$$

where L_T is a normalized partial derivative of the blackbody radiance with temperature and is given by Eq. (3-42).

Using the Wien's approximation to Planck's law we can simplify Eq. (3-42) as follows

$$L_T = \frac{x}{T} = \frac{C_2}{\lambda \cdot T^2} \tag{6-2}$$

where C_2=1.4388x10^4 - is the second radiation constant [μm K]

Performing the substitution of Eq. (6-2) into Eq. (6-1) and assuming that by setting the optical integration time the signal level is kept at the fixed value Q_{max} for all temperatures, we obtain the approximate expression for NEΔT

$$NE\Delta T = \frac{\lambda \cdot T^2}{C_2 \cdot \sqrt{Q_{max}}} \tag{6-3}$$

For a signal level of 10^6 electrons per pixel, temperature of 1000 °C, and peak wavelength of the filter of 1.5 μm the NEΔT computed from Eq. (6-3) is equal to 0.1689 which is in very good agreement with the rigorously obtained value shown in the Table 1. It should be noted, however, that Eq. (6-3) provides an accurate result only for $\lambda T<2900$ K since the Wien's approximation is not as accurate outside of this region.

At this point a very important implication of Eq. (6-3) should be emphasized. It follows from inspection of Eq. (6-3) that in order to achieve the best accuracy of narrow-band temperature measurement the peak wavelength of the filter should be selected at the shortest possible wavelength, provided that the signal level is kept constant by setting the optical integration time or by other means. However, if the signal level is not controlled during the measurements, the best accuracy is achieved by selecting the peak wavelength of the filter as close to the maximum of the spectral signal density as the charge handling capacity permits. This point may be clarified by inspection of Figure 16.

We now turn our attention to the noise equivalent temperature of the wideband temperature measurement. For the case of signal level fixed at 10^6 electrons per pixel and 1000 °C temperature of the blackbody radiator the value of NEΔT given in Table 1 is equal to 0.251 °C. This value of NEΔT is somewhat worse than the corresponding value for narrow-band measurement. In order to explain this fact we have to consider the blackbody

spectral radiance shown in Figure 1 and the spectral responsivity of PtSi Schottky-Barrier detector (SBD) shown in Figure 7. The inspection of this figure shows that for the temperature range approximately between 600 K and 1500 K the maximum of blackbody spectral radiance is within the bandwidth of PtSi SBD. Moreover, for this range of temperatures the PtSi SBD is sensitive to the radiation emitted at wavelengths only within a relatively small spectral interval around the maximum of the blackbody spectral radiance. Therefore, the detected radiation is approximately proportional to the fifth power of the radiator temperature, as given by Eq. (2-6). In other words, the spectral responsivity of the PtSi SBD can be considered as the spectral transmittance of a wide filter with center wavelength being within the proximity of the maximum of the blackbody spectral radiance. Substituting Eq. (2-6) into Eq. (3-38) and neglecting the correction for the filter shape we obtain the approximation of the signal detected by wideband measurement

$$S_{wide-band} = 1.288 \times 10^{11} \cdot G \cdot \frac{t_i}{Q_{el}} \cdot T^5 = const \cdot T^5 \qquad (6\text{-}4)$$

Substituting the Eq. (6-4) into the Eq. (3-14) and ignoring the readout noise the obtain

$$NE\Delta T = \frac{\sqrt{const \cdot T^5}}{4 \cdot const \cdot T^4} = \frac{1}{5 \cdot \sqrt{const \cdot T^3}} \qquad (6\text{-}5)$$

In the case of signal being kept at the fixed level Q_{max} by setting the optical integration time or other means Eq. (6-4) can be rewritten as

$$S_{wide-band} = const \cdot T^5 = Q_{max} \tag{6-6}$$

Substituting Eq. (6-6) into Eq. (6-5) we obtain an approximate expression for NEΔT of wideband temperature measurements

$$NE\Delta T = \frac{T}{5 \cdot \sqrt{Q_{max}}} \tag{6-7}$$

For a signal level of 10^6 electrons per pixel and temperature of 1000 °C, the NEΔT computed from Eq. (6-7) is equal to 0.2546 °C which is in good agreement with the rigorously obtained value shown in the Table 1.

At this point it might be interesting to compare the results obtained for wideband and narrow-band temperature measurements. Taking the ratio of Eq. (6-3) to Eq. (6-7) we have

$$\frac{NE\Delta T_{narrow-band}}{NE\Delta T_{wide-band}} = \frac{5 \cdot \lambda \cdot T}{C_2} = \frac{\lambda \cdot T}{2877.6} \tag{6-8}$$

It should be noted that the approximation given by Eq. (6-4) is only valid for the PtSi SBD viewing the target with temperature between 600 K and 1500 K since those assumptions were used in the derivation of this equation. For temperatures outside of this interval the spectral bandwidth of PtSi SBD does not contain the maximum of the blackbody spectral radiance. In that case the detected signal is approximately proportional to the fourth power of the target temperature as given by Eq. (2-7).

Concluding this section we note that in cases where enough signal is being detected to provide high signal-to-noise ratio the method of narrow band radiometry will yield higher temperature accuracy at elevated temperatures than wide-band measurement providing the optimum selection of the peak wavelength of the narrow-passband filter.

6.1.2 Ratio and Multi-wavelength Radiometry

In the method of ratio radiometry two signals are being used in order to infer the temperature of the radiant target and, therefore, the noise levels of both signals contribute to the uncertainty of the temperature measurement. Hence, it is beneficial to independently adjust the optical integration time of the imager for signal measurements at the two wavelengths thus achieving the highest possible signal-to-noise ratios for beach measurement. Assuming that the signal levels are controlled by this procedure and considering the

BLIP mode of imager operation we can express the NEΔT given by Eq. (4-4) as

$$NE\Delta T_{\lambda_1,\lambda_2} = \frac{\lambda_1 \cdot \lambda_2 \cdot T^2}{C_2 \cdot (\lambda_2 - \lambda_1)} \cdot \sqrt{\frac{2}{Q_{max}}} \qquad (6\text{-}9)$$

Inspection of this equation shows that temperature accuracy is affected by two factors:

(1) The smaller product of two wavelengths $\lambda_1 \cdot \lambda_2$ leads to the smaller NEΔT. Therefore, the center wavelength of one of the filters should be selected as short as the responsivity of the imager permits.

(2) The higher separation of two filters also leads to smaller NEΔT. Therefore, if the signal level is controlled for measurements at both wavelengths the filter with longer peak wavelength should be positioned as far from the first filter as the spectral responsivity of the imager permits. If the signal level is being controlled only for measurement at shorter wavelength then the optimum positioning of the filter with longer wavelength is unique for each temperature and can be determined from the data given in Figure 22.

Assuming that the signal level is fixed for both measurements at 10^6 electrons per pixel and the reasonable for PtSi SBD wavelength selections of

1.5 and 4.5 μm we can use Eq. (6-9) in order to develop this simple expression for NEΔT

$$NE\Delta T_{1.5,4.5} = 2.21\times10^{-7}\cdot T^{2} \qquad (6\text{-}10)$$

The value of NEΔT calculated based on Eq. (6-10) for target temperature of 1000 °C is equal to 0.358 °C. However, in order to provide meaningful comparison with the temperature accuracy of multi-wavelength radiometry the value of NEΔT shown in the Table 1 was obtained from Eq. (4-4) based on the assumption that only the highest of two signals is kept at the fixed level Q_{max} by the control of the optical integration time. The second signal (at longer wavelength) is measured with the integration time set during the first signal measurement. This leads to the higher value of resulting NEΔT because of the lower signal-to-noise ratio for the measurement at longer wavelength. However, this result can be meaningfully compared with the NEΔT of least-squares based techniques since in these techniques only a single value of the optical integration time is used for the signal measurements at all wavelengths.

In the case of multi-wavelength radiometry the target temperature is inferred from the signal measurements at more than two wavelengths. Each measurement used for the calculation of the target temperature has some noise level associated with it and some fraction of this noise is contributed to

the total uncertainty in the temperature measurement. However, in the case of gray or black targets with fixed integration time for measurements at all wavelengths the multi-wavelength technique is capable of providing greater accuracy than ratio radiometry. This is due to the fact that the extra measurements provide redundancy which is used to offset the effects of the temporal noise in the signal measurements. It should be noted, however, that the high accuracy of multi-wavelength radiometry is only achieved with the correct choice of the emissivity model.

The inspection of Table 1 shows that if the emissivity of the blackbody radiator is modeled with the quadratic emissivity model given by Eq. (5-23) then the accuracy of the multi-wavelength technique is inferior to that of ratio radiometry. This effect is due to the fact that the unnecessary unknown parameter in the model introduces an additional degree of freedom to the least-squares algorithm leading to a degradation in the quality of the solution.

It is important to recognize the compromise involved in the selection of the emissivity model. In order to correctly determine the temperature of the target with unknown emissivity it is necessary to provide a sufficiently complex and flexible emissivity model capable of accurate approximating of target spectral emissivity. On the other hand, too complex, overdetermined model will lead to a decrease in the resulting temperature accuracy of the

measurement due to the redundant degrees of freedom in the fitting algorithm. This point is illustrated in Figure 28.

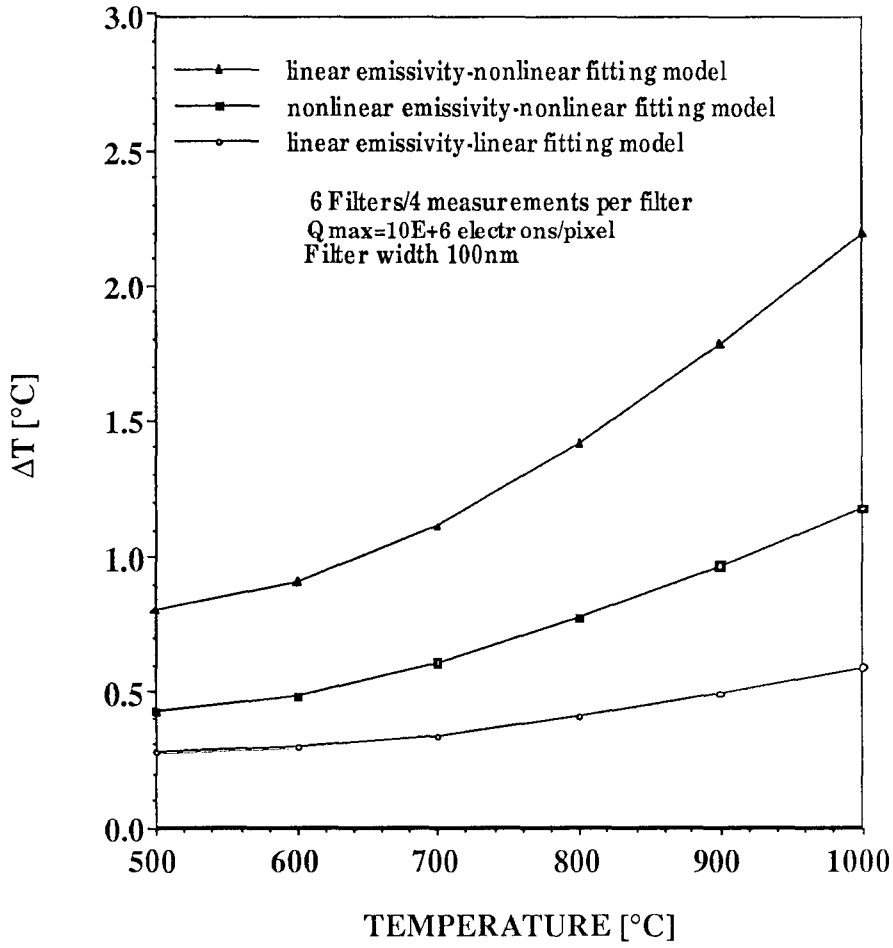

Figure 28 Accuracy of MWIP measurements with linear and quadratic emissivity models.

Inspection of Figure 28 shows that the temperature accuracy resulting from the application of MWIP to the targets which exhibit linear and quadratic characteristics of their spectral emissivity. The inspection of this

figure confirms that the best possible accuracy is achieved by employing the emissivity model most closely matching the spectral emissivity of the target. However, if no prior knowledge of the target emissivity exists, it may be beneficial to intentionally use a more complex emissivity model. This will result in some loss of accuracy but also provide the guarantee that a reasonable estimation of the target temperature can be obtained by MWIP. It is shown in Table 1 that selecting the emissivity model with too few parameters renders the MWIP algorithm ineffective for targets with relatively complex spectral emissivity.

6.2 Improvement of Temperature Accuracy

The temperature accuracy achievable by any of the described above radiometric methods is limited by the radiation shot noise, rms detector readout noise, inaccurate description of the spectral characteristics of the system, and other sources not accounted during the measurements. The effect of the shot noise and detector readout noise on the measurement accuracy can be reduced by increasing the effective signal level by temporal or spatial averaging of the detected signal.

6.2.1 Independently Repeated Measurements

All sources of noise present in the measurements of the emitted radiation can be classified in two categories:

(1) The temporal (time varying) noise sources represented by radiation shot noise and rms detector readout noise. The effect of these noise sources on the accuracy of the measurement is also time varying and can only be described in statistical terms.

(2) Permanent noise sources represented by the inaccuracies in the specifications of the instrument spectral characteristics. This includes the inaccurate knowledge of the detector spectral responsivity and spectral transmittance of any filters used during the measurement. In addition, such factors as scattering and reflection of the radiation can also be considered as the source of permanent noise.

It is well known from classical statistics [5] that the standard deviation of any measurement with a normally distributed random noise can be decreased by substituting the single measurement with an average of n measurements of the same source. In this case the improvement in resulting standard deviation of the measurement is proportional to the square root of the number of averaged independent measurements. This technique can be

applied to the reduction of the effects of temporal radiation and detector noise on the accuracy of the radiometric measurements. The resulting values of NEΔT for 4, 25 and 100 averaged measurements are shown in Tables 2-4.

The inspection of Tables 2-4 shows that in the cases of broadband, narrow-band, and ratio radiometry the resulting improvement in the temperature accuracy is exactly proportional to the square root of the number of averaged measurements. The improvement of the accuracy of MWIP methods is slightly lower due to the fact that some implicit averaging is already built-in in the least-squares fitting procedure.

Table 2 NEΔT resulting from 4 measurements per filter.

Method of Temperature Measurement	**Black Body** $\varepsilon = 1$ (°C)	**Color Body** $\varepsilon = a + b \cdot \lambda$ (°C)	**Color Body** $\varepsilon = a + b \cdot \lambda + c \cdot \lambda^2$ (°C)
Wide-Band Radiometry ($\Delta\lambda = 3$ μm)	0.126		
Narrow-Band Radiometry ($\lambda = 1.5$ μm)	0.085		
Ratio Radiometry ($\lambda_1 = 1.5$ μm , $\lambda_2 = 3.0$ μm)	0.282		
Multi Wavelength Radiometry (linear emissivity model)	0.170	0.594	56.0
Multi Wavelength Radiometry (quadratic emissivity model)	0.588	2.20	1.18

Table 3 NEΔT resulting from 25 measurements per filter.

Method of Temperature Measurement	Black Body $\varepsilon = 1$ (°C)	Color Body $\varepsilon = a + b \cdot \lambda$ (°C)	Color Body $\varepsilon = a + b \cdot \lambda + c \cdot \lambda^2$ (°C)
Wide-Band Radiometry ($\Delta\lambda$ = 3 μm)	0.050		
Narrow-Band Radiometry (λ = 1.5 μm)	0.034		
Ratio Radiometry (λ_1 = 1.5 μm , λ_2 = 3.0 μm)	0.113		
Multi Wavelength Radiometry (linear emissivity model)	0.091	0.290	56.0
Multi Wavelength Radiometry (quadratic emissivity model)	0.326	1.047	0.677

Table 4 NEΔT resulting from 100 measurements per filter.

Method of Temperature Measurement	Black Body $\varepsilon = 1$ (°C)	Color Body $\varepsilon = a + b \cdot \lambda$ (°C)	Color Body $\varepsilon = a + b \cdot \lambda + c \cdot \lambda^2$ (°C)
Wide-Band Radiometry ($\Delta\lambda$ = 3 μm)	0.025		
Narrow-Band Radiometry (λ = 1.5 μm)	0.017		
Ratio Radiometry (λ_1 = 1.5 μm , λ_2 = 3.0 μm)	0.056		
Multi Wavelength Radiometry (linear emissivity model)	0.049	0.161	56.0
Multi Wavelength Radiometry (quadratic emissivity model)	0.177	0.585	0.370

It might be interesting to note that in the case of temperature measurements by an IR imager with a large number of closely spaced

detectors this noise reduction technique does not necessarily require the independent signal measurements to be performed sequentually with the same detector. It may be assumed that a relatively small number of adjacent detectors measure the radiation emitted from a small surface area with the same temperature. Therefore, the signal levels detected by adjacent detectors can be considered as independent measurements of the same radiation signal. This approach represents the tradeoff between the resulting spatial resolution of the imager and the time required to obtain n independent signal measurements which can be averaged for the purpose of noise reduction.

6.2.2 Calibration

The technique of noise reduction effected by taking the average of independent measurements does not apply in the case of permanent, time independent noise sources, such as reflection, atmospheric absorption, and inaccurate specification of the spectral characteristics of the system. The primary method of the reduction of the effects of these noise sources on the accuracy of radiometric measurement is the calibration of the imager system. The properly performed calibration should provide an accurate description of the spectral characteristics of the system. An additional purpose of the calibration is to develop the correction factors which will allow one to offset

the effects of all other noise sources which are not accounted for by the system model.

One way to approach the problem of the calibration is based on the reference wavelength method described in Chapter 4. According to this method the spectral transmittance of the filter is described by its moments. These moments are determined by numerical integration of the Eq. (3-17) reproduced here for convenience

$$\int_0^{\infty} (\lambda - \lambda_o)^n \cdot \tau(\lambda) d\lambda = a_n \cdot \tau(\lambda_o) \cdot (\Delta\lambda)^{n+1} \qquad (3\text{-}17)$$

where $\Delta\lambda$ - is the bandwidth of the filter at half of its peak transmittance,

λ_o - is the mean wavelength of the filter corresponding to $a_1=0$.

The spectral transmission of the filter should be first determined by a spectroradiometer or other means. Coates [6] points out that better results may be obtained by analyzing the spectral characteristics of the entire optical system of the imager with an installed filter, rather than measuring the individual transmittances of the filter, lens of objective, etc. In other words, the commulative effect of the spectral characteristics of each element of the optical assembly can be considered as the spectral properties of the filter.

Once the spectral transmittance of the system has been measured, the value of each moment can be determined by numerical integration of

Eq. (3-17). Coates [5] notes that in most practical situations for roughly symmetrical filters with fractional bandwidth $\Delta\lambda/\lambda_o$ of 1.5% or less the signal accuracy of better than 0.01% can be achieved with measurement of filter transmittance to an accuracy of about 10%. Moreover, such accuracy of signal modeling is usually achieved with utilization of only the first three moments.

The second step in the calibration process involves the measurement of the output signal of the imager viewing the blackbody radiator with known temperature. Based on this measurement the actual value of the product $G \cdot R(\lambda_o)$ can be computed, where the coefficient G represents the geometrical characteristics of the system and is given by Eq. (3-40). Finally, it must be noted that additional calibration procedures might be needed depending on the particular conditions of the measurements.

CHAPTER 7

CONCLUSIONS

This thesis analyzes the limitations on of the accuracy of temperature measurements performed by the means of imaging pyrometry. The presented analysis is based on the developed radiometric model of an IR image sensor. This model places special emphasis on an accurate description of the spectral characteristics of the system. The application of reference wavelength approach for the description of the spectral transmittance of the optical system allowed to perform accuracy analysis which to our knowledge has not been published in the radiometric literature.

The analysis presented in this work provides the estimation of the temperature measurements accuracy achievable by the methods of wide-band, narrow-band, ratio, and multi-wavelength pyrometry.

It was demonstrated that the accuracy of the temperature measurements can be improved by controlling the optical integration time of the imager. This technique allows to maintain high signal-to-noise ratio, limited only by maximum charge handling capacity of the imager, Q_{max}. It was shown that wide-band ($\Delta\lambda$=3 μm) measurements performed by a 320x244 IR imager with PtSi Schottky-barrier detectors can yield temperature resolution of 0.25 °C in the case of a blackbody radiator at 1000 °C and the signal level of 10^6 electrons per pixel. For the case of

radiation detection through the 100-nm-wide Gaussian filter with peak wavelength at 1.5 μm the corresponding accuracy of the temperature measurements is 0.17 °C.

The method of ratio radiometry analyzed in this work provides the means of the temperature measurement of the graybody radiator with unknown emissivity. It might be interesting to note that for the case of blackbody radiator, the accuracy of ratio method is slightly inferior to the accuracy achievable by narrow-band radiometry. Furthermore, due to the unrealistic requirement of constant spectral emissivity, in many practical situations the method of ratio radiometry does not provide accurate temperature estimates [11].

The analysis presented in this thesis demonstrates, that the temperature of the remote radiant target with unknown emissivity can be successfully measured most efficiently by the means of multi-wavelength imaging pyrometry. In theory, the MWIP technique is capable of providing accurate estimation of the temperature of the radiator with arbitrary shape of the spectral emissivity. However, due to the practical limitations imposed on the spectral bandwidth and amount of measurements, some knowledge of the spectral emissivity of the target is desirable. The prior knowledge of the spectral characteristics of emissivity, permits to select emissivity model with optimum number of parameters, thus minimizing the degree of freedom of the least-squares algorithm used in MWIP.

The temperature accuracy of multi-wavelength pyrometry was analyzed for linear and quadratic emissivity models. The presented results show that for targets with linear spectral emissivity the MWIP with six 100-nm-wide filters is capable of providing temperature resolution of 0.6 °C for 1000 °C target temperature and maximum detected signal of 10^6 electrons per pixel. For the targets with quadratic emissivity the temperature accuracy of 6-filter MWIP was found to be about 1 °C for target temperature of 1000 °C at the maximum detected signal of $4x10^6$ electrons per pixel. For target temperature of 500 °C the corresponding accuracy was found to be 0.28 °C in the case of linear target emissivity and 0.42 in the case of quadratic target emissivity assuming a maximum detected signal of $4x10^6$ electrons per pixel. It should be noted that these results apply to the measurements with correctly selected emissivity models. The temperature measurements of the targets with linear emissivity by 6-filter MWIP using quadratic emissivity model yield the accuracy of about 1 °C for target temperature 1000 °C and $25x10^6$ electrons per pixel maximum signal. The use of linear emissivity model for temperature measurement of target with quadratic emissivity leads to rather high errors in the estimated temperature.

Finally, for the purpose of performing practical measurements, an accurate calibration of the optical system is necessary. It should also be mentioned, that the least-squares algorithm used in this work may not be

effective for real-time on-line measurements. The selection of the real-time least-squares based algorithm should take advantage of the past history and the dynamics of the system.

APPENDIX

Program Modeling Detected Signal

The following program performs the simulation of the signal detected by IR imager according to the model presented in Chapter 3.

```
# include <stdio.h>
# include <stdlib.h>
# include <math.h>
# define PI 3.141592653589793
# define A2 0.1803
# define A4 0.0976
# define C1 1.1911E+8
# define C2 1.4388E+4
# define AREA 1.6E-9
# define FILL 0.39
# define FN 2
# define FREQUENCY 30
# define ELECTRON 1.602177E-19
# define PSIMS 0.2272
# define CONE 0.12402
# define WIDTH 0.1
# define B1 0.225272727
# define B2 0.158575758
# define B3 -0.0148484848
# define ONE 1
# define NP 4
FILE *fp1;

long float HIGH,T;
int N;
```

```
/* This program simulates the signal detected by IR imager.
The signal has the noise level corresponding to shot noise+
readout noise of 200 electrons per pixel. The output is
formatted according to the requirements for the input to
least-squares routine*/
main()
{
 long float radiance();
 long float signal();
 long float sigma();
 long float random();
 long float t,lambda1,lambda2,noise,noisysig,l1,l2,step,maxsig;
 int i,k,rn0;

 fp1=fopen("SIGNAL.DAT","w");

printf("enter temperature");
scanf("%lf",&t);
printf("enter shortest wavelength");
scanf("%lf",&l1);
printf("enter longest wavelength");
scanf("%lf",&l2);
printf("enter number of filters");
scanf("%d",&N);
printf("enter number of measurements per filter");
scanf("%d",&k);
srand(100);
lambda1=l1;
step=(l2-lambda1)/(N-1);

/* calculate the HIGHT so that the maximum signal for this
temperature is equal 1.E+6 */

 maxsig=-1.;
```

```
 HIGHT=0.1;
 for(lambda2=l1; lambda2<=(l2+0.1*step); lambda2+=step*0.1) {
 if (signal(lambda2,t) > maxsig ) maxsig=signal(lambda2,t);}
 HIGHT=HIGHT*1.E+6/maxsig;

fprintf(fp1,"%2d\t%3d\t%3d\t%3d\t%10.5f\t%10.5f\n",k*N,ONE,NP,ONE,
WIDTH,HIGHT);
fprintf(fp1,"%5.3f\t%7.3f\t%7.3f\t%7.3f\n",0.1,0.1,0.1,100.0);

 for(lambda2=l1; lambda2<=(l2+0.1*step); lambda2+=step) {

for (i=1; i<=k; ++i) {
noise=sqrt(200*200+signal(lambda2,t))*random();
noisysig=signal(lambda2,t)+noise;

fprintf(fp1,"%20.15f\t%20.14f\n",lambda2,noisysig);
            }
}
fclose(fp1);
}

/* The following subroutine computes the blackbody radiance */
long float radiance(lambda, t)
long float lambda,t;
{
 long float x,l;
 x=C2/(lambda*t);
 l=(exp(x)-1.)*lambda*lambda*lambda*lambda*lambda;
 return(C1/l);
}

/* The following subroutine computes detected signal without noise */
long float signal(lambda , t)
long float lambda,t;
```

```
{
 long float radiance();
 long float sigma();
 long float response,s,emiss;

 response=1.-PSIMS*lambda/1.24;
 response*=CONE*response;   /* spectral responsivity of the imager */

 s=1.+(A2*WIDTH*WIDTH/(lambda*lambda))*sigma(lambda,t,response);
 s*=WIDTH*radiance(lambda,t);
 s*=(HIGHT*AREA*FILL*PI/(4.*FN*FN))*response;
 emiss=B1+B2*lambda+B3*lambda*lambda;  /* emissivity model */
 return(s*emiss/(FREQUENCY*ELECTRON));
}

/* The following subroutine computes the filter shape factors */
long float sigma(lambda, t,response)
long float lambda,t,response;
{
 long float x,r1,r2,l1,l2,l3,l4,emiss,e1,e2,sigm;
 x=C2/(lambda*t);
 emiss=B1+B2*lambda+B3*lambda*lambda;
 e1=(B2+2*B3*lambda)/emiss;
 e2=B3/emiss;
 r1=-(2.*CONE*PSIMS/1.24)*(1.-(PSIMS/1.24)*lambda);
 r1=r1/response;
 r2=2*CONE*PSIMS*PSIMS/(1.24*1.24);
 r2=r2/(2*response);
 l1=(x*exp(x))/(exp(x)-1.)-5.;
 l1=l1/lambda;
 l2=(x*x*exp(x))/((exp(x)-1.)*(exp(x)-1.));
 l2-=(((x*x/2.)+6.*x)*exp(x))/(exp(x)-1.);
 l2+=15.;
 l2=l2/(lambda*lambda);
```

```
 sigm=(l2+(r1+e1)*l1+r2+r1*e1+e2)*lambda*lambda;

 return(sigm);
}

/* The following subroutine represents random number generator.
The generated random numbers are normally distributed with the
mean 0 and standard deviation 1. This subroutine is utilized in
the simulation of the radiation and readout noises */
float random()
{
long float u1,u2,r,a;
u1=rand()*4.656612875E-10;
u2=rand()*4.656612875E-10;
r=sqrt(-2*log(u1));
a=2*PI*u2;
return(r*sin(a));
}
```

Program Performing Temperature Accuracy Estimation

The following program computes the temperature accuracy achievable by the methods of narrow-band, ratio, and multiwavelength radiometry. The computations are performed in accordance with the development of Chapters 3, 4, and 5.

```
# include <stdio.h>
# include <stdlib.h>
# include <math.h>
# define PI 3.141592653589793
# define A2 0.1803
# define A4 0.0976
```

```
# define C1 1.1911E+8
# define C2 1.4388E+4
# define AREA 1.6E-9
# define FILL 0.39
# define FN 2
# define FREQUENCY 30
# define ELECTRON 1.602177E-19
# define PSIMS 0.2272
# define CONE 0.12402
# define WIDTH 0.1
# define B1 0.68714286
# define B2 0.0085714286
# define B3 0.
# define ONE 1
# define NP 3

FILE *fp2,*fp1,*fp3;

long float x,l1,l2,l3,lt,l1t,l2t,e1,e2,ea,eb,r1,r2,ka,kb,k1,kt,kk;
long float sigmaa,sigmab,sigmal,sigmat;

/* This program calculates standard deviations of temperature for
the case of MWIP with the linear emissivity model. For linear model
the parameter IFIXB(3) should be equal to 0 in mwip.f
This version takes into account the derivatives of k(a,b,T,lambda)
The program also computes the temperature accuracy of narrow-band
and ratio radiometry*/

long float HIGHT,step;
int N;
main()
{
 long float radiance();
 long float signal();
```

```
long float sigma();
long float sdt();
long float emissivity ();
long float response ();
long float derivatives();
long float dtll();
long float dtl();
long float sdx,lambda1,lambda2,lambda,t,maxsig;
int k;

fp2=fopen("sdt_mwip.dat","w");

printf("enter temperature");
scanf("%lf",&t);
printf("enter shortest wavelength");
scanf("%lf",&l1);
printf("enter longest wavelength");
scanf("%lf",&l2);
printf("enter number of filters");
scanf("%d",&N);
printf("enter number of measurements per filter");
scanf("%d",&k);
printf("Enter procentage of error in positioning the filters");
scanf("%lf",&sdx);

sdx*=WIDTH;

 for(N=4; N<=10; ++N) {
 step=(lambda2-lambda1)/(N-1);

fprintf(fp2,"%4.2f\t%3d\t%2d\t",WIDTH,k,N);

      for(t=273.0+500.; t<=273.0+1100.; t+=100.0) {
```

```
/* calculate the HIGHT so that the maximum signal for this
temperature is equal 1.E+6 */

 maxsig=-1.;
 HIGHT=0.1;
 for(lambda=lambda1; lambda<=(lambda2+0.01*step); lambda+=0.1*step) {
 if (signal(lambda,t) > maxsig ) maxsig=signal(lambda,t);}
 HIGHT=HIGHT*1.E+6/maxsig;

      fprintf(fp2,"%4.3f\t",sdt(t,sdx,lambda1,lambda2,k));

      }
 fprintf(fp2,"\n");
}
fclose(fp2);
dtll(k,sdx);
dtl(k,sdx);
}

/* The following subroutine computes the blackbody radiance */
long float radiance(lambda, t)
long float lambda,t;
{
 long float l;
 l=(exp(x)-1.)*lambda*lambda*lambda*lambda*lambda;
 return(C1/l);
}

/* The following program computes the spectral responsivity
of the imager according to Fowler equation */
long float response(lambda)
long float lambda;
{
long float resp;
```

```
 resp=1.-PSIMS*lambda/1.24;
 resp*=CONE*resp;
return(resp);
}

/* Emissivity model */
long float emissivity(lambda)
long float lambda;
{
return(B1+B2*lambda+B3*lambda*lambda);
}

/* The following subroutine computes detected signal without noise */
long float signal(lambda , t)
long float lambda,t;
{
 long float radiance();
 long float sigma();
 long float emissivity ();
 long float response ();
 long float s,sigm,G;
 sigm=sigma(lambda,t);
 G=(HIGHT*AREA*FILL*PI/(4.*FN*FN))*WIDTH;
 kk=G*(1.+(A2*WIDTH*WIDTH/(lambda*lambda))*sigm);
 s=kk*response(lambda)*radiance(lambda,t)*emissivity(lambda);
 k1=G*A2*WIDTH*WIDTH/(lambda*lambda)*(sigmal-
2*sigm/lambda)/kk;
 ka=G*A2*WIDTH*WIDTH/(lambda*lambda)*sigmaa/kk;
 kb=G*A2*WIDTH*WIDTH/(lambda*lambda)*sigmab/kk;
 kt=G*A2*WIDTH*WIDTH/(lambda*lambda)*sigmat/kk;
 return(s/(FREQUENCY*ELECTRON));
}

/* The following program computes the partial derivatives
```

```
of the signal with respect to temperature, wavelength and
the parameters of the emissivity model */
long float derivatives(lambda,t)
long float lambda,t;
{
 long float radiance();
 long float sigma();
 long float emissivity ();
 long float response ();

 x=C2/(lambda*t);

 e1=(B2+2*B3*lambda)/emissivity(lambda);
 e2=B3/emissivity(lambda);
 ea=1./emissivity(lambda);
 eb=lambda/emissivity(lambda);

 r1=-(2.*CONE*PSIMS/1.24)*(1.-(PSIMS/1.24)*lambda);
 r1=r1/response(lambda);
 r2=CONE*PSIMS*PSIMS/(1.24*1.24);
 r2=r2/(response(lambda));

 l1=(x*exp(x))/(exp(x)-1.)-5.;
 l1=l1/lambda;
 l2=(x*x*exp(x))/((exp(x)-1.)*(exp(x)-1.));
 l2-=(((x*x/2.)+6.*x)*exp(x))/(exp(x)-1.);
 l2+=15.;
 l2=l2/(lambda*lambda);
 l3=(x*x*x/6.-7.*x*x/2.+21.*x-35.)/(lambda*lambda*lambda);
 lt=(x*exp(x))/(t*(exp(x)-1));
 l1t=(x*x*exp(x)*(x/(exp(x)-1)-1))/(C2*(exp(x)-1));
 l2t=x*(6.-x)/(lambda*lambda*t);
}
```

```
/* The following subroutine computes the filter shape factors */
long float sigma(lambda, t)
long float lambda,t;
{
 long float sigm;
 long float emissivity ();
 long float derivatives();

 derivatives(lambda,t);

 sigm=(l2+(r1+e1)*l1+r2+r1*e1+e2)*lambda*lambda;
 sigmaa=-
(lambda*lambda*B2)*(r1+l1)/(emissivity(lambda)*emissivity(lambda));

sigmab=(lambda*lambda*B1)*(r1+l1)/(emissivity(lambda)*emissivity(lamb
da));
 sigmat=lambda*lambda*(l2t+(r1+e1)*l1t);
 sigmal=3*l3-l1*l3+(2*r2-r1*r1-e1*e1)*l1+(r1+e1)*(2*l1-l2*l2);
 sigmal+=(2*r2-r1*r1)*e1-e1*e1*r1;
 sigmal*=lambda*lambda;
 sigmal+=2.*sigm/lambda;

 return(sigm);
}

/* The following program computes the resulting from MWIP
temperature accuracy (standard deviation) */
long float sdt(t,sdx,l1,l2,k)
long float t,sdx,l1,l2;
int k;
{
 long float denom,D,alfa[4][4],der[4];
 long float lambda;
 long float signal();
```

```
int j,m;

for(j=1; j<=NP; ++j) {
for(m=1; m<=NP; ++m) {
alfa[j][m]=0.;}}

for(lambda=l1; lambda<=(l2+0.1*step); lambda+=step) {

denom=1+signal(lambda,t)*sdx*sdx*(e1+k1+r1+l1)*(e1+k1+r1+l1);
der[1]=ea+ka;
der[2]=eb+kb;
der[3]=lt+kt;
for(j=1; j<=3; j+=1) {
for(m=1; m<=3; m+=1) {
alfa[j][m]+=k*signal(lambda,t)*der[j]*der[m]/denom;}}
}
D=alfa[1][1]*(alfa[2][2]*alfa[3][3]-alfa[3][2]*alfa[3][2]);
D=D-alfa[1][2]*(alfa[1][2]*alfa[3][3]-alfa[1][3]*alfa[2][3]);
D+=alfa[1][3]*(alfa[1][2]*alfa[2][3]-alfa[1][3]*alfa[2][2]);
return(sqrt((alfa[1][1]*alfa[2][2]-alfa[1][2]*alfa[1][2])/D));
}

/* The following program computes the accuracy of the
ratio radiometry */
long float dtll (k,sdx)
long float sdx;
int k;
{
long float lambda1,lambda2,lambda,maxsig,t,dt,s1,s2,ds1,ds2,dtds1,dtds2;
long float signal();

 fp1=fopen("dtll1000CQmax.dat","w");

t=1273.;
```

```
maxsig=-1.;
HIGHT=0.1;

for(lambda1=1.5; lambda1<=4.5; lambda1+=0.05) {

fprintf(fp1,"%4.2f\t%3d\t%4.1f\t%3.2f\t",WIDTH,k,t,lambda1);

for(lambda2=1.5; lambda2<=4.5; lambda2+=0.5) {

s1=signal(lambda1,t);
s2=signal(lambda2,t);
if (s1>s2) HIGHT=HIGHT*1.E+6/s1;
else
HIGHT=HIGHT*1.E+6/s2;

s1=signal(lambda1,t);
s2=signal(lambda2,t);

ds1=s1*(1./k+s1*sdx*sdx*(e1+k1+r1+l1)*(e1+k1+r1+l1));
ds2=s2*(1./k+s2*sdx*sdx*(e1+k1+r1+l1)*(e1+k1+r1+l1));

dtds1=lambda1*lambda2*t*t/(C2*(lambda2-lambda1)*s1);
dtds2=lambda1*lambda2*t*t/(C2*(lambda2-lambda1)*s2);

dt=sqrt(dtds1*dtds1*ds1+dtds2*dtds2*ds2);
printf("s1=%7.1f\ts2=%7.1f\n",s1,s2);
      fprintf(fp1,"%4.4f\t",dt);
      }
 fprintf(fp1,"\n");
}
fclose(fp1);
}
```

```
/* The following program computes the accuracy of
narrow-band radiometry */
long float dtl (k,sdx)
long float sdx;
int k;
{
long float lambda,maxsig,sig,t,dt,ds,dsdt;
long float signal();
fp3=fopen("dtlQmax10E6.dat","w");

 for(lambda=1.5; lambda<=4.5; lambda+=0.1) {

fprintf(fp3,"%4.2f\t%3d\t%3.2f\t",WIDTH,k,lambda);

 for(t=500+273.;t<=1100+273.;t+=100.) {

/* calculate the HIGHT so that the maximum signal
is equal to 1.E+6 */

 HIGHT=0.1;
 maxsig=signal(lambda,t);
 HIGHT=HIGHT*1.E+6/maxsig;

sig=signal(lambda,t);
ds=sig*(1./k+sig*sdx*sdx*(e1+k1+r1+l1)*(e1+k1+r1+l1));
dsdt=sig*(lt+kt);
dt=sqrt(ds)/dsdt;

      fprintf(fp3,"%4.4f\t",dt);
      }
 fprintf(fp3,"\n");
}
fclose(fp3);
}
```

User-Supplied Subroutine for Least-Squares Package ODRPACK

This subroutine specifies the fitting function and the environment parameters for the leas-squares package ODRPACK.

```
      PROGRAM MWIP
C  ODRPACK ARGUMENT DEFINITIONS
C     ==> FCN     NAME OF THE USER SUPPLIED FUNCTION SUBROUTINE
C     ==> N       NUMBER OF OBSERVATIONS
C     ==> M       COLUMNS OF DATA IN THE EXPLANATORY VARIABLE
C     ==> NP      NUMBER OF PARAMETERS
C     ==> NQ      NUMBER OF RESPONSES PER OBSERVATION
C    <==> BETA    FUNCTION PARAMETERS
C     ==> Y       RESPONSE VARIABLE
C     ==> LDY     LEADING DIMENSION OF ARRAY Y
C     ==> X       EXPLANATORY VARIABLE
C     ==> LDX     LEADING DIMENSION OF ARRAY X
C     ==> WE      "EPSILON" WEIGHTS
C     ==> LDWE    LEADING DIMENSION OF ARRAY WE
C     ==> LD2WE   SECOND DIMENSION OF ARRAY WE
C     ==> WD      "DELTA" WEIGHTS
C     ==> LDWD    LEADING DIMENSION OF ARRAY WD
C     ==> LD2WD   SECOND DIMENSION OF ARRAY WD
C     ==> IFIXB   INDICATORS FOR "FIXING" PARAMETERS (BETA)
C     ==> IFIXX   INDICATORS FOR "FIXING" EXPLANATORY VARIABLE (X)
C     ==> LDIFX   LEADING DIMENSION OF ARRAY IFIXX
C     ==> JOB     TASK TO BE PERFORMED
C     ==> NDIGIT  GOOD DIGITS IN SUBROUTINE FUNCTION RESULTS
C     ==> TAUFAC  TRUST REGION INITIALIZATION FACTOR
C     ==> SSTOL   SUM OF SQUARES CONVERGENCE CRITERION
C     ==> PARTOL  PARAMETER CONVERGENCE CRITERION
C     ==> MAXIT   MAXIMUM NUMBER OF ITERATIONS
```

```
C     ==> IPRINT   PRINT CONTROL
C     ==> LUNERR   LOGICAL UNIT FOR ERROR REPORTS
C     ==> LUNRPT   LOGICAL UNIT FOR COMPUTATION REPORTS
C     ==> STPB     STEP SIZES FOR FINITE DIFFERENCE DERIVATIVES WRT
BETA
C     ==> STPD     STEP SIZES FOR FINITE DIFFERENCE DERIVATIVES WRT
DELTA
C     ==> LDSTPD   LEADING DIMENSION OF ARRAY STPD
C     ==> SCLB     SCALE VALUES FOR PARAMETERS BETA
C     ==> SCLD     SCALE VALUES FOR ERRORS DELTA IN EXPLANATORY
VARIABLE
C     ==> LDSCLD   LEADING DIMENSION OF ARRAY SCLD
C    <==> WORK     DOUBLE PRECISION WORK VECTOR
C     ==> LWORK    DIMENSION OF VECTOR WORK
C    <==  IWORK    INTEGER WORK VECTOR
C     ==> LIWORK   DIMENSION OF VECTOR IWORK
C    <==  INFO     STOPPING CONDITION

C PARAMETERS SPECIFYING MAXIMUM PROBLEM SIZES HANDLED BY
THIS DRIVER
C    MAXN        MAXIMUM NUMBER OF OBSERVATIONS
C    MAXM        MAXIMUM NUMBER OF COLUMNS IN EXPLANATORY
VARIABLE
C    MAXNP       MAXIMUM NUMBER OF FUNCTION PARAMETERS
C    MAXNQ       MAXIMUM NUMBER OF RESPONSES PER OBSERVATION

C PARAMETER DECLARATIONS AND SPECIFICATIONS
      INTEGER
LDIFX,LDSCLD,LDSTPD,LDWD,LDWE,LDX,LDY,LD2WD,LD2WE,
     +        LIWORK,LWORK,MAXM,MAXN,MAXNP,MAXNQ
      PARAMETER (MAXM=5,MAXN=600,MAXNP=5,MAXNQ=1,
     +        LDY=MAXN,LDX=MAXN,
     +        LDWE=MAXN,LD2WE=1,LDWD=1,LD2WD=1,
     +        LDIFX=1,LDSTPD=1,LDSCLD=1,
```

```
     +       LWORK=18 + 11*MAXNP + MAXNP**2 + MAXM + MAXM**2 +
     +          4*MAXN*MAXNQ + 6*MAXN*MAXM +
2*MAXN*MAXNQ*MAXNP +
     +          2*MAXN*MAXNQ*MAXM + MAXNQ**2 +
     +          5*MAXNQ + MAXNQ*(MAXNP+MAXM) +
LDWE*LD2WE*MAXNQ,
     +       LIWORK=20+MAXNP+MAXNQ*(MAXNP+MAXM))

C  VARIABLE DECLARATIONS
      INTEGER       I,INFO,IPRINT,J,JOB,L,LUNERR,LUNRPT,M,MAXIT,N,
     +          NDIGIT,NP,NQ
      INTEGER       IFIXB(MAXNP),IFIXX(LDIFX,MAXM),IWORK(LIWORK)
      DOUBLE PRECISION PARTOL,SSTOL,TAUFAC
      DOUBLE PRECISION
BETA(MAXNP),SCLB(MAXNP),SCLD(LDSCLD,MAXM),
     +          STPB(MAXNP),STPD(LDSTPD,MAXM),
     +          WD(LDWD,LD2WD,MAXM),WE(LDWE,LD2WE,MAXNQ),
     +          WORK(LWORK),X(LDX,MAXM),Y(LDY,MAXNQ)
       DOUBLE PRECISION WIDTH,HEIGHT
         COMMON /MINE/ WIDTH,HEIGHT
      EXTERNAL      FCN


C  SPECIFY DEFAULT VALUES FOR DODRC ARGUMENTS
      WE(1,1,1)  = -1.0D0
      WD(1,1,1)  = -1.0D0
      IFIXB(1)   = -1
      IFIXX(1,1) =  0
      JOB        =  12
      NDIGIT     = -1
      TAUFAC     = -1.0D0
      SSTOL      = -1.0D0
      PARTOL     = -1.0D0
      MAXIT      =  1000
```

```
      IPRINT    = -1
      LUNERR    = -1
      LUNRPT    = -1
      STPB(1)   = -1.0D0
      STPD(1,1) = -1.0D0
      SCLB(1)   = -1.0D0
      SCLD(1,1) = -1.0D0

C  SET UP ODRPACK REPORT FILES
      LUNERR =  9
      LUNRPT =  9
      OPEN (UNIT=9,FILE='REPORT.mine')

C  READ PROBLEM DATA, AND SET NONDEFAULT VALUE FOR ARGUMENT
IFIXX
      OPEN (UNIT=5,FILE='SIGNAL.DAT')
      READ (5,FMT=*) N,M,NP,NQ,WIDTH,HEIGHT
      READ (5,FMT=*) (BETA(I),I=1,NP)
      DO 10 I=1,N
        READ (5,FMT=*) (X(I,J),J=1,M),(Y(I,L),L=1,NQ)
C       IF (X(I,1).EQ.0.0D0 .OR. X(I,1).EQ.100.0D0) THEN
C         IFIXX(I,1) = 0
C       ELSE
C         IFIXX(I,1) = 1
C       END IF
        WE(I,1,1)=1.0D0/(200.0D0*200.0D0+Y(I,1))
   10 CONTINUE

C  SPECIFY TASK: EXPLICIT ORTHOGONAL DISTANCE REGRESSION
C             WITH USER SUPPLIED DERIVATIVES (CHECKED)
C             COVARIANCE MATRIX CONSTRUCTED WITH RECOMPUTED
DERIVATIVES
C             DELTA INITIALIZED TO ZERO
C             NOT A RESTART
```

```
C  AND INDICATE SHORT INITIAL REPORT
C          SHORT ITERATION REPORTS EVERY ITERATION, AND
C          LONG FINAL REPORT
      JOB    = 00012
      IPRINT = 2113

C  COMPUTE SOLUTION
      CALL DODRC(FCN,
     +          N,M,NP,NQ,
     +          BETA,
     +          Y,LDY,X,LDX,
     +          WE,LDWE,LD2WE,WD,LDWD,LD2WD,
     +          IFIXB,IFIXX,LDIFX,
     +          JOB,NDIGIT,TAUFAC,
     +          SSTOL,PARTOL,MAXIT,
     +          IPRINT,LUNERR,LUNRPT,
     +          STPB,STPD,LDSTPD,
     +          SCLB,SCLD,LDSCLD,
     +          WORK,LWORK,IWORK,LIWORK,
     +          INFO)
      END

      SUBROUTINE FCN(N,M,NP,NQ,
     +               LDN,LDM,LDNP,
     +               BETA,XPLUSD,
     +               IFIXB,IFIXX,LDIFX,
     +               IDEVAL,F,FJACB,FJACD,
     +               ISTOP)

C  SUBROUTINE ARGUMENTS
C     ==> N      NUMBER OF OBSERVATIONS
C     ==> M      NUMBER OF COLUMNS IN EXPLANATORY VARIABLE
C     ==> NP     NUMBER OF PARAMETERS
C     ==> NQ     NUMBER OF RESPONSES PER OBSERVATION
```

```
C     ==> LDN     LEADING DIMENSION DECLARATOR EQUAL OR
EXCEEDING N
C     ==> LDM     LEADING DIMENSION DECLARATOR EQUAL OR
EXCEEDING M
C     ==> LDNP    LEADING DIMENSION DECLARATOR EQUAL OR
EXCEEDING NP
C     ==> BETA    CURRENT VALUES OF PARAMETERS
C     ==> XPLUSD  CURRENT VALUE OF EXPLANATORY VARIABLE, I.E., X +
DELTA
C     ==> IFIXB   INDICATORS FOR "FIXING" PARAMETERS (BETA)
C     ==> IFIXX   INDICATORS FOR "FIXING" EXPLANATORY VARIABLE (X)
C     ==> LDIFX   LEADING DIMENSION OF ARRAY IFIXX
C     ==> IDEVAL  INDICATOR FOR SELECTING COMPUTATION TO BE
PERFORMED
C     <== F       PREDICTED FUNCTION VALUES
C     <== FJACB   JACOBIAN WITH RESPECT TO BETA
C     <== FJACD   JACOBIAN WITH RESPECT TO ERRORS DELTA
C     <== ISTOP   STOPPING CONDITION, WHERE
C                   0 MEANS CURRENT BETA AND X+DELTA WERE
C                     ACCEPTABLE AND VALUES WERE COMPUTED
SUCCESSFULLY
C                   1 MEANS CURRENT BETA AND X+DELTA ARE
C                     NOT ACCEPTABLE;  ODRPACK SHOULD SELECT VALUES
C                     CLOSER TO MOST RECENTLY USED VALUES IF POSSIBLE
C                  -1 MEANS CURRENT BETA AND X+DELTA ARE
C                     NOT ACCEPTABLE;  ODRPACK SHOULD STOP

C  INPUT ARGUMENTS, NOT TO BE CHANGED BY THIS ROUTINE:
      INTEGER         I,IDEVAL,ISTOP,L,LDIFX,LDM,LDN,LDNP,M,N,NP,NQ
      DOUBLE PRECISION BETA(NP),XPLUSD(LDN,M)
      INTEGER         IFIXB(NP),IFIXX(LDIFX,M)
C  OUTPUT ARGUMENTS:
      DOUBLE PRECISION
F(LDN,NQ),FJACB(LDN,LDNP,NQ),FJACD(LDN,LDM,NQ)
```

```
C  LOCAL VARIABLES
     INTRINSIC      DEXP
     DOUBLE PRECISION T,LAMBDA,EMISS,RESP,SIGMA,S,E1,E2,HEIGHT,PI,
    +L1,L2,LB,R1,R2,X,A2,C1,C2,AREA,FILL,FN,CONV,PSIMS,CONE,WIDTH
C DEFINE COMMON BLOCK FOR PASSING WIDTH AND HEIGHT
          COMMON /MINE/ WIDTH,HEIGHT
C PARAMETER DECLARATIONS
          PI=3.14159265358979323846264338327 9D0
       A2=0.1803D0
       C1=1.1911D+8
       C2=1.4388D+4
       AREA=1.6D-9
       FILL=0.39D0
       FN=2.D0
       CONV=2.083D+17
       PSIMS=0.2272D0
       CONE=0.12402D0
C
C RENAMING SOME VARIABLES
          T=BETA(4)
C  CHECK FOR UNACCEPTABLE VALUES FOR THIS PROBLEM
     IF (T .LT. 0.0D0) THEN
       ISTOP = 1
       RETURN
     ELSE
       ISTOP = 0
     END IF
C
C  COMPUTE PREDICTED VALUES
     IF (MOD(IDEVAL,10).GE.1) THEN
       DO 110 L = 1,NQ
         DO 100 I = 1,N
C COMPUTE SIGNAL
C
```

```
C RADIANCE
C
      LAMBDA=XPLUSD(I,1)
    X=C2/(LAMBDA*T)
    LB=(DEXP(X)-1.0D0)*LAMBDA*LAMBDA*LAMBDA*LAMBDA*LAMBDA
    LB=C1/LB
C
C RESPONSIVITY
C
    RESP=1.0D0-PSIMS*LAMBDA/1.24D0
    RESP=CONE*RESP*RESP
C
C EMISSIVITY
C
      EMISS=BETA(1)+BETA(2)*LAMBDA+BETA(3)*LAMBDA*LAMBDA
C
C VARIOUS DERIVATIVES
C
    R1=-(2.0D0*CONE*PSIMS/1.24D0)*(1.0D0-(PSIMS/1.24D0)*LAMBDA)
    R1=R1/RESP
    R2=2.0D0*CONE*PSIMS*PSIMS/(1.24D0*1.24D0)
    R2=R2/(2.0D0*RESP)
    L1=(X*DEXP(X))/(DEXP(X)-1.0D0)-5.0D0
    L1=L1/LAMBDA
    L2=(X*X*DEXP(X))/((DEXP(X)-1.0D0)*(DEXP(X)-1.0D0))
    L2=L2-(((X*X/2.0D0)+6.0D0*X)*DEXP(X))/(DEXP(X)-1.0D0)
    L2=L2+15.0D0
    L2=L2/(LAMBDA*LAMBDA)
      E1=(BETA(2)+2.0D0*BETA(3)*LAMBDA)/EMISS
      E2=(2.0D0*BETA(3))/(2.0D0*EMISS)
    SIGMA=(L2+(R1+E1)*L1+R2+R1*E1+E2)*LAMBDA*LAMBDA
C
C SIGNAL
C
```

```
S=EMISS*WIDTH*(1.0D0+(A2*WIDTH*WIDTH/(LAMBDA*LAMBDA))*SIGMA)*
LB
      S=S*(HEIGHT*AREA*FILL*PI/(4.0D0*FN*FN))*RESP*CONV
C OUTPUT FUNCTION (CORRECTED FOR INTEGRATION TIME AJUSTMENTS)
      F(I,L)=S
  100     CONTINUE
  110   CONTINUE
    END IF
    RETURN
    END
```

REFERENCES

1. DeWitt, D. P., and F. P. Incropera. "Physics of Thermal Radiation," in *Theory and Practice of Radiation Thermometry*, John Wiley & Sons, New York (1988)

2. Nutter, G. D. "Radiation Thermometers," in *Theory and Practice of Radiation Thermometry*, John Wiley & Sons, New York (1988)

3. Kosonocky, W. F. "Review of Infrared Image Sensors with Schottky-Barrier," Mita Press, Tokyo (1991)

4. Wolfe, W. L. "Radiometry," *Appl. Opt and Opt. Eng.* 8, 137 (1980)

5. Bevington, P. R. "Data Reduction and Error Analysis for the Physical Sciences," McGraw-Hill Book Co., New York (1969)

6. Coates, P. B. "Wavelength Specification in Optical and Photoelectric Pyrometry," *Metrologia* 13, 1 (1977)

7. J. Bezemer, "Spectral Sensitivity Corrections for Optical Standard Pyrometers," *Metrologia* 10, 47 (1974)

8. "Coates, P. B. Multi-Wavelength Pyrometry," *Metrologia* 17, 103 (1981)

9. Khan, M. A., et. al. "Noncontact Temperature Measurement: Interpolation Based Techniques," *Rev. Sci. Instrum.* 62, 393 (1991)

10. Tenney, A. S. "Radiation Ratio Thermometry," in *Theory and Practice of Radiation Thermometry*, John Wiley & Sons, New York (1988)

11. Khan, M. A., et. al. "Noncontact Temperature Measurement: Least Squares Based Techniques," *Rev. Sci. Instrum.* 62, 403 (1991)

12. Gardner, J. L. "Computer Modelling of a Multiwavelength Pyrometry for Measuring True Surface Temperature," *High Temp.-High Pressures* 12, 699 (1980)

13. DeWitt, D. P., and J.C. Richmond. "Thermal Radiative Properties of Materials," in *Theory and Practice of Radiation Thermometry*, John Wiley & Sons, New York (1988)

14. Boggs, P. T., et. al. "User's Reference Guide for ODRPACK Version 2.00 Software for Weighted Orthogonal Distance Regression," Natioanl Institute of Standards and Technology (1992)

15. Sato, T. "Spectral Emissivity of Silicon," *Japaneese J. of Appl. Phys.* 6, 339 (1967)